SPACE MAPPING FRAMEWORKS FOR MODELING AND DESIGN OF MICROWAVE CIRCUITS

To my parents

SPACE MAPPING FRAMEWORKS FOR MODELING AND DESIGN OF MICROWAVE CIRCUITS

By

MOSTAFA A. ISMAIL, M.Sc. (Eng.)

A Thesis

Submitted to the School of Graduate Studies

in Partial Fulfillment of the Requirements

for the Degree

Doctor of Philosophy

McMaster University

April 2001

DOCTOR OF PHILOSOPHY (2001) McMASTER UNIVERSITY
(Electrical and Computer Engineering) Hamilton, Ontario

TITLE: **Space Mapping Frameworks for Modeling and Design of Microwave Circuits**

AUTHOR: Mostafa A. Ismail
M.Sc. (Eng.)
(Faculty of Engineering, Cairo University)

SUPERVISOR: J.W. Bandler, Professor Emeritus, Department of Electrical and Computer Engineering
B.Sc. (Eng.), Ph.D., D.Sc. (Eng.) (University of London)
D.I.C. (Imperial College)
P.Eng. (Province of Ontario)
C.Eng. FIEE (United Kingdom)
Fellow, IEEE
Fellow, Royal Society of Canada
Fellow, Engineering Institute of Canada

NUMBER OF PAGES: xviii, 164

ABSTRACT

This thesis contributes to computer-aided design and modeling of microwave circuits exploiting space mapping technology. Comprehensive frameworks for enhancing available empirical models or creating new ones are presented. A novel technique for microwave circuit design is also presented.

A comprehensive framework to engineering device modeling which we call Generalized Space Mapping (GSM) is introduced. GSM aims at significantly enhancing the accuracy of available empirical models of microwave devices by utilizing a few relevant full-wave EM simulations. Three fundamental illustrations are presented: a basic Space Mapping Super Model (SMSM), Frequency-Space Mapping Super Model (FSMSM) and Multiple Space Mapping (MSM). Two variations of MSM are presented: MSM for Device Responses (MSMDR) and MSM for Frequency Intervals (MSMFI). A novel criterion to discriminate between coarse models of the same device is also presented.

A new computer-aided modeling methodology to develop broadband physics-based models for passive components is presented. Full-wave EM simulators, artificial neural networks, multivariable rational functions, dimensional analysis and frequency mapping are coherently integrated to establish broadband models. Frequency mapping is used to develop the frequency-dependent empirical models. Useful properties of the

frequency mapping are utilized in the modeling process. Transformations from frequency-dependent models to frequency-independent ones are also considered. The passivity conditions of the frequency-dependent empirical model are also considered.

We present a novel design framework for microwave circuits. We expand the original space mapping technique by allowing preassigned parameters (which are not used in optimization) to change in some components of the coarse model. We refer to those components as “relevant” components and we present a method based on sensitivity analysis to identify them. As a result, the coarse model can be calibrated to align with the fine model. Our algorithm establishes a mapping from some of the optimizable parameters to the preassigned parameters of the relevant components. This mapping is updated iteratively until we reach the optimal solution.

ACKNOWLEDGEMENTS

The author wishes to express his sincere appreciation to Dr. J.W. Bandler, director of research in the Simulation Optimization Systems Research Laboratory at McMaster University and President of Bandler Corporation, for his expert guidance, continued assistance, encouragement and supervision throughout the course of this work.

The author would like also to express his appreciation to Dr. Natalia Georgieva of McMaster University, for her continued encouragement and useful discussions as a colleague in the Simulation Optimization Systems Research Laboratory at McMaster University from 1999 to 2000, and also as a Supervisory Committee member. Thanks are extended to Dr. J.P. Reilly and Dr. A.D. Spence, Supervisory Committee members, for their continuing interest.

The author thanks Dr. Q.J. Zhang of Carleton University for useful discussions during earlier parts of this work. The author also thanks Dr. R.M. Biernacki and Dr. S.H. Chen, now with Agilent EEsof EDA, Santa Rosa, CA, for their concept of the Space Mapping Super Model while they were with Optimization Systems Associates Inc.

The author would like to thank his colleagues Dr. M.H. Bakr, J.E. Rayas-Sánchez, T. Chen, F. Guo, Q.S. Cheng and A.S. Mohamed for their nice company, productive collaboration and stimulating discussions.

The author has greatly benefited from working with the OSA90/hope™ and

Empipe™ microwave computer-aided design systems developed by Optimization Systems Associates Inc., now part of Agilent EEsof EDA. The author is also grateful to Dr. J.C. Rautio, President, Sonnet Software, Inc., Liverpool, NY, for making ***em***™ available and to Agilent Technologies, Santa Rosa, CA, for making Momentum™ available.

The author would like to express his appreciation to Dr. K. Madsen of the Institute of Mathematical Modeling, the Technical University of Denmark, for discussions at both McMaster University and the Technical University of Denmark. The author would like also to thank D.G. Swanson, Jr., of Bartley R.F. Systems, Amesbury, MA, for discussions while visiting the Simulation Optimization Systems Research Laboratory at McMaster University in 1998. The author greatly benefited from his expertise and knowledge in microwave design.

Financial assistance was awarded to the author from several sources: from the Natural Sciences and Engineering Research Council of Canada through grants OGP0007239, STP0201832 and STR234854-00, through the Micronet Network of Centres of Excellence, from the Department of Electrical and Computer Engineering through a Teaching Assistantship and Scholarship, and through a Nortel Networks Ontario Graduate Scholarship in Science and Technology (OGSST).

Finally, thanks are due to my family for encouragement, understanding, patience and continuous support.

CONTENTS

LIST OF FIGURES

LIST OF TABLES

Chapter 1

INTRODUCTION

Over the past four decades computer-aided design (CAD) techniques have been utilized in circuit design. The use of iterative optimization in circuit design was strongly advocated by (Temes and Calahan 1967). Since then optimization techniques have been extensively developed and applied for design and modeling of microwave circuits. Areas of application include filter design, design centering, yield enhancement, robust device modeling and fault diagnosis (Bandler 1969), (Bandler and Salama 1985), (Bandler, Kellermann and Madsen 1985) and (Bandler and Chen 1988), and others. Efficient optimization of large microwave systems is presented in Bandler and Zhang (1987).

Electromagnetic (EM) simulators have added a new dimension to CAD of microwave circuits. Microwave engineers can validate their designs without building actual prototypes. Excellent agreement between efficient EM field solvers and measurements has been reported in Rautio and Harrington (1987a and 1987b). There are two types of EM simulators: so-called "2.5-D" EM simulators, which analyze planar structures and 3-D EM simulators, which analyze arbitrary 3-D structures. The 2.5-D software is based on the method of moments (Harrington 1967) while 3-D software is frequently based on finite-element analysis, finite-difference time domain (FDTD) or TLM method (Hoefer 1992). Examples of commercial 2.5-D and 3-D EM simulators include Sonnet's ***em***™ (***em*** 1997), Momentum™ (Momentum 1999), Agilent HFSS™

(Agilent HFSS 1999) and Ansoft HFSS™. Methods of using commercial EM simulators in circuit design and modeling are addressed in Jain and Onno (1997) and Swanson (1998).

The Geometry Capture concept by Bandler, Biernacki and Chen (1996 and 1999) has made automated electromagnetic optimization realizable. This concept was implemented in Empipe™ (Empipe 1997) and Empipe3D™ (Empipe3D 1997) to perform 2.5-D and 3-D EM optimization, respectively. The Empipe family is based on the OSA90/hope™ platform (OSA90/hope 1997). EM optimization of planar and 3-D microwave structures has been reported in Bandler, Biernacki, Chen, Swanson and Ye (1994), Bandler, Biernacki, Chen, Getsinger, Grobelny, Moskowitz and Talisa (1995), Bandler, Biernacki, Chen, Hendrick and Omeragić (1997) and Swanson (1995).

Response surface modeling and model-reduction techniques are very important directions of microwave CAD. Efficient interpolation techniques have been developed for microwave circuit design and modeling. For example, Maximally Flat Quadratic Interpolation (MFQI) was presented in Bandler, Biernacki, Chen, Grobelny and Ye 1993 as a powerful tool for EM yield optimization. The MFQI technique is implemented in Empipe™ and Empipe3D™. A multidimensional Cauchy interpolation technique was presented in Peik, Mansour and Chow (1998) for optimization and Monte Carlo analysis of microwave circuits. An adaptive frequency sampling technique was introduced in Dhaene, Ureel, Faché and De Zutter (1995) to approximate microwave responses in a certain frequency range of interest with a minimum number of EM simulations. Model-reduction techniques have been exploited for design and analysis of high-speed circuits in Dounavis, Gad, Achar and Nakhla (2000).

Artificial neural networks have been introduced to microwave CAD in Zaabab, Zhang and Nakhla (1994). They have been combined with EM simulators to develop accurate models for emerging microwave devices (Wang and Zhang 1997, Watson and Gupta 1996 and 1997 and Bandler, Ismail, Rayas-Sánchez and Zhang 1999). They have been also used for microwave filter design and modeling (Burrascano, Dionigi, Fancelli and Mongiardo 1998) and (Bakr, Bandler, Ismail, Rayas-Sánchez and Zhang 2000).

Circuit-theoretic models (circuit simulators) have been used extensively for microwave design and analysis. They are simple and efficient but may lack the necessary accuracy or have limited validity range. Examples of commercial circuit simulators with optimization capabilities include OSA90/hope™ (OSA90/hope 1997) and Agilent ADS™ (ADS 1999). Field-theoretic models (EM simulators) on the other hand are more accurate but CPU intensive. Efficient techniques have been developed to exploit the efficiency of circuit-theoretic models and the accuracy of field-theoretic models. Space Mapping (Bandler, Biernacki, Chen, Grobelny and Hemmers 1994) directs the bulk of CPU intensive optimization to the circuit-theoretic models while preserving the accuracy offered by the field-theoretic models. Companion (circuit-theoretic) models were exploited in Pavio (1999) for EM optimization. Another technique that compensates the interaction between nonadjacent elements of a microwave structure by adding circuit components is presented in Ye and Mansour (1997).

The objective of this thesis is to summarize our developments in modeling and optimization of microwave circuits. These developments include the Generalized Space Mapping (GSM) framework for device modeling (Bandler, Georgieva, Ismail, Rayas-Sánchez and Zhang 1999 and 2001) and broadband modeling of microwave passive devices exploiting frequency mapping (Bandler, Ismail and Rayas-Sánchez 2000 and

2001a). They also include an expanded space mapping (ESM) optimization algorithm exploiting preassigned parameters (Bandler, Ismail and Rayas-Sánchez 2001b and 2001c).

In Chapter 2, we review some essential concepts in circuit optimization such as error functions, design specifications, norms and objective functions. The review follows the work of Bandler (1969), Bandler and Charalambous (1972), Charalambous (1973), Rizk (1979), Bandler and Chen (1988) and Grobelny (1995). We also review the original space mapping algorithm (Bandler, Biernacki, Chen, Grobelny and Hemmers 1994) as well as recent developments in space mapping algorithms for modeling and optimization of microwave circuits. Dimensional analysis is an important tool for device modeling. An example showing the application of dimensional analysis in device modeling is presented.

In Chapter 3, we present a comprehensive framework to engineering device modeling. We consider the Generalized Space Mapping (GSM) approach for microwave device modeling (Bandler, Georgieva, Ismail, Rayas-Sánchez and Zhang 1999 and 2001). Three fundamental illustrations are presented: a basic Space Mapping Super Model (SMSM), Frequency-Space Mapping Super Model (FSMSM) and Multiple Space Mapping (MSM). Two variations of MSM are also presented: MSM for Device Responses (MSMDR) and MSM for Frequency Intervals (MSMFI). We present two algorithms to implement MSMDR and MSMFI. We also present novel criteria to differentiate between coarse models of the same device. The chapter is concluded with some modeling examples including a microstrip line, a microstrip right angle bend, a microstrip step junction and a microstrip shaped T-junction, yielding remarkable improvement within regions of interest.

In Chapter 4, we address the issue of developing broadband empirical models of microwave passive devices. A new computer-aided modeling methodology to develop physics-based models for passive components valid in a broad frequency band is presented (Bandler, Ismail, Rayas-Sánchez 2000 and 2001a). Full-wave EM simulators, artificial neural networks, multivariable rational functions, dimensional analysis and frequency mapping are coherently integrated to establish broadband models. We consider both frequency-independent and frequency-dependent empirical models. Frequency mapping is used to develop the frequency-dependent empirical models. Useful properties of the frequency mapping are also presented and utilized in the modeling process. We also consider the transformation from frequency-dependent models into frequency-independent ones. The chapter is concluded by developing broadband empirical models for typical microwave devices such as a microstrip right angle bend, a microstrip via, a microstrip double-step junction and a CPW step junction.

In Chapter 5, we summarize the expanded space mapping design framework exploiting preassigned parameters (Bandler, Ismail and Rayas-Sánchez 2001b and 2001c). The chapter starts by introducing some concepts and notation. Some key preassigned parameters (which are not used in optimization) are allowed to change in some of the coarse model components (we call them "relevant" components) in order to calibrate the coarse model with the fine model. A decomposition technique based on sensitivity analysis is presented to partition the coarse model components into two sets. The key preassigned parameters (KPP) are allowed to change in the first set and they are kept intact in the second set. The Expanded Space Mapping Design Framework (ESMDF) algorithm calibrates the coarse model iteratively by extracting the KPP of the relevant components. It establishes a mapping from some of the optimizable parameters

to the preassigned parameters. This mapping is sparse and needs few fine model simulations to be fully established. Trust region methodology is used to optimize the enhanced (calibrated) coarse model. The algorithm terminates if certain relevant stopping criteria are satisfied. We also address software implementation of the algorithm as well as interfacing with commercial EM simulators. The algorithm has been applied to several microwave design problems including a three-section microstrip transformer, an HTS filter and a stopband microstrip filter with open stubs.

We conclude in Chapter 6 along with suggestions for further research.

The circuit examples included in this thesis have been prepared using OSA90/hope™ (OSA90/hope 1997) circuit simulation and optimization system, Empipe™ (Empipe 1997), the EM simulator Sonnet's ***em***™ (***em*** 1997) and the EM simulator Momentum™ (Momentum 1999).

The author contributed substantially to the following original developments presented in this thesis:

(1) Development of a generic space mapping formulation for microwave device modeling.

(2) Development of a comprehensive modeling framework to enhance empirical models of passive devices and to differentiate between empirical models of the same device.

(3) Development of broadband empirical models of microwave passive devices.

(4) Introducing the concept of key preassigned parameters to microwave circuit design.

(5) Development and implementation of the expanded space mapping algorithm for

circuit optimization exploiting key preassigned parameters.

(6) Development of a software tool to drive EM simulators (which has parameterization capabilities) from any Microsoft Windows based programming environment such as Matlab™ (Matlab 1999).

Chapter 2

BASIC CONCEPTS IN MODELING AND OPTIMIZATION

2.1 INTRODUCTION

In this chapter, we review concepts and techniques for design and modeling of microwave circuits. First we define typical design specifications for microwave problems. Error functions, norms and objective functions are also formulated. Our definitions follow work done by Bandler (1969), Bandler and Charalambous (1972), Charalambous (1973), Rizk (1979), Bandler and Chen (1988) and Grobelny (1995).

We also review the space mapping (SM) concept for microwave design and modeling. This review introduces notation we will use through out this work. We start with the original space mapping approach to circuit design (Bandler, Biernacki, Chen, Grobelny and Hemmers 1994). Other space mapping algorithms for circuit design are briefly contrasted. We also review the application of the space mapping technique to modeling.

Finally, we review the method of dimensional analysis for device modeling. The basic theorem in dimensional analysis was proved by Buckingham (Middendorf 1986). Dimensional analysis aims at reducing the number of variables a physical quantity

depends upon. It is applicable to all scientific and engineering problems.

2.2 DESIGN SPECIFICATIONS, ERROR FUNCTIONS AND NORMS

2.2.1 Design Specifications and Error Functions

Let the responses of interest of a microwave circuit be

$$\boldsymbol{R}(\boldsymbol{\varphi},\psi)=[R_1(\boldsymbol{\varphi},\psi)\;\; R_2(\boldsymbol{\varphi},\psi)\cdots R_r(\boldsymbol{\varphi},\psi)]^T \tag{2-1}$$

where $\boldsymbol{\varphi}\in\Re^n$ represents the circuit designable parameters and ψ is an independent variable such as frequency, time or temperature (Bandler and Rizk 1979) and (Rizk 1979). The circuit response could be a function of more than one independent variable. In this work, we will deal only with one independent variable, namely, the frequency ω. Therefore, from now on we will refer to the independent variable ψ as ω. A typical design problem implies that the circuit responses (2-1) should satisfy some specifications. These specifications are considered functions only of the independent variable ω. The specifications can be single, upper or lower specifications. In this work, we will consider upper and lower specifications.

An upper specification is defined such that the desired response of the circuit should be less than this specification. A lower specification is defined such that the desired response should be higher than this specification. Typical microwave design problems may involve upper, lower or both specifications.

Each circuit response $R_i(\boldsymbol{\varphi},\omega)$ in (2-1) can be associated with an upper specification $S_{ui}(\omega)$, a lower specification $S_{li}(\omega)$ or both. In practical microwave

circuit design each specification is defined over a discrete set of frequencies. Let $S_{ui}(\omega)$ be defined over the discrete frequency set Ω_{ui}. Similarly, the lower specification $S_{li}(\omega)$ is defined over the discrete set of frequencies Ω_{li}. The sets Ω_{ui} and Ω_{li} may not be disjoint.

Consider lower and upper specifications, the error functions will take the form (Bandler 1969)

$$\begin{aligned} \boldsymbol{e}_{li}(\boldsymbol{\varphi},\omega) &= w_{li}(\omega)\,[S_{li}(\omega) - R_i(\boldsymbol{\varphi},\omega)]\,,\ \omega \in \Omega_{li} \\ \boldsymbol{e}_{ui}(\boldsymbol{\varphi},\omega) &= w_{ui}(\omega)\,[R_i(\boldsymbol{\varphi},\omega) - S_{ui}(\omega)]\,,\ \omega \in \Omega_{ui} \end{aligned} \tag{2-2}$$

where $w_{li}(\omega)$ and $w_{ui}(\omega)$ are nonnegative weighting factors. The error functions in (2-2) are defined such that positive (negative) values for the errors indicate violation (satisfaction) of the design specifications (Chen 1987). The error vector

$$\boldsymbol{e}(\boldsymbol{\varphi}) = [e_1(\boldsymbol{\varphi})\ \ e_2(\boldsymbol{\varphi}) \cdots e_{Ne}(\boldsymbol{\varphi})]^T \tag{2-3}$$

contains the error functions defined by (2-2) for all responses in (2-1) and over all frequency samples. The number of error functions (N_e) depends on whether the ith response $R_i(\boldsymbol{\varphi},\omega)$ has an upper, lower or both specifications imposed on it. Define b_{li} by

$$b_{li} = \begin{cases} 1 & \text{if a lower specification } S_{li}(\omega) \text{ exists for } R_i(\boldsymbol{\varphi},\omega) \\ 0 & \text{otherwise} \end{cases} \tag{2-4}$$

Similarly, b_{ui} is defined by

$$b_{ui} = \begin{cases} 1 & \text{if an upper specification } S_{ui}(\omega) \text{ exists for } R_i(\boldsymbol{\varphi},\omega) \\ 0 & \text{otherwise} \end{cases} \tag{2-5}$$

Notice that b_{ui} and b_{li} can not be zero at the same time since at least $S_{ui}(\omega)$, $S_{li}(\omega)$ or

both should exist for the circuit response $R_i(\boldsymbol{\varphi},\omega)$ (otherwise we would not include this response in (2-1)). Therefore, the total number of error functions N_e is given by

$$N_e = \sum_{i=1}^{r} b_{li} \left|\Omega_{li}\right| + b_{ui} \left|\Omega_{ui}\right| \tag{2-6}$$

where $\left|\ \right|$ denotes the set cardinality.

For example, Fig. 2.1(a) shows typical specifications for a bandpass filter design problem. The response of interest is the scattering parameter S_{21} and both lower and upper specifications exist. The lower specification $S_l(\omega)$ is defined in the passband and the upper specification $S_u(\omega)$ is defined in the stopband. The lower specification contains 4 frequency samples while the upper specification contains 8 frequency samples. The components of the error vector $\boldsymbol{e}$ are shown in Fig. 2.1(b).

2.2.2 Vector Norms and Objective Functions

Circuit design implies solving the optimization problem

$$\underset{\boldsymbol{\varphi}}{\text{minimize}} \quad U(\boldsymbol{e}(\boldsymbol{\varphi})) \tag{2-7}$$

where U is an objective function, $\boldsymbol{e}$ is the vector of error functions (2-3) and $\boldsymbol{\phi}$ represents the design parameters. Very often we set U to a suitable norm which gives a measure of how much the error functions satisfy (violate) the specifications.

The ℓ_p norm is defined by

$$\left\|\boldsymbol{e}(\boldsymbol{\varphi})\right\|_p = \left[\sum_{j=1}^{N_e} \left|e_j(\boldsymbol{\varphi})\right|^p\right]^{1/p} \tag{2-8}$$

The parameter p has an important implication. Large (small) values of p put more emphasis on the error functions (e_j's) that have larger (smaller) values (Chen 1987).

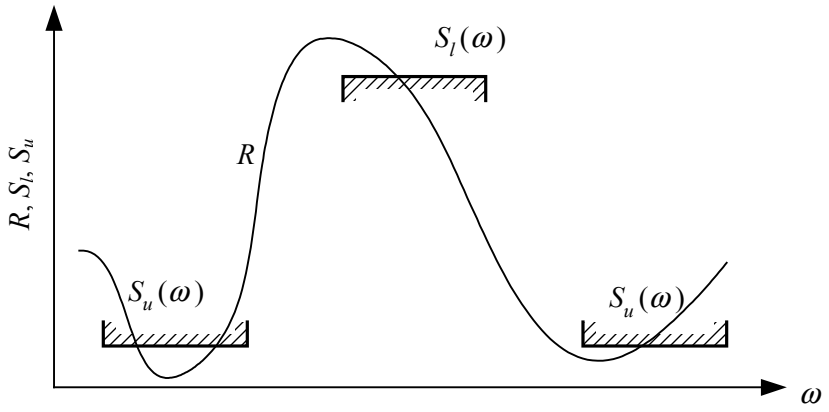

(a)

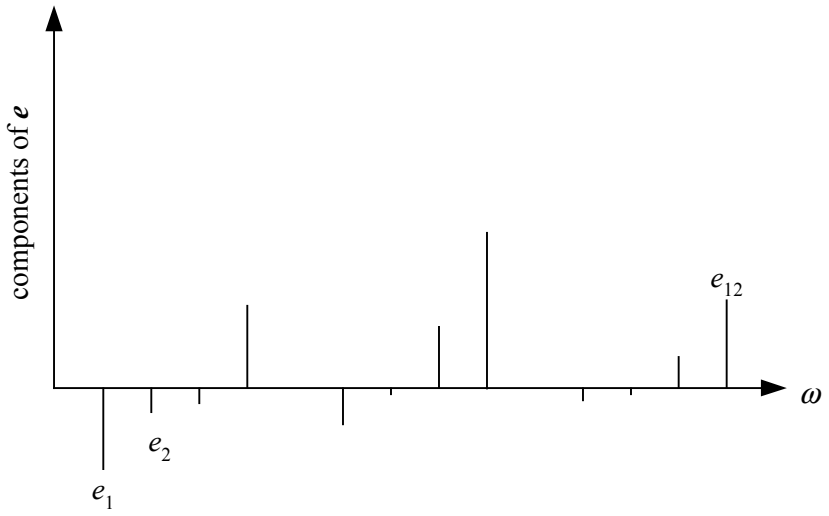

(b)

Fig. 2.1 Illustration of upper and lower specifications and error functions for a typical bandpass filter design.

Special cases include least square (p=2), which is the most widely used norm. It has nice features such as differentiability and, moreover, it involves a quadratic function in $\boldsymbol{\phi}$ if the error functions are linear in $\boldsymbol{\phi}$.

When p=1 we have the ℓ_1 norm which puts more emphasis on small error

function values. Therefore, it is widely used in data fitting problems and robust device modeling (Bandler, Chen and Daijavad 1986). Also it is used in analog fault location (Bandler and Salama 1985).

The most popular norm in filter design is the minimax norm (ℓ_∞ norm) defined by

$$\left\|\boldsymbol{e}(\boldsymbol{\varphi})\right\|_\infty = \max_j \left|e_j(\boldsymbol{\varphi})\right| \tag{2-9}$$

This norm puts emphasis on the worst case errors. It is suitable for filter design problems in which we wish to obtain equal-ripple responses. Another important norm is the Huber norm (Huber 1981, Bandler, Chen, Biernacki, Gao, Madsen and Yu 1993a and 1993b) defined by

$$H(\boldsymbol{e}) = \sum_{i=1}^{N_e} \rho(e_i) \tag{2-10}$$

where

$$\rho(e_i) = \begin{cases} e_i^2/2 & \text{if} \quad |e_i| \le K \\ K|e_i| - K^2/2 & \text{if} \quad |e_i| > K \end{cases} \tag{2-11}$$

where K is a positive constant. The Huber norm is treated as a hybrid of the ℓ_1 and ℓ_2 norms. It is robust against large errors and flexible with respect to small variations in data (see Bandler, Chen, Biernacki, Gao, Madsen and Yu 1993a and 1993b). A comparison between ℓ_1, ℓ_2 and the Huber norm in data fitting was presented in Bandler, Chen, Biernacki, Gao, Madsen and Yu (1993a) and (1993b). In Chapter 3, 4 and 5, we will use the Huber norm as an objective function for the parameter extraction (PE) process.

When we set the objective function U in (2-7) to the ℓ_p norm of the error vector

$\boldsymbol{e}$ (with $p > 0$) we are basically interested in driving the error functions to zero. This is because we are seeking the minimal value of the absolute of the error functions. For example, if we managed to drive the objective function to zero, this would mean that we obtained a solution which makes the circuit responses exactly match the specifications over the frequency samples of interest. In practical circuit design we are not only interested in satisfying the specifications but also exceeding them as much as possible. Bandler and Charalambous (1972) and Charalambous (1973) considered this case and proposed the generalized least pth (ℓ_p) objective. This objective function is defined by

$$H_p(\boldsymbol{e}) = \begin{cases} H_p^+(\boldsymbol{e}(\boldsymbol{\varphi})) = \left[\sum_{j \in \boldsymbol{J}} [e_j(\boldsymbol{\varphi})]^p \right]^{1/p} & \text{if } \boldsymbol{J}(\boldsymbol{\varphi}) \neq \varnothing \\ H_p^-(\boldsymbol{e}(\boldsymbol{\varphi})) = -\left[\sum_{j=1}^{N_e} [-e_j(\boldsymbol{\varphi})]^{-p} \right]^{-1/p} & \text{if } \boldsymbol{J}(\boldsymbol{\varphi}) = \varnothing \end{cases} \tag{2-12}$$

The index $\boldsymbol{J}$ in (2-12) is given by

$$\boldsymbol{J} = \{ j \,|\, e_j(\boldsymbol{\varphi}) \geq 0 \} \tag{2-13}$$

The function $H_p^+(\boldsymbol{e}(\boldsymbol{\varphi}))$ in (2-12) is concerned with the responses that violate the specifications (their associated errors are positive). Minimizing this function forces the responses to only satisfy the specifications. In order to exceed the specifications as much as possible we minimize the function $H_p^-(\boldsymbol{e}(\boldsymbol{\varphi}))$ in (2-12). The ($-p$) in the definition of $H_p^-(\boldsymbol{e}(\boldsymbol{\varphi}))$ indicates that the larger the value of p the more emphasis is given to the minimum error (Bandler and Charalambous 1972). Minimizing $H_p^-(\boldsymbol{e}(\boldsymbol{\varphi}))$ will tend to maximize the minimum amount by which the specifications are exceeded (Bandler and Charalambous 1972). A special case of the generalized least pth ℓ_p objective is the

generalized minimax function

$$\boldsymbol{H}_{\infty}(\boldsymbol{e}(\boldsymbol{\varphi})) = \max_{j=1,\cdots,N_e} \{e_j(\boldsymbol{\varphi})\} \tag{2-14}$$

which is used in the Chebyshev design of filters.

Another norm, which is similar to the ℓ_2 but is defined for matrices, is the Frobenius norm. The Frobenius norm of a matrix $\boldsymbol{A} = [a_{ij}]$, $i = 1, \ldots, k$ and $j = 1, \ldots, l$ is defined by

$$\|\boldsymbol{A}\|_F = \left[\sum_{i=1}^{k} \sum_{j=1}^{l} \left| a_{ij} \right|^2 \right]^{1/2} \tag{2-15}$$

2.3 SPACE MAPPING TECHNOLOGY

In this section, we review some of the space mapping (SM) based techniques for modeling and optimization of microwave circuits. The basic concept was first published in Bandler, Biernacki, Chen, Grobelny and Hemmers (1994). Space mapping assumes that there are two models to represent a microwave structure: a "coarse" model and a "fine" model. It also assumes that there exists a mapping between the parameters of the coarse model and those of the fine model. SM based algorithms differ in the way this mapping is approximated, initialized and updated. According to their application they are divided into two classes: SM based algorithms for design optimization and SM based algorithms for device modeling. A review of SM based algorithms for optimization can be found in (Bakr, Bandler, Madesn and Søndergaard 2000).

2.3.1 Fine and Coarse Models

Fine models are considered the reference models in SM. They are assumed to be

very accurate but time intensive. Typically they represent a solution of Maxwell equations using commercial EM simulators (Sonnet's ***em***, Agilent Momentum and Agilent HFSS) or in-house EM simulators. They may also represent measurements (if available) of the actual device. During the development and testing of SM based algorithms we can consider detailed circuit-based models as "fine" models.

Coarse models are considered approximate. They are assumed to be very fast to simulate but less accurate than fine models. Typically, they represent circuit-based models with empirical models for the circuit components. They may also represent a solution of Maxwell equations using fast EM simulators such as those based on the Mode-Matching technique (Bandler, Biernacki, Chen and Omeragić 1997 and 1999) or Method-of-Moment EM simulators with a very coarse mesh (Bandler, Biernacki, Chen, Grobelny and Hemmers 1994).

2.3.2 Basic Notation and Definitions

Let $\boldsymbol{x}_f \in \Re^n$ represent the designable parameters of the fine model. Similarly, let $\boldsymbol{x}_c \in \Re^n$ represent the designable parameters of the coarse model. Both $\boldsymbol{x}_f$ and $\boldsymbol{x}_c$ represent corresponding designable parameters. The space of $\boldsymbol{x}_f$ is called the fine model space while that of $\boldsymbol{x}_c$ is called the coarse model space.

The vector $\boldsymbol{R}_f(\boldsymbol{x}_f, \Omega) \in \Re^{FL}$ represents a complete set of basic responses of the fine model (such as the real and imaginary parts of the S-parameters) at the point $\boldsymbol{x}_f$ and over a set of discrete frequencies Ω. The number of basic responses is L and the number of discrete frequencies in the set Ω is F. Similarly, the vector $\boldsymbol{R}_c(\boldsymbol{x}_c, \Omega) \in \Re^{FL}$

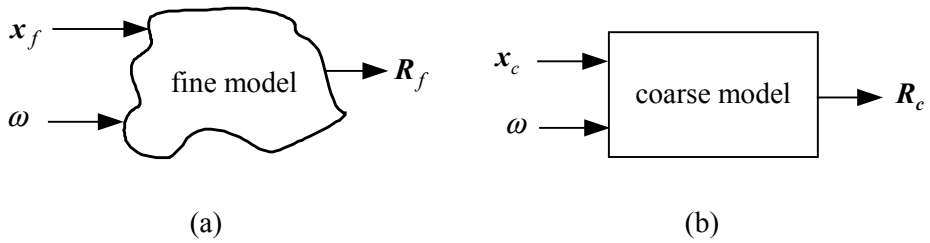

Fig. 2.2 The fine model (a), and the coarse model (b).

represents a complete set of basic responses for the coarse model at the point $\boldsymbol{x}_c$ and over the set $\boldsymbol{\Omega}$. Fig. 2.2 illustrates these concepts.

In the original space mapping approach (Bandler, Biernacki, Chen, Grobelny and Hemmers 1994) it is assumed that there exists a mapping from the fine model space to the coarse model space

$$\boldsymbol{x}_c = \boldsymbol{P}(\boldsymbol{x}_f) : \Re^n \mapsto \Re^n \tag{2-16}$$

such that the coarse model response at $\boldsymbol{x}_c$ matches the fine model response at $\boldsymbol{x}_f$. For a given $\boldsymbol{x}_f$ in the fine model space the corresponding point $\boldsymbol{x}_c$ in the coarse is obtained by solving the optimization problem

$$\boldsymbol{x}_c = \arg\min_{\boldsymbol{x}_c} \left\| \boldsymbol{R}_f(\boldsymbol{x}_f, \Omega) - \boldsymbol{R}_c(\boldsymbol{x}_c, \Omega) \right\| \tag{2-17}$$

where $\| \ \|$ is a suitable norm. This is called parameter extraction (PE) and it is essential in any space mapping based algorithm.

2.3.3 Space Mapping Optimization

Space Mapping was originally presented as an optimization tool. Three main tasks are performed in SM based algorithms for optimization: coarse model optimization, updating the mapping $\boldsymbol{P}$ and parameter extraction optimization (2-17). The optimal

solution of the coarse model is obtained by solving

$$\boldsymbol{x}_c^* = \arg\min_{\boldsymbol{x}_c} U(\boldsymbol{R}_c(\boldsymbol{x}_c, \Omega)) \tag{2-18}$$

where U is a suitable objective function (see Section 2.2.2).

2.3.3.1 The Original SM Algorithm

The original space mapping algorithm (Bandler, Biernacki, Chen, Grobelny and Hemmers 1994) uses linear approximation to approximate the mapping $\boldsymbol{P}$

$$\boldsymbol{x}_c = \boldsymbol{B}\,\boldsymbol{x}_f + \boldsymbol{c} \tag{2-19}$$

where $\boldsymbol{B} \in \Re^{nxn}, \boldsymbol{c} \in \Re^n$ are to be determined. Some base points are selected around the optimal coarse model solution $\boldsymbol{x}_c^*$ in the fine model space. The corresponding points in the coarse model space are obtained by performing parameter extraction optimization (2-17) at each point. The initial mapping is then evaluated by solving a system of linear equations. At the ith iteration the algorithm compares the fine model response at $\boldsymbol{x}_f^{(i)} = \boldsymbol{B}_i^{-1}\boldsymbol{x}_c^* - \boldsymbol{c}_i$ and the optimal coarse model response. If they do not agree the algorithm performs parameter extraction optimization (2-17) to get a new pair of points $(\boldsymbol{x}_f^{(i)}, \boldsymbol{x}_c^{(i)})$. This pair of points is added to the set of base points and the mapping is then updated by solving a linear system of equations. The algorithm converges when the fine model response is sufficiently close to the optimal coarse model response. The following steps summarize the original space mapping algorithm (Bandler, Biernacki, Chen, Grobelny and Hemmers 1994)

Step 0 Initialize $\boldsymbol{x}_f^{(1)} = \boldsymbol{x}_c^*$. If $\left\| \boldsymbol{R}_c(\boldsymbol{x}_c^*) - \boldsymbol{R}_f(\boldsymbol{x}_f^{(1)}) \right\| \le \varepsilon$, stop.

Step 1 Select a set X_f of m_b base points in the fine model space by perturbation

around $\boldsymbol{x}_f^{(1)}$.

Step 2 Obtain the corresponding set X_c in the coarse model by performing parameter extraction optimization (2-17) to all points in the set X_f.

Step 3 Initialize $i = 0$ and $m_i = m_b$.

Step 4 Compute the mapping parameters $\boldsymbol{B}_i$ and $\boldsymbol{c}_i$.

Step 5. Set $\boldsymbol{x}_f^{(m_i+1)} = \boldsymbol{B}_i^{-1}\boldsymbol{x}_c^* - \boldsymbol{c}_i$.

Step 6 If $\left\|\boldsymbol{R}_c(\boldsymbol{x}_c^*) - \boldsymbol{R}_f(\boldsymbol{x}_f^{(m_i+1)})\right\| \le \varepsilon$, stop.

Step 7 Perform parameter extraction optimization (2-17) to get $\boldsymbol{x}_c^{(m_i+1)}$ corresponding to $\boldsymbol{x}_f^{(m_i+1)}$.

Step 8 Add $\boldsymbol{x}_f^{(m_i+1)}$ to X_f and $\boldsymbol{x}_c^{(m_i+1)}$ to X_c.

Step 9 Set $i = i+1$, $m_i = m_i + 1$ and go to step 4.

The mapping parameters $\boldsymbol{B}_i$ and $\boldsymbol{c}_i$ are updated as follows. Assume that the set X_f contains m_i points

$$X_f = \{\boldsymbol{x}_f^{(1)}, \boldsymbol{x}_f^{(3)}, \cdots, \boldsymbol{x}_f^{(m_i)}\} \tag{2-20}$$

The corresponding set X_c in the coarse model space is given by

$$X_c = \{\boldsymbol{x}_c^{(1)}, \boldsymbol{x}_c^{(3)}, \cdots, \boldsymbol{x}_c^{(m_i)}\} \tag{2-21}$$

where every point in X_c is obtained by performing parameter extraction optimization (2-17) to the corresponding point in X_f. Substituting the points in X_f and X_c in (2-19) we get (Bandler, Biernacki, Chen, Grobelny and Hemmers 1994)

$$[\boldsymbol{x}_c^{(1)}\ \boldsymbol{x}_c^{(2)}\cdots\boldsymbol{x}_c^{(m_i)}]=[\boldsymbol{c}_i\ \boldsymbol{B}_i]\begin{bmatrix}1 & 1 & \cdots & 1\\ \boldsymbol{x}_f^{(1)} & \boldsymbol{x}_f^{(2)} & \cdots & \boldsymbol{x}_f^{(m_i)}\end{bmatrix} \tag{2-22}$$

The solution of the system of linear equations (2-22) is given by

$$\boldsymbol{A}_i^T=(\boldsymbol{D}^T\boldsymbol{D})^{-1}\boldsymbol{D}^T\boldsymbol{E} \tag{2-23}$$

where

$$\boldsymbol{A}_i=[\boldsymbol{c}_i\ \boldsymbol{B}_i] \tag{2-24a}$$

$$\boldsymbol{D}^T=\begin{bmatrix}1 & 1 & \cdots & 1\\ \boldsymbol{x}_f^{(1)} & \boldsymbol{x}_f^{(2)} & \cdots & \boldsymbol{x}_f^{(m_i)}\end{bmatrix} \tag{2-24b}$$

$$\boldsymbol{E}^T=[\boldsymbol{x}_c^{(1)}\ \boldsymbol{x}_c^{(2)}\cdots\boldsymbol{x}_c^{(m_i)}] \tag{2-24c}$$

2.3.3.2 Other Space Mapping Optimization Algorithms

The aggressive space mapping algorithm (Bandler, Biernacki, Chen, Hemmers and Madsen 1995) uses linear approximation to approximate the mapping $\boldsymbol{P}$. A unit mapping $\boldsymbol{x}_f=\boldsymbol{x}_c$ is used as an initial value for $\boldsymbol{P}$. The mapping is iteratively updated using the Broyden formula (Broyden 1965). Aggressive space mapping is more efficient than the original space mapping algorithm in the sense that it does need the overhead fine model simulations performed at the base points to build the initial mapping.

A trust region methodology has been combined with the aggressive space mapping algorithm in Bakr, Bandler, Biernacki, Chen and Madsen (1998). The authors call this algorithm TRASM, which stands for trust region aggressive space mapping. The authors in Bakr, Bandler, Georgieva and Madsen (1999) use a hybrid approach to obtain the optimal solution of the fine model. They use the TRASM algorithm to get close to the solution, then they use direct optimization to find the optimal solution of the fine

model.

The authors in Bakr, Bandler, Madsen, Rayas-Sánchez and Søndergaard (2000) exploit a surrogate model approach combined with space mapping approach for optimization. They consider a surrogate model, which is a convex combination of the mapped coarse model (the coarse model with the mapping $\boldsymbol{P}$) and a linearized fine model. An object oriented CAD system (SMX) implementing the surrogate model-based space mapping algorithm is presented in Bakr, Bandler, Cheng, Ismail and Rayas-Sánchez (2001). Besides being an optimization system, SMX provides an efficient technique for interfacing to commercial EM/circuit simulators.

Other types of space mapping based algorithms for optimization use artificial neural-networks to approximate the mapping $\boldsymbol{P}$. Bakr, Bandler, Ismail, Rayas-Sánchez and Zhang (2000) adaptively enhance the coarse model by establishing the mapping $\boldsymbol{P}$ by a neural-network. The mapping is updated at every iteration by retraining the neural-network. An approach similar to aggressive space mapping which uses a neural network to approximate the mapping $\boldsymbol{P}$ is presented in Bandler, Ismail, Rayas-Sánchez and Zhang (2001).

2.3.4 Space Mapping for Device Modeling

Space mapping based algorithms for device modeling aim at enhancing the coarse model in a region of interest. A set of base points is selected in the region of interest and a mapping is established such that the coarse model matches the fine model. The coarse model combined with the mapping $\boldsymbol{P}$ is called an enhanced coarse model. It is designed to be as almost as accurate as the fine model and almost as fast as the coarse model. The enhanced coarse model can be used (within the region of interest) for

statistical analysis such as yield estimation and for optimization.

Bandler, Ismail, Rayas-Sánchez and Zhang (1999) approximate the mapping $\boldsymbol{P}$ in a region of interest by an artificial neural network. They have also exploited useful concepts such as partial space mapping and frequency mapping. The authors in Bakr, Bandler, Georgieva (1999) introduced a space mapping modeling technique called space derivative mapping. They approximate the mapping $\boldsymbol{P}$ by a linear mapping in a region of interest. The Jacobian of $\boldsymbol{P}$ is calculated in terms of the Jacobian of the fine model and that of the coarse model. The Jacobian of the fine and coarse model models is computed by perturbation.

We will show in Chapter 3 how to generalize the space mapping concept to provide a comprehensive modeling framework for microwave devices.

2.4 DIMENSIONAL ANALYSIS

Dimensional analysis (Middendorf 1986) is a powerful tool for device modeling. It aims at reducing the number of variables a physical quantity depends upon. It was used in Watson, Mah and Liou (1999) to reduce the number of input variables of artificial neural networks. In this Section, we illustrate this concept through a microwave-modeling problem.

Dimensional analysis is based on Buckingham's theorem (Middendorf 1986). This theorem states that "if an equation is dimensionally homogeneous it can be reduced to a relationship among a complete set of dimensionless products of the system variables". The dimensionless products are called Pi (π) terms. In physical phenomena the equations expressing the relationships among the variables are dimensionally homogeneous. Therefore, the method applies to all engineering and scientific analysis.

The method tells us that if a complete set of dimensionless products can be found the governing equations of the system can be developed. It combines the basic variables into multiple-variable terms to express a physical quantity.

The set of dimensionless products is complete when each product is independent and any other dimensionless product that can be formed from the variables is a product of powers of the π terms in the set.

In Chapter 4, we will show how to exploit dimensional analysis in creating broadband empirical models for microwave devices.

2.4.1 Microstrip Via Example

Here, we consider modeling the microstrip via in Fig. 2.3(a). The equivalent circuit model is an inductor L to ground (Fig. 2.3(b)). The geometrical parameters are W_0, W, D and H (the substrate height). It is required to apply dimensional analysis to determine the dependency of the inductance L on the via parameters. The set of variables are L, W_0, W, D and the permeability μ_0 (we can use the speed of light c instead of μ_0). A typical dimensionless product takes the form

$$\pi = H^{x_1} W^{x_2} W_0^{x_3} D^{x_4} L^{x_5} \mu_0^{x_6} \tag{2-25}$$

where $x_1, \ldots, x_6$ are yet to be determined. Using the SI system of units,

$$\text{units of } \pi = (\text{M})^{x_1} (\text{M})^{x_2} (\text{M})^{x_3} (\text{M})^{x_4} (\text{Kg M S}^{-2} \text{ A}^{-2})^{x_5} (\text{Kg M}^2 \text{ S}^{-2} \text{ A}^{-2})^{x_6} \tag{2-26}$$

where Kg, M, S and A are the units of the SI system. Rearranging,

$$\text{units of } \pi = \text{Kg}^{x_5+x_6} \text{ M}^{x_1+x_2+x_3+x_4+x_5+2x_6} \text{ S}^{-2x_5-2x_6} \text{ A}^{-2x_5-2x_6} \tag{2-27}$$

But since π is dimensionless,

$$\begin{aligned} & x_5 + x_6 = 0 \\ & x_1 + x_2 + x_3 + x_4 + x_5 + 2x_6 = 0 \\ & -2x_5 - 2x_6 = 0 \\ & -2x_5 - 2x_6 = 0 \end{aligned} \tag{2-28}$$

The coefficient matrix of the system of simultaneous linear equations in (2-28) is given by

$$\boldsymbol{C} = \begin{bmatrix} 0 & 0 & 0 & 0 & 1 & 1 \\ 1 & 1 & 1 & 1 & 1 & 2 \\ 0 & 0 & 0 & 0 & 1 & 1 \\ 0 & 0 & 0 & 0 & 1 & 1 \end{bmatrix} \tag{2-29}$$

The coefficients of the matrix $\boldsymbol{C}$ can be obtained directly as shown in TABLE 2.1.

Any solution of (2-28) will result in a dimensionless π term. Furthermore, from matrix algebra the number of independent solutions (m) of the simultaneous equations is given by

$$m = n - \text{Rank}(\boldsymbol{C}) \tag{2-30}$$

where n is the total number of variables. The rank of the matrix $\boldsymbol{C}$ is 2, therefore we have 4 independent π terms. These terms can be obtained by solving the systems in (2-28). Since we have four equations and six unknowns, two of the unknowns can be expressed in terms of the other 4, which are called the excess variables. That is,

$$\begin{aligned} & x_5 = -x_6 \\ & x_1 = -x_2 - x_3 - x_4 - x_6 \end{aligned} \tag{2-31}$$

where the excess variables are x_2, x_3, x_4 and x_6. A solution of (2-31) is given in TABLE 2.2.

Substituting the values of the x's in (2-26) we get the following π-terms

$$\pi_1 = \frac{W}{H},\ \pi_2 = \frac{W_0}{H},\ \pi_3 = \frac{D}{H},\ \pi_4 = \frac{L}{\mu_0 H} \tag{2-32}$$

Let

$$\pi_2' = \frac{\pi_2}{\pi_1} = \frac{W_0}{W},\ \pi_3' = \frac{\pi_3}{\pi_1} = \frac{D}{W} \tag{2-33}$$

Applying Buckingham's theorem the relation between the independent π-terms can take the form

$$\pi_4 = f(\pi_1, \pi_2', \pi_3') \tag{2-34}$$

That is,

$$L = H\mu_0\ \ f(\frac{W}{H}, \frac{W_0}{W}, \frac{D}{W}) \tag{2-35}$$

Therefore, applying dimensional analysis reduces the number of parameters the inductance L depends upon from 4 to 3.

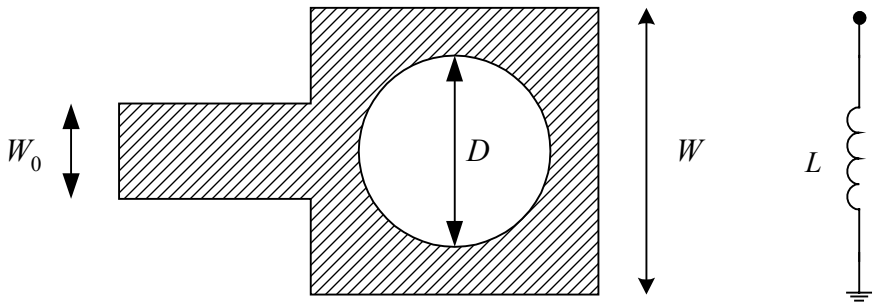

Fig. 2.3 The microstrip via: (a) the physical structure, (b) the circuit model.

TABLE 2.1

DETERMINING THE COEFFICIENT MATRIX OF THE SYSTEM IN (2-27) DIRECTLY FROM THE UNITS OF THE VIA PARAMETERS

	x_1	x_2	x_3	x_4	x_5	x_6
	H	W	W_0	D	L	μ_0
Kg	0	0	0	0	1	1
M	1	1	1	1	1	1
S	0	0	0	0	0	0
A	0	0	0	0	–2	–2

TABLE 2.2

A SOLUTION OF THE SYSTEM OF LINEAR EQUATIONS IN (2-31)

x_2	x_3	x_4	x_6	x_5	x_1
1	0	0	0	0	–1
0	1	0	0	0	–1
0	0	1	0	0	–1
0	0	0	1	–1	–1

2.5 CONCLUDING REMARKS

We have reviewed some fundamental concepts in circuit optimization and modeling. Design responses, error functions and design specifications have been addressed. Circuit design and modeling involve minimizing an objective function. This objective function is represented by a suitable norm of an error vector. Relevant norms and their applications to circuit design and modeling have been presented.

We have reviewed the space mapping concept for circuit design and modeling. Space mapping considers two kinds of models: a "fine" model and a "coarse" model. Different kinds of "fine" and "coarse" models of microwave circuits have been discussed. SM directs the bulk of CPU intensive optimization to the coarse model. The fine model is simulated a few times for verification and alignment.

Space mapping based algorithms are classified according to their application: (1) SM based algorithms for circuit modeling, and (2) SM based algorithms for circuit optimization. In SM based algorithms for optimization a mapping between the coarse model and fine model parameters is updated iteratively. SM was originally conceived for circuit optimization.

We have reviewed the original space mapping algorithm (Bandler, Biernacki, Chen, Grobelny and Hemmers 1994). We have also provided a survey of recent developments in SM algorithms for circuit optimization. The SM concept has been exploited for circuit modeling.

Finally, we review the method of dimensional analysis and its application to device modeling.

Chapter 3

GENERALIZED SPACE MAPPING FOR DEVICE MODELING

3.1 INTRODUCTION

In this chapter, we present a novel technique to enhance empirical models of microwave passive devices. We generalize the Space Mapping (Bandler, Biernacki, Chen, Grobelny and Hemmers 1994), the Frequency Space Mapping (Bandler, Biernacki, Chen, Hemmers and Madsen 1995) and the Multiple Space Mapping (Bandler, Biernacki, Chen and Wang 1998) concepts to build a new engineering device modeling framework. We refer to the concept generically as the Generalized Space Mapping (GSM) concept (Bandler, Georgieva, Ismail, Rayas-Sánchez and Zhang 1999 and 2001).

The mathematical formulation of GSM is not complicated. It is expected to be useful in assisting designers to evaluate the accuracy of empirical models and/or to discriminate between them. Intuitively meaningful quantitative measures of model accuracy can be developed through careful interpretations of GSM. Significant enhancement of the accuracy of available empirical models of microwave devices can be realized.

We start the chapter by describing the GSM concepts. Three fundamental cases

are presented: Space Mapping Super Model (SMSM) which maps designable device parameters, a basic Frequency-Space Mapping Super Model (FSMSM) which maps the frequency variable as well as the designable device parameters and Multiple Space Mapping (MSM). We present two variations of MSM: MSM for Device Responses (MSMDR) and MSM for Frequency Intervals (MSMFI). Two algorithms to implement MSMDR and MSMFI are also presented. Next we discuss the implementation of GSM. This is followed by some modeling examples.

3.2 THE GSM CONCEPT

Consider a microwave device which can be represented by two possible physically consistent models: a "coarse" model and a "fine" model (Bandler, Biernacki, Chen, Grobelny and Hemmers 1994). Recall from Chapter 2 that the coarse model is typically a circuit based model and the fine model is typically a full-wave EM simulator. The physical parameters of the microwave device are represented by $\boldsymbol{x}_f \in \Re^n$.

The vectors $\boldsymbol{R}_c(\boldsymbol{x}_f, \omega), \boldsymbol{R}_f(\boldsymbol{x}_f, \omega) \in \Re^L$ represent a complete set of responses for the coarse and fine model, respectively, at the point $\boldsymbol{x}_f$ and frequency ω. These responses are typically the real and imaginary parts of the scattering (S) parameters. In general, the response $\boldsymbol{R}_c(\boldsymbol{x}_f, \omega)$ deviates from the response $\boldsymbol{R}_f(\boldsymbol{x}_f, \omega)$ produced by an EM simulator. Therefore, the aim is to find a mapping from the fine model parameters and the frequency variable to a new set of parameters and a new frequency variable so that the responses of the two models match. Mapping the space parameters was introduced by Bandler, Biernacki, Chen, Grobelny and Hemmers (1994) and mapping the frequency variable was introduced later by Bandler, Biernacki, Chen, Hemmers and

Madsen (1995). The mapped coarse model parameters are represented by $\boldsymbol{x}_c \in \Re^n$ and the mapped frequency variable is represented by ω_c. We call this scheme Frequency-Space Mapping Super Model (FSMSM) as illustrated in Fig. 3.1. A special case of FSMSM is to map only the fine model parameters and leave the frequency variable unchanged. We call this Space Mapping Super Model (SMSM), as illustrated in Fig. 3.2. Once FSMSM or SMSM are established the enhanced coarse model (see Fig. 3.3) can be utilized for analysis or design purposes. We will compare the FSMSM and SMSM in one of the examples.

The mapping relating the fine model parameters and frequency to the coarse model parameters and frequency is given by

$$[\boldsymbol{x}_c \quad \omega_c]^T = \boldsymbol{P}(\boldsymbol{x}_f, \omega) \tag{3-1}$$

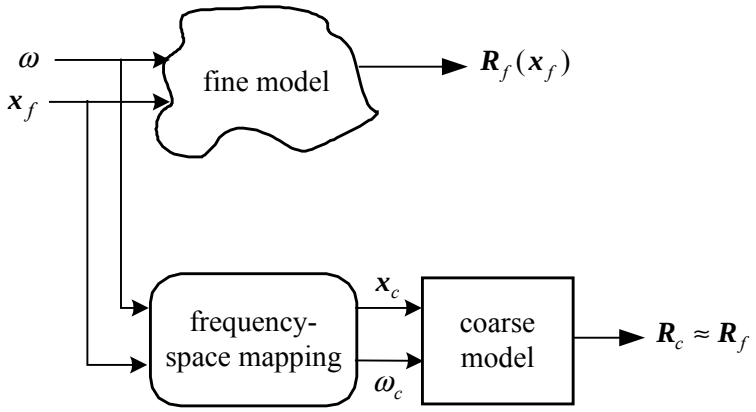

Fig. 3.1 The Frequency-Space Mapping Super Model (FSMSM) concept.

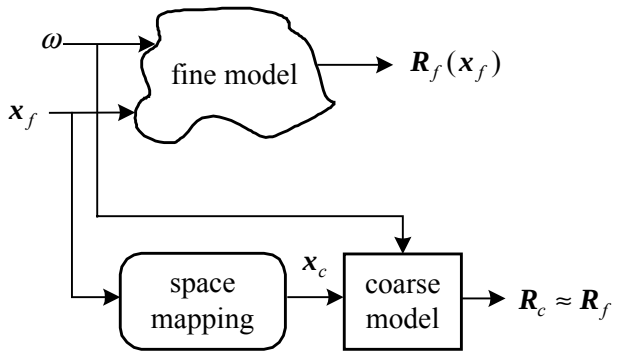

Fig. 3.2 The Space Mapping Super Model (SMSM) concept.

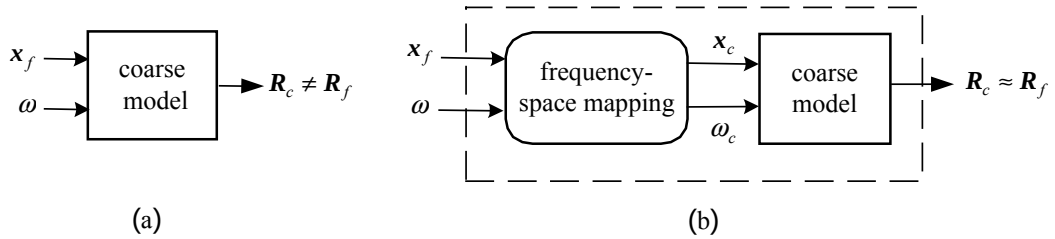

Fig. 3.3 The coarse model (a), and the enhanced coarse model (b).

or, in matrix form, assuming a linear mapping,

$$\begin{bmatrix} \boldsymbol{x}_c \\ \omega_c^{-1} \end{bmatrix} = \begin{bmatrix} \boldsymbol{c} \\ \delta \end{bmatrix} + \begin{bmatrix} \boldsymbol{B} & \boldsymbol{s} \\ \boldsymbol{t}^T & \sigma \end{bmatrix} \begin{bmatrix} \boldsymbol{x}_f \\ \omega^{-1} \end{bmatrix} \tag{3-2}$$

where $\boldsymbol{c}$, $\boldsymbol{s}$, $\boldsymbol{t} \in \Re^n$, $\boldsymbol{B} \in \Re^{nxn}$, δ, σ are the parameters characterizing the mapping $\boldsymbol{P}$. Notice that in (3-2) we map the inverse of the frequency (which is proportional to the wavelength) instead of the frequency itself. This has produced better results in all the models we considered than mapping the frequency directly. It can also be justified by the fact that in most microwave structures shrinking the structure would lead to a shift of its spectral characteristics to higher frequencies (shorter wavelengths).

The mapping parameters in (3-2) can be evaluated by solving the optimization

problem

$$\min_{\boldsymbol{c},\boldsymbol{B},\boldsymbol{s},\delta,\boldsymbol{t},\sigma} \left\| \begin{bmatrix} \boldsymbol{e}_1^T & \boldsymbol{e}_2^T & \cdots & \boldsymbol{e}_N^T \end{bmatrix}^T \right\| \tag{3-3}$$

subject to suitable constraints, where $\| \ \|$ is a suitable norm, N is the total number of fine model simulations and $\boldsymbol{e}_k$ is an error vector given by

$$\boldsymbol{e}_k = \boldsymbol{R}_f(\boldsymbol{x}_{f_i}, \omega_j) - \boldsymbol{R}_c(\boldsymbol{x}_c, \omega_c), \tag{3-4a}$$

$$\begin{bmatrix} \boldsymbol{x}_c & \omega_c \end{bmatrix}^T = \boldsymbol{P}(\boldsymbol{x}_{f_i}, \omega_j) \tag{3-4b}$$

with

$$i = 1, \cdots, B_p \tag{3-5a}$$

$$j = 1, \cdots, F_p \tag{3-5b}$$

$$k = j + (i-1)F_p \tag{3-5c}$$

where B_p is the number of base points and F_p is the number of frequency points per frequency sweep. The total number of fine model simulations is $N = B_p\ F_p$. The constraints we impose on the mapping parameters are that the mapping parameters should be as close as possible to the parameters corresponding to a unit mapping $\boldsymbol{x}_c = \boldsymbol{x}_f$ and $\omega_c = \omega$, which corresponds to $\boldsymbol{c} = \boldsymbol{0}$, $\boldsymbol{B} = \boldsymbol{I}$, $\boldsymbol{s} = \boldsymbol{0}$, $\delta = 0$, $\boldsymbol{t} = \boldsymbol{0}$, $\sigma = 1$. These constraints are justified by the fact that the coarse model embodies the physical characteristics of the fine model. Therefore, the optimum values of the mapping parameters should not severely deviate from the values corresponding to a unit mapping. To include these constraints, the optimization problem in (3-3) is modified as follows

$$\min_{\boldsymbol{c},\boldsymbol{B},\boldsymbol{s},\delta,\boldsymbol{t},\sigma} \left\| \begin{bmatrix} \boldsymbol{e}_1^T & \boldsymbol{e}_2^T \cdots \boldsymbol{e}_N^T & \boldsymbol{c}^T & \boldsymbol{s}^T & \boldsymbol{t}^T & \Delta\boldsymbol{b}_1^T & \Delta\boldsymbol{b}_2^T \cdots \Delta\boldsymbol{b}_n^T & \Delta\sigma & \delta \end{bmatrix}^T \right\| \tag{3-6}$$

where the error vectors $\boldsymbol{e}_1, \boldsymbol{e}_2, \cdots, \boldsymbol{e}_N$ are defined by (3-4a), the vectors

$\Delta \boldsymbol{b}_1,\ \Delta \boldsymbol{b}_2, \cdots,\ \Delta \boldsymbol{b}_n$ are the columns of the matrix $\Delta \boldsymbol{B}$ given by

$$\Delta \boldsymbol{B} = \boldsymbol{B} - \boldsymbol{I} \tag{3-7}$$

and $\Delta\sigma$ is defined by

$$\Delta\sigma = \sigma - 1 \tag{3-8}$$

The numerical values of the mapping parameters in (3-6) can give the designer physically-based intuitive information on the entire modeling process. The deviation of the optimal values of these parameters from those corresponding to a unit mapping indicates the degree of proximity between the coarse and fine model. This important feature can be used to compare two coarse models. The coarse model with less deviation should be more accurate. Let β be the deviation of the mapping parameters from the parameters corresponding to a unit mapping, that is

$$\beta = \left\| [\boldsymbol{c}^T\ \boldsymbol{s}^T\ \boldsymbol{t}^T\ \Delta \boldsymbol{b}_1^T\ \Delta \boldsymbol{b}_2^T \cdots \Delta \boldsymbol{b}_n^T\ \Delta\sigma\ \ \delta]^T \right\| \tag{3-9}$$

where $\Delta \boldsymbol{b}_1,\ \Delta \boldsymbol{b}_2, \cdots, \Delta \boldsymbol{b}_n$ and $\Delta\sigma$ are defined by (3-7) and (3-8), respectively. Therefore, based on the value of β, we can discriminate between various coarse models of the same device. The smaller the value of β the closer the coarse model is to the fine model. We will demonstrate this feature in one of the examples.

3.3 MULTIPLE SPACE MAPPING (MSM)

Multiple Space Mapping (MSM) was introduced in Bandler, Biernacki, Chen and Wang (1998). We present two variations of MSM for device modeling. We refer to them as MSM for Device Responses (MSMDR) and MSM for Frequency Intervals (MSMFI). In MSMDR we divide the device response vector $\boldsymbol{R}$ (in both models) into L

subsets of responses (or vectors) $\boldsymbol{R}_i, i = 1, 2, ..., L$. An individual mapping is established for each subset of responses as illustrated in Fig. 3.4. In MSMFI we divide the frequency range of interest into M intervals and evaluate a separate mapping for each interval, as illustrated in Fig. 3.5 (the switch in Fig. 3.5 is controlled by the frequency variable). The important questions are how we partition these responses into a set of sub-responses and how we divide the frequency range into a set of intervals. There was no guide in Bandler, Biernacki, Chen and Wang (1998) regarding answers to these questions. The following algorithms implement MSMDR and MSMFI.

3.3.1 MSMDR Algorithm

MSMDR algorithm divides the device responses in an iterative manner while establishing a separate mapping for each set of sub-responses. First it establishes a

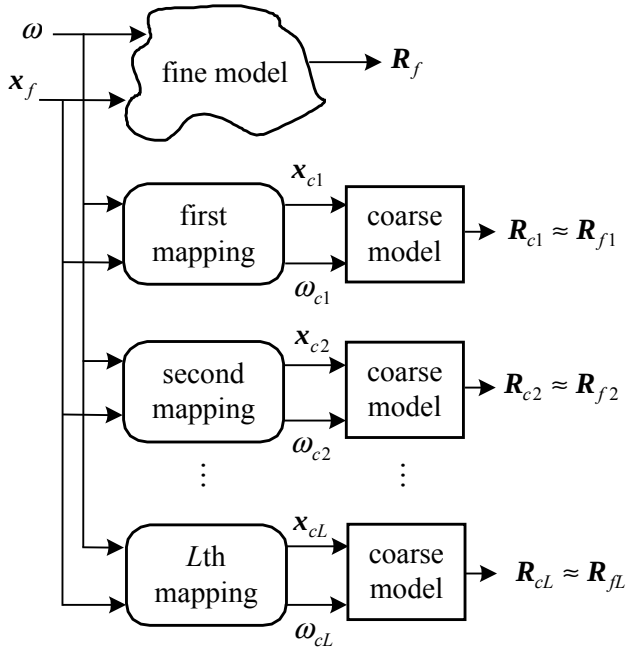

Fig. 3.4 The Multiple Space Mapping for Device Responses (MSMDR).

mapping targeting all responses. Then it assigns this mapping to the set of sub-responses satisfying a specified accuracy. It repeats the previous steps recursively on the remaining responses (which do not satisfy the required accuracy). The algorithm stops when all responses are exhausted. The following steps summarize the algorithm implementing MSMDR:

Step 1 Initialize i=1 and let $\boldsymbol{R}$ contain all responses.

Step 2 Establish a mapping $\boldsymbol{P}_i$, by solving (3-6), targeting all responses in $\boldsymbol{R}$.

Step 3 Assign the mapping $\boldsymbol{P}_i$ to the set of sub-responses $\boldsymbol{R}_i \subset \boldsymbol{R}$ that satisfies the error criteria $\left\| \boldsymbol{R}_{f_i} - \boldsymbol{R}_{c_i} \right\| \le \varepsilon$, where ε is a small positive number and $\boldsymbol{R}_{f_i}$, $\boldsymbol{R}_{c_i}$ are the fine and the coarse model sub-responses, respectively.

Step 4 Replace $\boldsymbol{R}$ by $\boldsymbol{R} - \boldsymbol{R}_i$ and increment i.

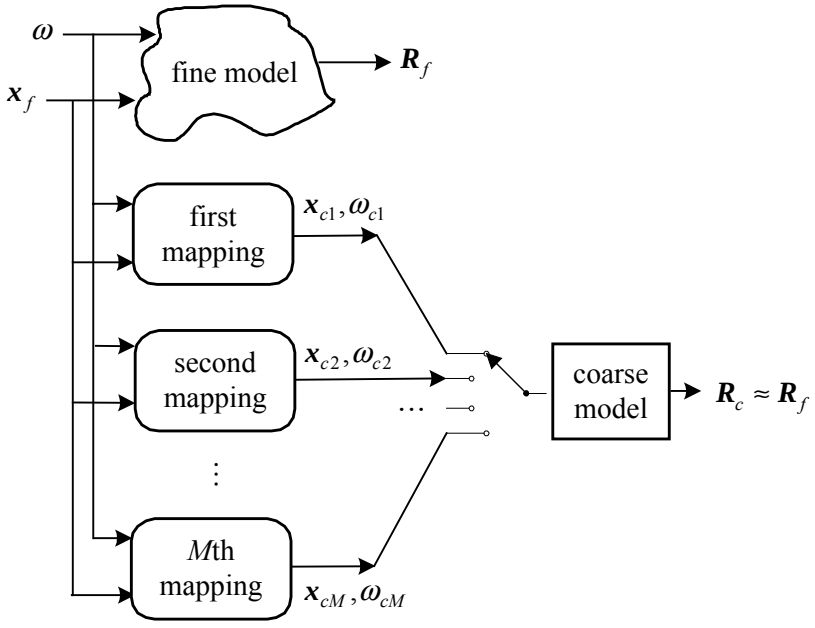

Fig. 3.5 The Multiple Space Mapping for Frequency Intervals (MSMFI).

Step 5 If $\boldsymbol{R}$ is not empty go to step 2, otherwise stop.

3.3.2 MSMFI Algorithm

MSMFI algorithm is similar to MSMDR algorithm. First the algorithm establishes a mapping targeting all set of responses $\boldsymbol{R}$ in the whole frequency range $\omega_{\min} \le \omega \le \omega_{\max}$. Then it assigns this mapping to the frequency interval $\omega_{\min} \le \omega \le \omega_{\mathrm{l}}$ (where ω_{l} belongs to the frequency range of interest) in which the set of responses $\boldsymbol{R}$ satisfies a certain specified accuracy. It repeats the previous steps recursively until covering the whole frequency range. The following steps summarize the MSMFI algorithm:

Step 1 Initialize *i*=1 and let the frequency interval $\Omega = [\omega_{\min}, \omega_{\max}]$.

Step 2 Establish a mapping $\boldsymbol{P}_i$, by solving (3-6), in the frequency range defined by Ω.

Step 3 Assign the mapping $\boldsymbol{P}_i$ to the frequency interval $\Omega_i \subset \Omega$ in which the error criteria $\left\| \boldsymbol{R}_f - \boldsymbol{R}_c \right\| \le \varepsilon$ is satisfied, where ε is a small positive number and $\boldsymbol{R}_f$, $\boldsymbol{R}_c$ are the fine and the coarse model responses, respectively.

Step 4 Replace Ω by $\Omega - \Omega_i$ and increment *i*.

Step 5 If Ω is not empty go to step 2, otherwise stop.

The validity of the algorithm is based on the assumption that the error between the coarse and fine model response is monotonically increasing with frequency. We have to emphasize that both MSMFI and MSMDR cost the same number of fine model simulations (EM simulations) required to establish a single mapping for the whole frequency range. However, they can dramatically enhance the coarse model, as we will see in the examples.

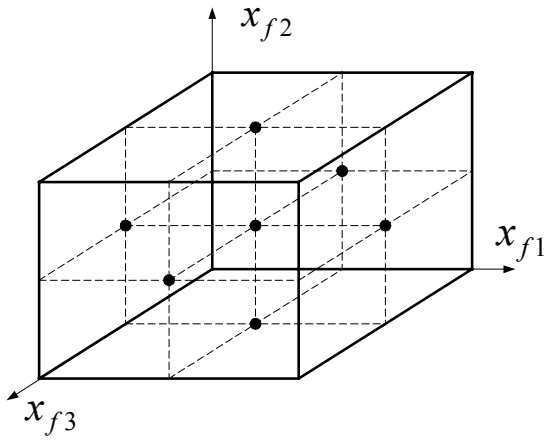

Fig. 3.6 Distribution of the base points in the region of interest for a 3-dimensional space.

3.4 IMPLEMENTATION OF GSM

The optimization problem in (3-6) is solved using the Huber optimizer (Bandler, Chen, Biernacki, Gao, Madsen and Yu 1993a and 1993b), implemented in OSA90/hope™. The set of base points $\{\boldsymbol{x}_{f_i}, i = 1, 2, ..., B_p\}$ in the region of interest is taken as in Fig. 3.6 (Biernacki, Bandler, Song and Zhang 1989). According to this distribution the number of base points is $2n+1$, where n is the number of fine model parameters. The starting values for the mapping parameters $\boldsymbol{c}$, $\boldsymbol{B}$, $\boldsymbol{s}$, δ, $\boldsymbol{t}$, σ are $\mathbf{0}$, $\boldsymbol{I}$, $\mathbf{0}$, 0, $\mathbf{0}$, 1, respectively, which correspond to the unit mapping $\boldsymbol{x}_c = \boldsymbol{x}_f$ and $\omega_c = \omega$. The software tools needed for the implementation of GSM are an optimizer (the Huber optimizer is recommended), a suitable circuit simulator which can handle simple matrix operations and a suitable full-wave EM simulator.

3.5 EXAMPLES

We present four typical modeling problems: a microstrip line, a microstrip right angle bend, a microstrip step junction and a microstrip shaped T-junction. To display the results in a compact way we define the error E_{ij} as the modulus of the difference between the scattering parameter S_{ij}^f computed by the fine model and the scattering parameter S_{ij}^c computed by the coarse model

$$E_{ij} = \left| S_{ij}^f - S_{ij}^c \right| = \sqrt{(\mathrm{Re}[S_{ij}^f] - \mathrm{Re}[S_{ij}^c])^2 + (\mathrm{Im}[S_{ij}^f] - \mathrm{Im}[S_{ij}^c])^2} \tag{3-10}$$

where i=1,2,..., N_p and j=1, 2,..., N_p (N_p is the number of ports of the microwave device). The error E_{ij} is a measure of both the error in the magnitude and the phase of the scattering parameters S_{ij}^c. We refer to E_{ij} simply as the error in the scattering parameter S_{ij}.

3.5.1 Microstrip Line

In this example, we compare SMSM and FSMSM. Both modeling approaches are used to enhance the transmission line model of a microstrip line. The fine model is analyzed by Sonnet's ***em***™ (***em*** 1997) and the "coarse" model is a built-in element of OSA90/hope™. The fine and coarse models are shown in Fig. 3.7. The structure in Fig. 3.7(a) is parameterized using Geometry Capture by Bandler, Biernacki and Chen (1996 and 1999) implemented in Empipe™ (Empipe 1997).

The fine and coarse model parameters are given by

$$\boldsymbol{x}_f = [L\ W\ H\ \varepsilon_r]^T,\ \boldsymbol{x}_c = [L_c\ W_c\ H_c\ \varepsilon_{rc}]^T$$

The region of interest is given in TABLE 3.1. The frequency range is 20 GHz to 30 GHz

with a step of 2 GHz (F_p = 6). The characteristic impedance Z_0 of the transmission line is computed in terms of the width W_c, the substrate height H_c and the relative dielectric constant ε_{rc} using the quasi-static model in Pozar (1990). Only 9 points (B_p = 9) in the region of interest were used to develop SMSM or FSMSM.

We developed SMSM and FSMSM for the microstrip line and the corresponding mapping parameters for each case are given in TABLE 3.2. Notice that in the case of SMSM the mapping parameters $\boldsymbol{s}, \delta, \boldsymbol{t}, \sigma$ are fixed and in the case of FSMSM the computed value of $\boldsymbol{t}$ is $\mathbf{0}$, which means that the coarse model frequency does not depend on the fine model parameters (it only depends on the fine model frequency). The microstrip transmission line SMSM and FSMSM is tested at 50 uniformly distributed random points in the region of interest. The error in S_{21} defined by (3-10) for the microstrip transmission line model is shown in Fig. 3.8(a). Fig. 3.8(b) and (c) show the error in S_{21} by the microstrip transmission line SMSM and by the microstrip transmission line FSMSM, respectively. The error of the microstrip transmission line FSMSM is approximately 4 times less than the corresponding error of the microstrip transmission line SMSM. The time taken by the EM solver and by the Huber optimizer is 90 s and 30 s, respectively, on an HP C200-RISC workstation.

TABLE 3.1

REGION OF INTEREST FOR THE
MICROSTRIP TRANSMISSION LINE

Parameter	Minimum value	Maximum value
W	20 mil	30 mil
H	8 mil	16 mil
ε_r	8	10

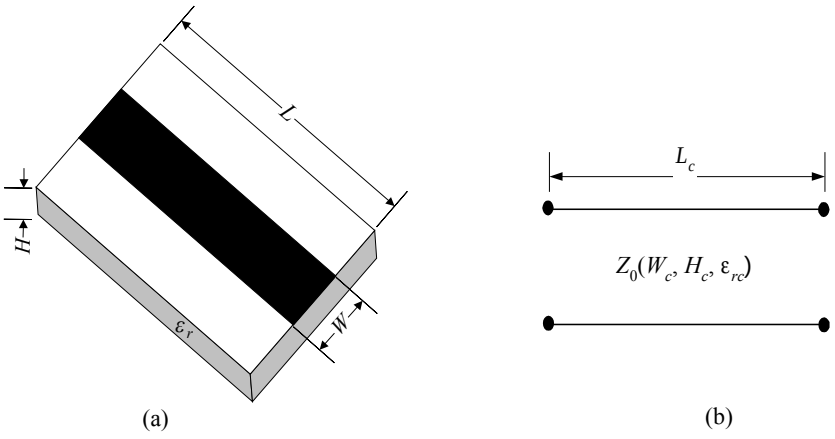

Fig. 3.7 Microstrip line models: (a) the fine model; (b) the coarse model.

TABLE 3.2

THE SMSM AND FSMSM MAPPING PARAMETERS
FOR THE MICROSTRIP TRANSMISSION LINE

	SMSM	FSMSM
$\boldsymbol{B}$	$\begin{bmatrix} 1.015 & -0.002 & -0.007 & -0.022 \\ -0.001 & 0.992 & 0.020 & 0.023 \\ -0.008 & 0.001 & 0.985 & 0.027 \\ 0.009 & -0.004 & 0.044 & 1.028 \end{bmatrix}$	$\begin{bmatrix} 1.026 & -0.005 & 0.006 & -0.021 \\ -0.009 & 0.965 & -0.011 & 0.017 \\ -0.002 & 0.004 & 0.979 & 0.022 \\ 0.019 & -0.001 & 0.020 & 1.025 \end{bmatrix}$
$\boldsymbol{c}$	$[-0.011 \quad -0.008 \quad 0.012 \quad -0.036]^T$	$[-0.013 \quad 0.001 \quad 0.011 \quad -0.010]^T$
$\boldsymbol{s}$	$\mathbf{0}$ (fixed)	$[-0.006 \quad 0 \quad 0.002 \quad -0.002]^T$
$\boldsymbol{t}$	$\mathbf{0}$ (fixed)	$\mathbf{0}$
σ	1 (fixed)	1.035
δ	0 (fixed)	0.001

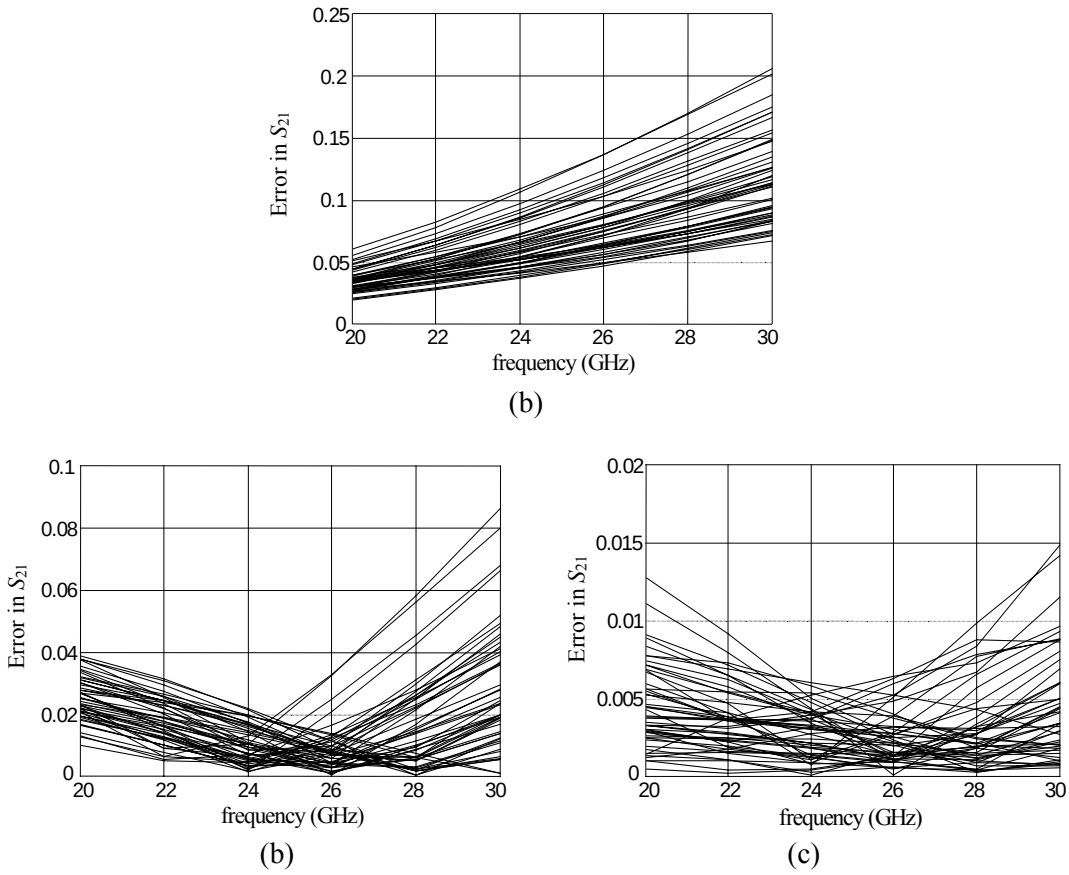

Fig. 3.8 Error in S_{21} with respect to ***em***™: (a) by the microstrip transmission line model; (b) by the microstrip transmission line SMSM; (c) by the microstrip transmission line FSMSM.

3.5.2 Microstrip Right Angle Bend

In this example, we compare two coarse models for the microstrip right angle bend in Fig. 3.9(a). The first coarse model is taken from Gupta, Garg and Bahl (1979) and is referred to as Gupta's model. The second coarse model is taken from Kirschning, Jansen and Koster (1983) and is referred to as Jansen's model. Both coarse models provide empirical formulas for the LC circuit in Fig. 3.9(b). The fine model is analyzed

by Sonnet's ***em***™ (***em*** 1997). The fine and coarse model parameters are given by

$$\boldsymbol{x}_f = [W\ H\ \varepsilon_r]^T,\ \boldsymbol{x}_c = [W_c\ H_c\ \varepsilon_{rc}]^T$$

The region of interest is given in TABLE 3.3. The frequency range is 1 GHz to 31 GHz with a step of 2 GHz (F_p = 16). The number of base points in the region of interest is 7 (B_p = 7).

The FSMSM was developed for the two coarse models. The corresponding mapping parameters are given in TABLE 3.4. The enhanced Gupta model and the enhanced Jansen model were tested at 50 random points in the region of interest. The error in S_{11} by Gupta's model and by Jansen's model are shown in Fig. 3.10. The error in S_{11} by the enhanced Gupta model and by the enhanced Jansen model are shown in Fig. 3.11.

It is difficult to compare the two coarse models since Jansen's model is slightly more accurate at lower frequencies (see Fig. 3.10) and Gupta's model is slightly more accurate at higher frequencies. However, after developing FSMSM for each coarse model we can compare the two coarse models according to the criteria in Section 3.2. The values of β given by (3-9) for the enhanced Gupta model and for the enhanced Jansen model are 3.4 and 3.5, respectively. We notice that the value of β in both cases is approximately the same, which means that the accuracy of both coarse models with respect to the fine model is comparable. The time taken by the EM solver and by the Huber optimizer is 6 min and 40 s, respectively, on an HP C200-RISC workstation.

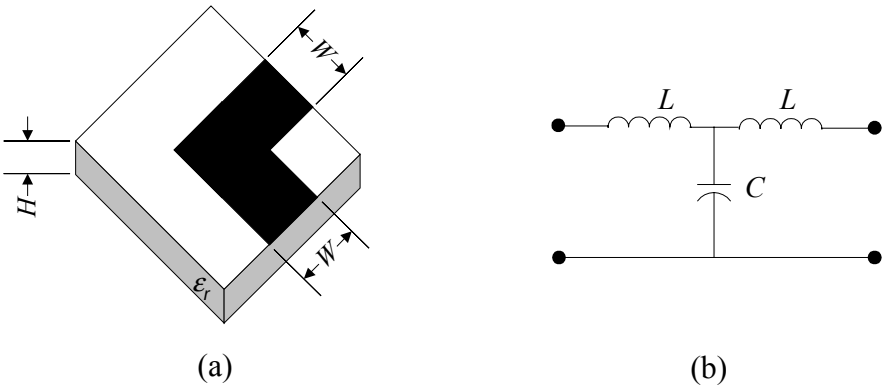

Fig. 3.9 Microstrip right angle bend: (a) the fine model; (b) the coarse model.

TABLE 3.3

REGION OF INTEREST FOR THE MICROSTRIP RIGHT ANGLE BEND

Parameter	Minimum value	Maximum value
W	20 mil	30 mil
H	8 mil	16 mil
ε_r	8	10

TABLE 3.4

THE FSMSM MAPPING PARAMETERS FOR
THE MICROSTRIP RIGHT ANGLE BEND

	Gupta's model	Jansen's model
$\boldsymbol{B}$	$\begin{bmatrix} 1.291 & 0.207 & 0.189 \\ 0.067 & 0.613 & -0.094 \\ 0.092 & -0.066 & 0.918 \end{bmatrix}$	$\begin{bmatrix} 2.768 & 0.314 & 0.276 \\ -0.042 & 1.282 & 0.318 \\ -0.018 & -0.013 & 0.421 \end{bmatrix}$
$\boldsymbol{c}$	$[0.094 \quad -0.174 \quad 0.123]^T$	$[0.048 \quad -0.012 \quad 0.031]^T$
$\boldsymbol{s}$	$[0.109 \quad -0.296 \quad 0.183]^T$	$[0.001 \quad -0.053 \quad 0.250]^T$
$\boldsymbol{t}$	$[-0.001 \quad -0.002 \quad -0.002]^T$	$[-0.001 \quad -0.002 \quad -0.001]^T$
σ	3.269	2.343
δ	0.019	0.015

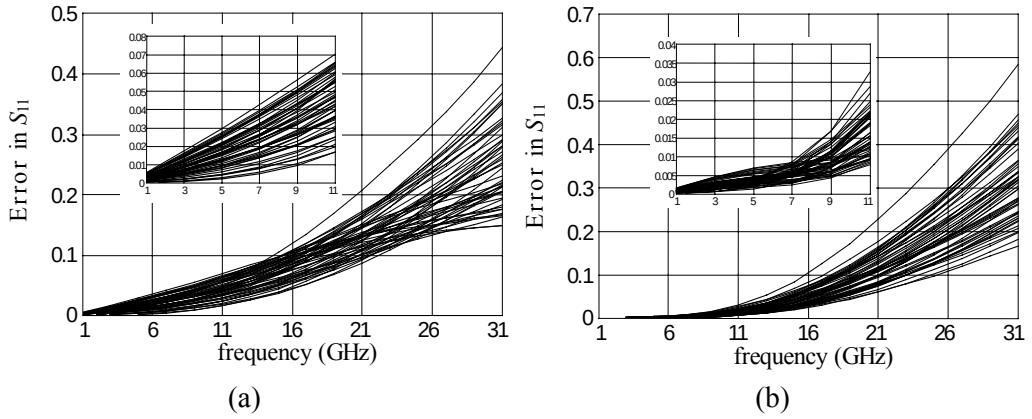

Fig. 3.10 Error in S_{11} of the microstrip right angle bend with respect to ***em***™: (a) by Gupta's model; (b) by Jansen's model.

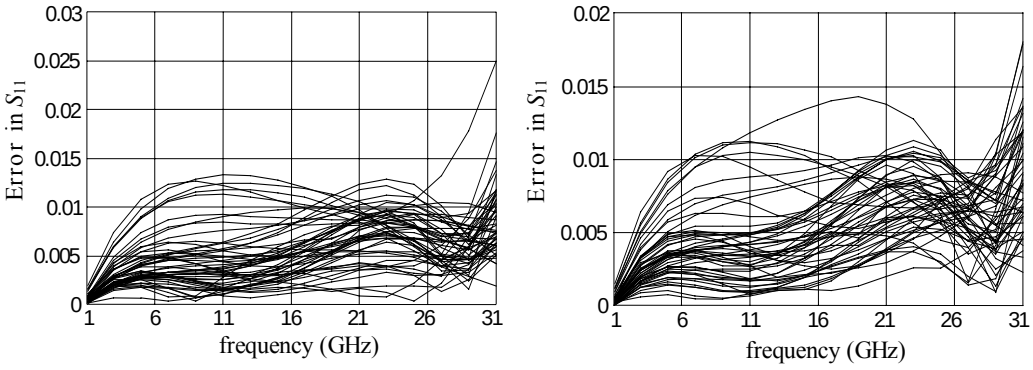

Fig. 3.11 Error in S_{11} of the microstrip right angle bend with respect to ***em***™: (a) by the enhanced Gupta model; (b) by the enhanced Jansen model.

3.5.3 Microstrip Step Junction

In this example, we demonstrate the MSMDR. The fine model of the microstrip step junction (Fig. 3.12) is analyzed by Sonnet's ***em***™ (***em*** 1997). The "coarse" model is a built-in element of OSA90/hope™. The fine and coarse model parameters are given by

$$\boldsymbol{x}_f = [W_1\ W_2\ H\ \varepsilon_r\ ]^T,\ \boldsymbol{x}_c = [W_{1c}\ W_{2c}\ H_c\ \varepsilon_{rc}\ ]^T$$

The region of interest is given in TABLE 3.5. The frequency range is 2 GHz to 40 GHz with a step of 2 GHz (F_p = 20). The number of base points in the region of interest is 9 (B_p = 9). There are six responses to be matched: the real and imaginary parts of S_{11}, S_{21} and S_{22}. We will show that one mapping targeting all these responses is not sufficient to achieve the required accuracy at the base points. The required accuracy is $E_{ij} \le 0.03$, i=1, 2 and j= 1, 2, where E_{ij} is defined by (3-10). Fig. 3.13(a) shows the error in S_{11} before applying any modeling technique while Fig. 3.13(b) shows it after developing a single mapping for all responses. We notice that the results obtained by a single mapping

do not satisfy the required accuracy.

The MSMDR algorithm (in Section 3.3.1) was applied to align the two models. The algorithm partitioned the responses into two groups {Im[S_{11}], Im[S_{21}], Im[S_{22}], Re[S_{21}])} and {Re[S_{11}], Re[S_{22}]} and developed a separate mapping for each group of responses. The corresponding mapping parameters for each group are given in TABLE 3.6. Fig. 3.13(c) shows the error in S_{11} at the base points after applying the MSMDR algorithm. We notice that the specified accuracy is achieved. The enhanced coarse model of the step junction was tested at 50 uniformly distributed random points. The errors in S_{11} and S_{21} by the coarse model are shown in Fig. 3.14(a) and (b), respectively. The errors in S_{11} and S_{21} by the enhanced coarse model are shown in Fig. 3.15(a) and (b), respectively.

The histograms of the error in S_{21} at 40 GHz (which is the maximum error in the frequency range 2 GHz to 40 GHz) by the coarse model and by the enhanced coarse model are shown in Fig. 3.16(a) and (b), respectively. The mean and standard deviation for the two cases are also shown in Fig. 3.16(a) and (b). The time taken by the EM solver and by the Huber optimizer is 19 min and 2.5 min, respectively, on an HP C200-RISC workstation.

TABLE 3.5

REGION OF INTEREST FOR THE MICROSTRIP STEP JUNCTION

Parameter	Minimum value	Maximum value
W_1	20 mil	40 mil
W_2	10 mil	20 mil
H	10 mil	20 mil
ε_r	8	10

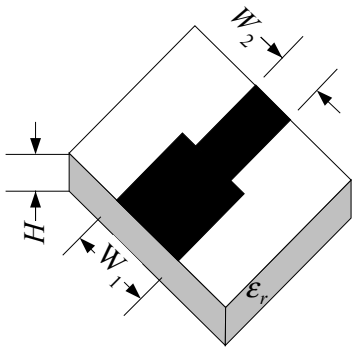

Fig. 3.12 Microstrip step junction.

TABLE 3.6

THE MSMDR MAPPING PARAMETERS FOR THE MICROSTRIP STEP JUNCTION

	Target responses are {Im[S_{11}], Im[S_{21}], Im[S_{22}], Re[S_{21}])}	Target responses are {Re[S_{11}], Re[S_{22}]}
$\boldsymbol{B}$	$\begin{bmatrix} 0.764 & 0.033 & -0.062 & 0.074 \\ 0.191 & 0.632 & 0.255 & -0.502 \\ -0.023 & 0.116 & 1.485 & 0.018 \\ 0.676 & -0.365 & -0.111 & 0.177 \end{bmatrix}$	$\begin{bmatrix} 3.071 & -0.008 & -0.010 & -0.004 \\ 0.008 & 0.202 & 0.032 & 0.004 \\ -0.001 & 0.001 & 1.152 & 0.000 \\ -0.077 & -0.118 & -0.002 & 1.241 \end{bmatrix}$
$\boldsymbol{c}$	$[0.002 \quad -0.002 \quad 0.002 \quad -0.006]^T$	$[-0.001 \quad 0.001 \quad 0.000 \quad -0.003]^T$
$\boldsymbol{s}$	$[-0.003 \quad 0.004 \quad -0.001 \quad -0.002]^T$	$\mathbf{0}$
$\boldsymbol{t}$	$[-0.001 \quad 0.000 \quad -0.005 \quad 0.000]^T$	$[-0.001 \quad 0.000 \quad -0.007 \quad 0.003]^T$
σ	1.546	5.729
δ	0.113	0.065

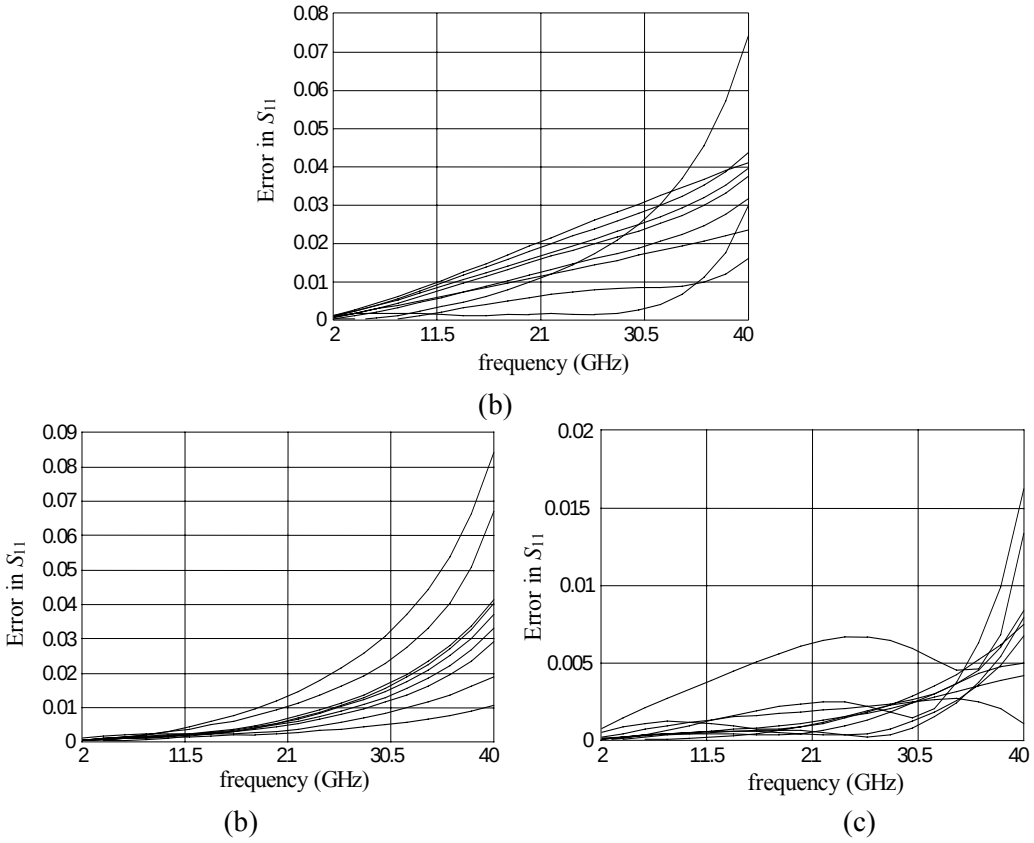

Fig. 3.13 Error in S_{11} of the microstrip step junction with respect to ***em***™: (a) before applying any modeling technique; (b) after applying FSMSM; (c) after applying the MSMDR algorithm.

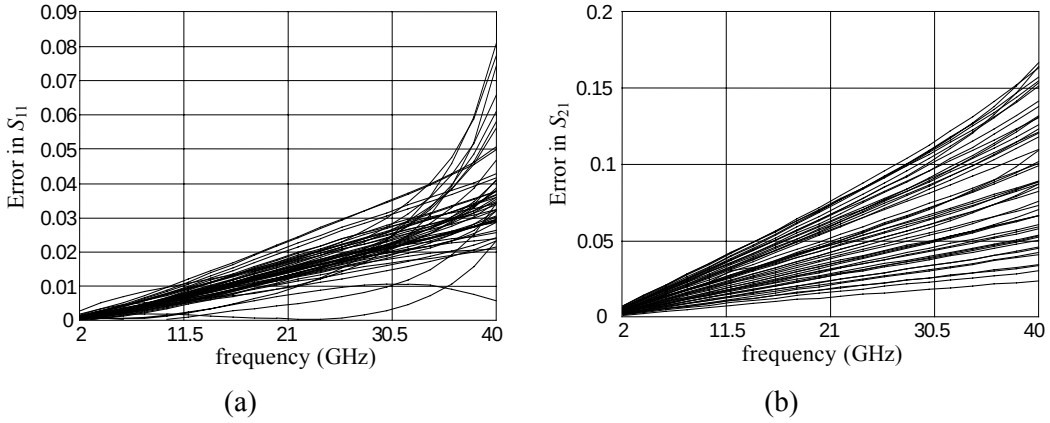

Fig. 3.14 Error of the microstrip step junction coarse model with respect to ***em***™: (a) in S_{11}; (b) in S_{21}.

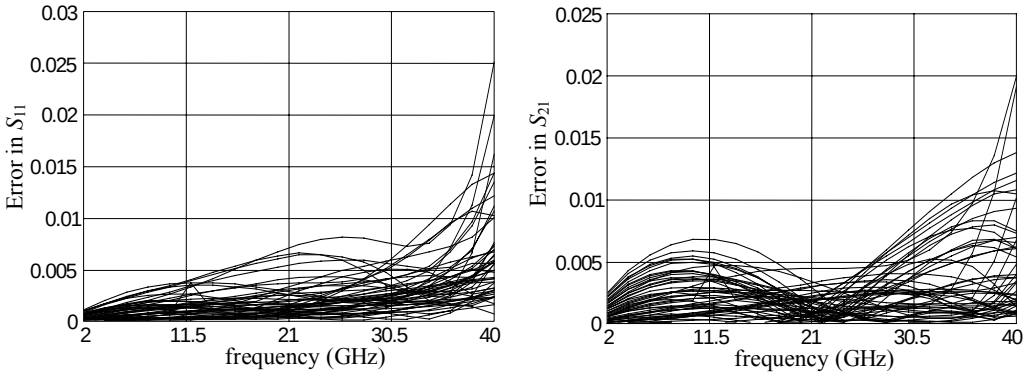

(a) (b)

Fig. 3.15 Error of the microstrip step junction enhanced coarse model with respect to ***em***™: (a) in S_{11}; (b) in S_{21}.

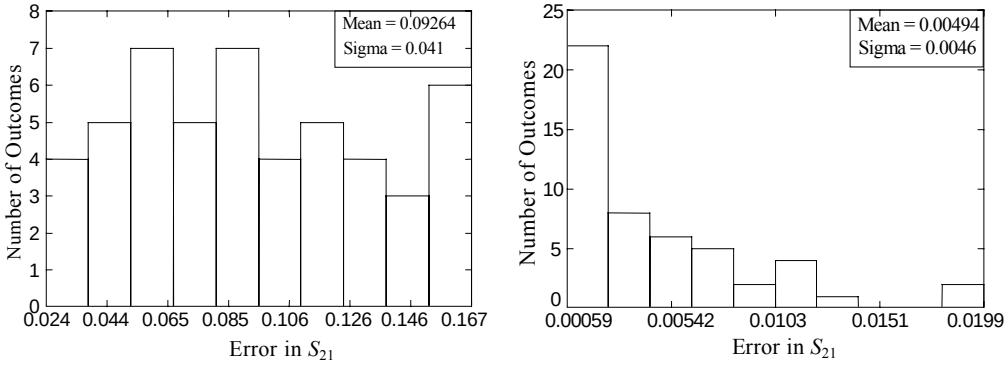

(a) (b)

Fig. 3.16 Histogram of the error in S_{21} of the microstrip step junction for 50 points in the region of interest at 40 GHz: (a) by the coarse model; (b) by the enhanced coarse model.

3.5.4 Microstrip Shaped T-Junction

In this example, we consider a shaped T-junction (Fig. 3.17(a)). This T-junction was introduced in Dydyk (1977) to compensate discontinuities. It was recently compared in Bandler, Bakr, Georgieva, Ismail and Swanson (1999) with the other T-junction

configurations in the literature. The T-junction is symmetric in the sense that all input lines have the same width w. The fine model is analyzed by Sonnet's ***em***™ (***em*** 1997) and the coarse model is composed of empirical models of simple microstrip elements (see Fig. 3.17b) of OSA90/hope™. The fine and coarse model parameters are given by

$$\boldsymbol{x}_f = [\, w \;\; h \;\; w_1 \;\; w_2 \;\; x \;\; y \;\; \varepsilon_r \,]^T, \quad \boldsymbol{x}_c = [\, w_c \;\; h_c \;\; w_{1c} \;\; w_{2c} \;\; x_c \;\; y_c \;\; \varepsilon_{cr} \,]^T .$$

The region of interest is given in TABLE 3.7 and the frequency range used is 2 GHz to 20 GHz with a step of 2 GHz (F_p = 10). The width w of the input lines is determined in terms of h and ε_r so that the characteristic impedance of the input lines is

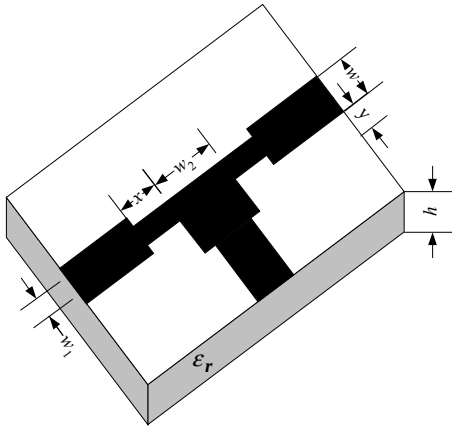

(a)

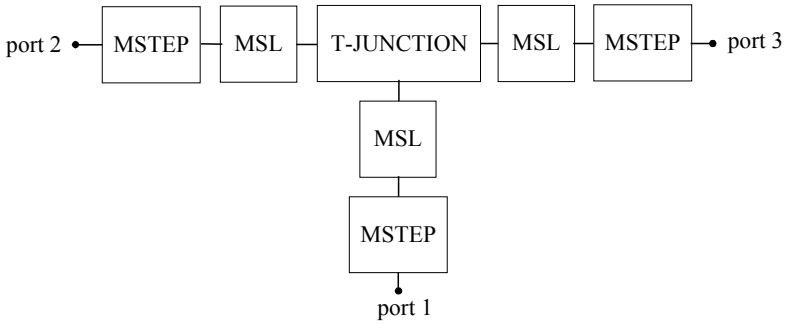

(b)

Fig. 3.17 Microstrip shaped T-junction: (a) the physical structure (fine model); (b) the coarse model.

50 ohm. The width w_1 is taken as 1/3 of the width w. The width w_2 is obtained so that the characteristic impedance of the microstrip line after the step connected to port 2 is twice the characteristic impedance of the microstrip line after the step connected to port 1 (see Fig. 3.17b). The number of base points in the region of interest is 9 ($B_p = 9$).

The MSMFI algorithm (in Section 3.3.2) was applied to enhance the accuracy of the T-Junction coarse model. The algorithm partitioned the total frequency range into two intervals: 2 GHz to 16 GHz and 16 GHz to 20 GHz. The corresponding mapping parameters for each interval are given in TABLE 3.8. Fig. 3.18(a) and (b) show $|S_{11}|$ and $|S_{22}|$ by Sonnet's ***em***™ (***em*** 1997), the T-junction coarse model and the T-junction enhanced coarse model at two test points in the region of interest. To perform a more comprehensive test, 50 random points are generated in the region of interest. The coarse model errors in S_{11} and in S_{22} defined by (3-10) are shown in Fig. 3.19(a) and (b), respectively. The enhanced coarse model errors in S_{11} and in S_{22} are shown in Fig. 3.20(a) and (b), respectively. The time taken by the EM solver and by the Huber optimizer is 11 min and 23 min, respectively, on an HP C200-RISC workstation.

TABLE 3.7

REGION OF INTEREST FOR THE MICROSTRIP SHAPED T-JUNCTION

Parameter	Minimum value	Maximum value
h	15 mil	25 mil
x	5 mil	10 mil
y	15 mil	25 mil
ε_r	8	10

The enhanced coarse model for the shaped T–Junction can be utilized in optimization. For example, the T-junction is optimized to achieve the minimum possible mismatch at the three ports. The optimization variables are x and y, the other parameters are kept fixed (w = 24 mil, h = 25 mil and $\varepsilon_r = 9.9$) (see Bandler, Bakr, Georgieva, Ismail and Swanson 1999). The specifications are

$$|S_{11}| \le 1/3, \quad |S_{22}| \le 1/3 \text{ for } 2 \text{ GHz} \le \omega \le 20 \text{ GHz}$$

The minimax optimizer in OSA90/hope™ reached the solution x = 4.31 mil and y = 19.77 mil. The magnitude of S_{11} and S_{22} obtained by Sonnet's ***em***™ (***em*** 1997), the coarse model and the enhanced coarse model are shown in Fig. 3.21(a) and (b). We notice a good agreement between the results obtained by the enhanced coarse model and by Sonnet's ***em***™ (***em*** 1997).

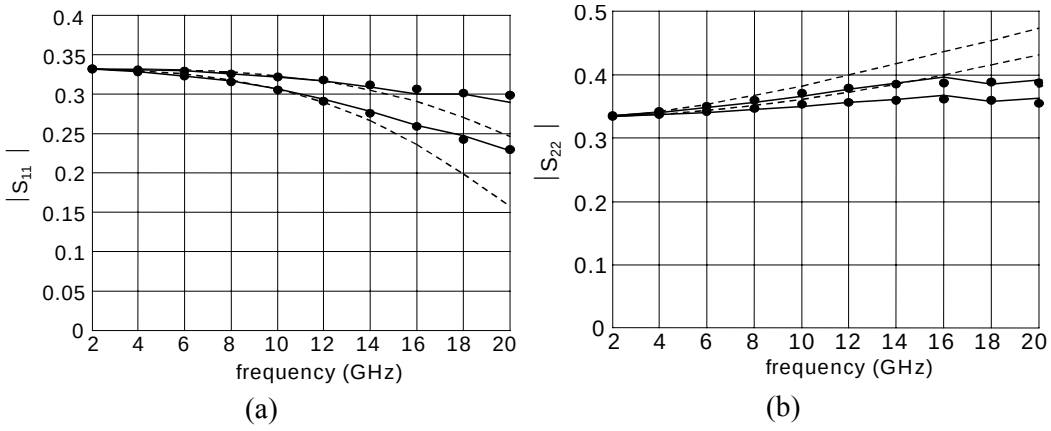

Fig. 3.18 Responses of the shaped T-Junction at two test points in the region of interest by ***em***™ (•), by the coarse model (---) and by the enhanced coarse model (—): (a) $|S_{11}|$; (b) $|S_{22}|$.

TABLE 3.8

THE MSMFI MAPPING PARAMETERS
FOR THE MICROSTRIP SHAPED T-JUNCTION

	2 GHz to 16 GHz	16 GHz to 20 GHz
$\boldsymbol{B}$	$\begin{bmatrix} 1.12 & 0.09 & 0.04 & 0.16 & 0.00 & -0.04 & 0.19 \\ 0.02 & 0.78 & 0.00 & -0.15 & -0.33 & -0.02 & 0.24 \\ 0.10 & 0.17 & 1.04 & 0.20 & -0.31 & -0.08 & -0.07 \\ -0.06 & 0.10 & -0.02 & 1.00 & 0.15 & -0.07 & -0.34 \\ 0.04 & 0.01 & 0.01 & 0.04 & 1.07 & -0.08 & -0.11 \\ -0.13 & -0.13 & -0.04 & -0.21 & 0.21 & 0.98 & 0.54 \\ -0.07 & 0.10 & -0.02 & -0.02 & -0.15 & 0.00 & 0.59 \end{bmatrix}$	$\begin{bmatrix} 0.99 & 0.04 & -0.00 & 0.02 & -0.02 & -0.04 & 0.06 \\ 0.05 & 0.86 & 0.02 & -0.06 & -0.22 & 0.06 & 0.00 \\ -0.01 & 0.14 & 0.99 & 0.08 & -0.26 & -0.08 & 0.04 \\ -0.10 & -0.07 & -0.03 & 0.88 & 0.11 & -0.06 & -0.21 \\ 0.1 & 0.03 & 0.03 & 0.11 & 1.09 & 0.02 & -0.13 \\ -0.13 & -0.02 & -0.04 & -0.13 & 0.24 & 1.07 & 0.25 \\ -0.13 & 0.20 & -0.04 & 0.01 & -0.1 & 0.01 & 0.92 \end{bmatrix}$
$\boldsymbol{c}$	$[0.02 \quad 0.04 \quad -0.01 \quad -0.05 \quad -0.01 \quad 0.06 \quad -0.09]$	$[0.01 \quad 0.01 \quad -0.01 \quad -0.03 \quad -0.01 \quad 0.02 \quad -0.03]^T$
$\boldsymbol{s}$	$[-0.04 \quad 0.29 \quad -0.18 \quad -0.04 \quad 0.06 \quad -0.05 \quad -0.50]$	$[0.00 \quad 0.01 \quad -0.01 \quad 0.00 \quad 0.00 \quad 0.00 \quad -0.02]^T$
$\boldsymbol{t}$	$\mathbf{0}$	$[0.01 \quad 0.00 \quad -0.02 \quad 0.00 \quad 0.00 \quad 0.00 \quad 0.00]^T$
σ	0.64	0.966
δ	–0.008	–0.004

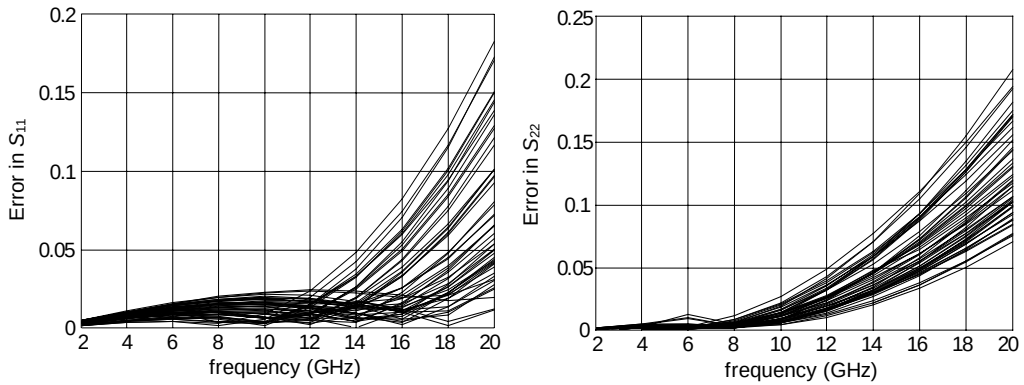

(a) (b)

Fig. 3.19 Error of the shaped T-Junction coarse model with respect to ***em***™: (a) in S_{11}; (b) in S_{22}.

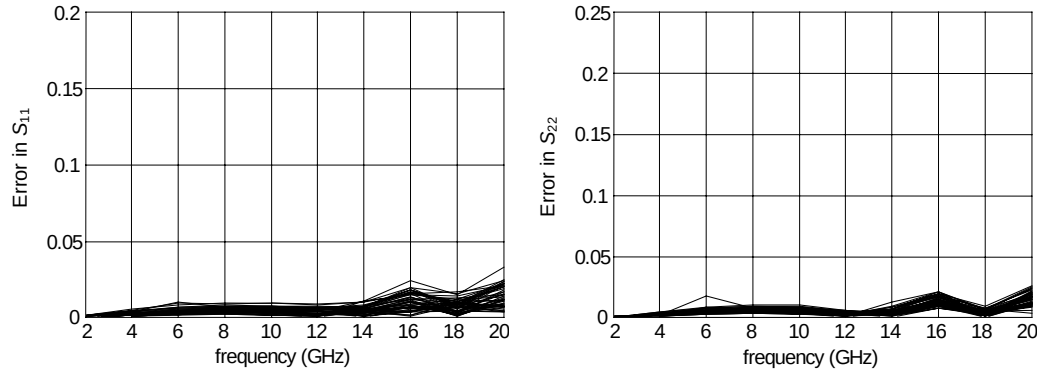

(a) (b)

Fig. 3.20 Error of the shaped T-Junction enhanced coarse model with respect to ***em***™: (a) in S_{11}; (b) in S_{22}.

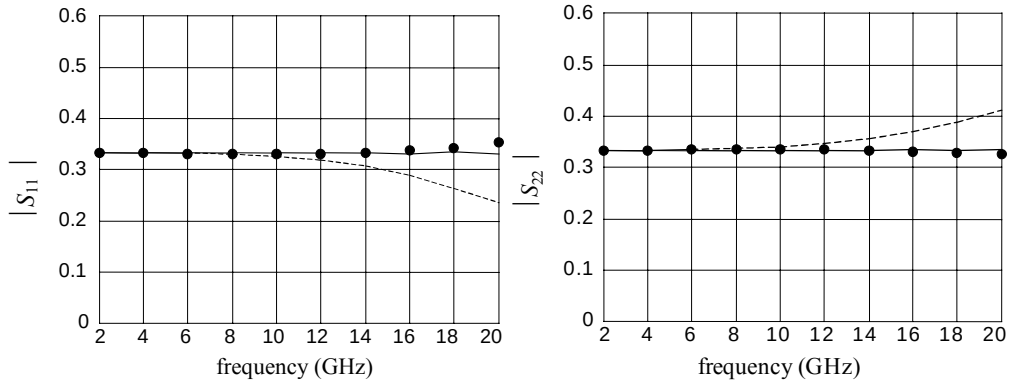

Fig. 3.21 Responses of the optimum shaped T-Junction by ***em***™ (•), by the coarse model (---) and by the enhanced coarse model (—): (a) $|S_{11}|$; (b) $|S_{22}|$.

3.6 CONCLUDING REMARKS

We have proposed the Generalized Space Mapping (GSM) approach to microwave device modeling. It is used to enhance the accuracy of existing empirical models. Three derivative concepts have been illustrated: the SMSM concept, the FSMSM concept and the MSM concept. Two variations of MSM have been presented: MSMDR and MSMFI. Our approach typically uses only a few EM simulations to dramatically enhance the accuracy of existing empirical device models.

GSM involves only simple matrix operations, which makes it an effective CAD tool in terms of CPU time, memory requirement, ease of use and accuracy. It also preserves the compactness and simplicity of the original empirical models. We have applied the GSM approach to some modeling problems, a microstrip line, a microstrip right angle bend, a microstrip step junction and a microstrip shaped T-junction, yielding remarkable improvement within the regions of interest.

Chapter 4

BROADBAND MODELING OF MICROWAVE PASSIVE DEVICES THROUGH FREQUENCY MAPPING

4.1 INTRODUCTION

We present a new computer-aided modeling methodology to develop physics-based empirical models for microwave passive components. We integrate in a coherent way EM simulators, artificial neural networks, multivariable rational functions, dimensional analysis and frequency mapping to establish models valid over broad frequency ranges. We consider frequency-independent empirical models (FIEM) and frequency-dependent empirical models (FDEM). In the FDEM we use the frequency mapping approach (Bandler, Biernacki, Chen, Hemmers and Madsen 1995 and Bandler, Ismail, Rayas-Sánchez and Zhang 1999) which implicitly introduces frequency dependency into the model elements. We also exploit the odd property of the frequency mapping, that is the transformed frequency must be an odd function of the original

frequency. Artificial neural networks or rational functions are used to approximate these elements as well as the frequency mapping. Rational functions enable us to transform a simple FDEM to an equivalent FIEM. This transformation can be expedited by impedance synthesis (Temes and Lapatra 1977), as we will see in the examples. The passivity of the FDEMs is also considered. Dimensional analysis (Middendorf 1986 and Watson, Mah and Liou 1999) determines the functionality of the model elements and the frequency mapping on the geometrical and physical parameters of the components. It also reduces the amount of training data required in the approximation process. The data required to develop the empirical models is obtained by accurate but time intensive full-wave EM simulators ("fine" models: see Chapter 2).

Equivalent circuits can be obtained from the literature or can be visualized by microwave engineers through their understanding and expertise of microwave components. We believe that, though simple, they have advantages over black-box modeling of microwave components since they embody physical characteristics (at least at low frequencies) of the actual components. A shortcoming is that those equivalent circuits may fail to give good accuracy at high frequencies due to dispersion. We address dispersive effects by introducing frequency dependency into the elements of the equivalent circuits.

We start the chapter by describing the process of creating FIEMs and FDEMs. Then we discuss some useful properties of the frequency mapping. Next we consider the transformation from FDEMs into FIEMs as well as the passivity conditions of the FDEMs. Multivariable rational functions are also described. Finally, we consider various modeling examples, including a microstrip right angle bend, a microstrip via, a microstrip double-step junction (to be used as a basic element of constructing a model for

nonuniform or tapered microstrip transmission lines) and a CPW step junction.

4.2 FREQUENCY INDEPENDENT EMPIRICAL MODELS (FIEM)

Consider a microwave component modeled by a fine model (typically a full-wave EM simulator) and a circuit model (empirical model). We assume that the topology of the equivalent circuit is known but the empirical formulas of their elements are to be determined. This concept is shown in Fig. 4.1. The vector $\boldsymbol{x}_f$ is an n-dimensional vector representing the parameters of the microwave component and ω is the frequency. The vectors $\boldsymbol{R}_f$ and $\boldsymbol{R}_c$ represent a complete set of responses (typically the real and imaginary parts of S-parameters) of the fine and circuit model responses, respectively. The development of the FIEM is shown in Fig. 4.2. The vector $\boldsymbol{y}$ is an l-dimensional vector representing the empirical formulas of the elements of the circuit model. Applying dimensional analysis (Middendorf 1986) the vector $\boldsymbol{y}$ becomes a function of an n_d dimensional vector $\boldsymbol{x}_d$ ($n_d < n$), which we call the reduced input parameter vector (we will show in the examples how to construct this vector). We approximate $\boldsymbol{y}$ through artificial neural network (Zaabab, Zhang and Nakhla 1995 and Watson and Gupta 1996) or multivariable rational functions (Leung and Haykin 1993) in a certain region of parameters and frequency as

$$\boldsymbol{y} \approx \boldsymbol{Q}(\boldsymbol{x}_d, \boldsymbol{w}) \tag{4-1}$$

where $\boldsymbol{w}$ is a set of unknown parameters. The set $\boldsymbol{w}$ is evaluated by solving the optimization problem

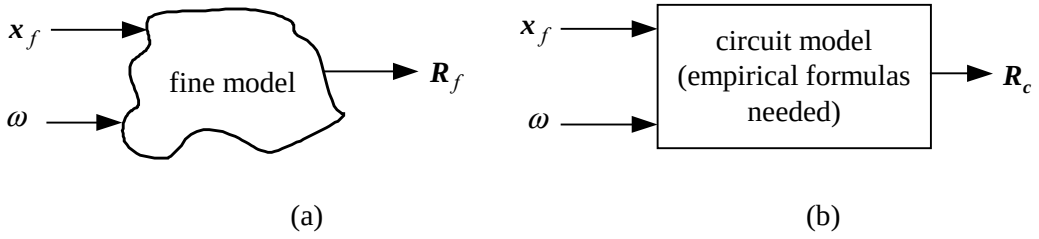

Fig. 4.1 The fine model (a), and the circuit model (b).

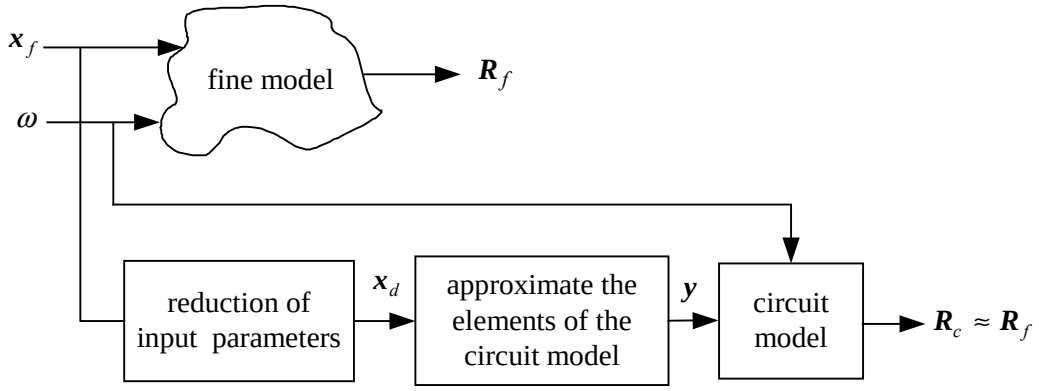

Fig. 4.2 The development of the frequency-independent empirical models.

$$\min_{\boldsymbol{w}} \left\| \; [\boldsymbol{e}_{11}^T \cdots \boldsymbol{e}_{1M}^T \; \boldsymbol{e}_{21}^T \cdots \boldsymbol{e}_{2M}^T \cdots \boldsymbol{e}_{N1}^T \cdots \boldsymbol{e}_{NM}^T]^T \right\| \tag{4-2}$$

where $\| \; \|$ is a suitable norm, N is the total number of training points, M is the number of frequency points per frequency sweep and $\boldsymbol{e}_{ij}$ is an error vector given by

$$\boldsymbol{e}_{ij} = \boldsymbol{R}_f(\boldsymbol{x}_{f_i}, \omega_j) - \boldsymbol{R}_c(\boldsymbol{Q}(\boldsymbol{x}_{di}, \boldsymbol{w}), \omega_j) \tag{4-3}$$

The norm in (4-2) is the Huber norm (see Section 2.2.2) and the optimization problem in (4-2) is solved by the Huber optimizer implemented in OSA90/hope™ (OSA90/hope 1997). The training points are selected according to the Central Composite Design (Montgomery 1991) and more training points are added if necessary.

4.3 FREQUENCY DEPENDENT EMPIRICAL MODELS (FDEM)

Two approaches can be used to introduce frequency dependency to the elements of the FDEM. One approach is to introduce the frequency dependency directly to the vector $\boldsymbol{y}$ (Fig. 4.3). The second approach exploits the frequency mapping (transformation) concept (Bandler, Ismail and Rayas-Sánchez 2000 and 2001a) where we simulate the circuit model at a different frequency from the fine model. We call this frequency the circuit model frequency ω_c. Frequency mappings (transformations) have roots in classical filter design, for example, low-pass to band-pass or high-pass transformations (Collin 1966). The development of the FDEM using this approach is shown in Fig. 4.4. The dependency of ω_c on ω as well as the physical parameters is determined by applying dimensional analysis. Artificial neural networks or multivariable rational functions are used to approximate $\boldsymbol{y}$ and ω_c as

$$\boldsymbol{y} \approx \boldsymbol{Q}(\boldsymbol{x}_d, \boldsymbol{w}_1) \tag{4-4a}$$

$$\omega_c \approx \Omega(\boldsymbol{x}_d, \omega, \boldsymbol{w}_2) \tag{4-4b}$$

where $\boldsymbol{w}_1$ and $\boldsymbol{w}_2$ are unknown parameters. These parameters are evaluated by solving the optimization problem in (4-2) with the error vector $\boldsymbol{e}_{ij}$ given by

$$\boldsymbol{e}_{ij} = \boldsymbol{R}_f(\boldsymbol{x}_{f_i}, \omega_j) - \boldsymbol{R}_c(\boldsymbol{Q}(\boldsymbol{x}_{d\,i}, \boldsymbol{w}_1), \Omega(\boldsymbol{x}_{d\,i}, \omega_j, \boldsymbol{w}_2)) \tag{4-5}$$

4.3.1 Properties of the Frequency Mapping

Simulating the circuit model at a different frequency from that of the fine model is an implicit way of introducing frequency dependency to the elements of the circuit model. For example, if the device is lossless the circuit model contains only lossless

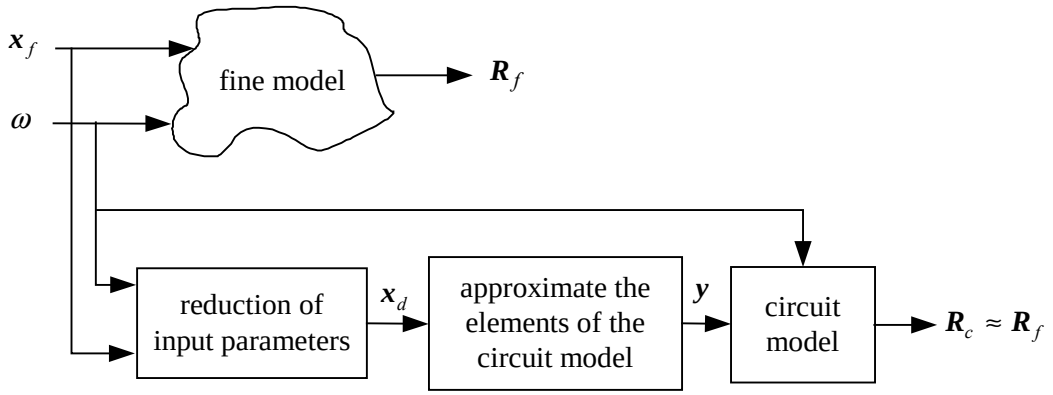

Fig. 4.3 The development of the frequency-dependent empirical models with circuit model elements explicitly function of frequency.

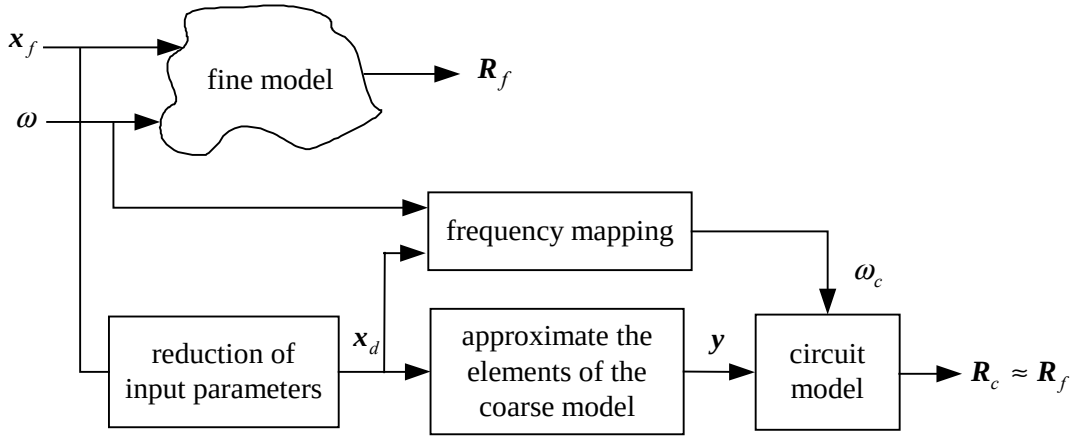

Fig. 4.4 The development of the frequency-dependent empirical models with the circuit model elements implicitly function of frequency through frequency mapping.

lumped-elements (inductors and capacitors). In this case, a FDEM simulated at ω_c and with a circuit element vector $\boldsymbol{y}$ is equivalent to a FDEM simulated at ω and with a circuit elements vector $\boldsymbol{y}_1$ given by

$$\boldsymbol{y}_1 = (\omega_c / \omega)\boldsymbol{y} \tag{4-6}$$

This can be proved as follows. For any inductor L and capacitor C (simulated at frequency ω_c) in $\boldsymbol{y}$ we have

$$Z_L = j\omega_c L = j\,\omega(L\omega_c/\omega) \tag{4-7a}$$

$$Y_C = j\omega_c C = j\,\omega(C\omega_c/\omega) \tag{4-7b}$$

Therefore, the circuit elements vector $\boldsymbol{y}_1$ (simulated at frequency ω) is related to the vector $\boldsymbol{y}$ by (4-6). Furthermore, the frequency ω_c should be an odd function of ω. This results from the even and odd properties (Collin 1966) of an arbitrary frequency-dependent impedance $Z(\omega)$, where the real (imaginary) part should be an even (odd) function of frequency. For example, if an inductor L is simulated at frequency ω_c the equivalent impedance $Z_L = j\omega_c L$ is purely imaginary, hence Z_L and consequently ω_c should be odd function of ω. The odd property is also preserved when using the frequency mapping to transform a low-pass filter into a high- or a band-pass filter (Collin 1966). We use this property in conjunction with dimensional analysis to further reduce the number of parameters of the artificial neural network or the multivariable rational function approximating ω_c.

4.3.2 Transformation of FDEMs into FIEMs

The advantage of using a multivariable rational function to approximate the frequency mapping is that we can transform the FDEM into an equivalent FIEM. This transformation involves one-port impedance synthesis, which states that the impedance we want to realize should be a positive real rational function (Temes and Lapatra 1977). For example, the impedances associated with an inductor L and a capacitor C (simulated at ω_c) in the circuit elements vector $\boldsymbol{y}$ are $Z_L = j\omega_c L$ and $Z_C = 1/(j\omega_c C)$, respectively. Those impedances can be realized using any of the one-port impedance synthesis techniques such as the first Foster realization or second Foster realization or ladder

realization (Temes and Lapatra 1977). In the examples presented here, we notice that the frequency ω_c takes the form

$$\omega_c = \omega \frac{f_1 - \omega^2 f_2}{f_3 - \omega^2 f_4} \tag{4-8}$$

where f_1, f_2, f_3 and f_4 are functions of the device physical parameters. Therefore, the impedances associated with an inductor L and a capacitor C in the circuit elements vector $\boldsymbol{y}$ are given by

$$Z_L = j\,\omega L \frac{f_1 - \omega^2 f_2}{f_3 - \omega^2 f_4} \tag{4-9a}$$

$$Z_C = \frac{1}{j\omega C} \frac{f_3 - \omega^2 f_4}{f_1 - \omega^2 f_2} \tag{4-9b}$$

We believe that (4-8) may be useful for other devices such as microstrip mitered bends, microstrip step junctions, etc.

4.3.3 Passivity of the FDEMs

The FDEM of a microwave component is passive if the equivalent impedance of each element (inductor or capacitor) of the circuit model is realizable. That is, the equivalent impedances given by (4-9a) and (4-9b) are realizable. An impedance $Z(s)$, where $s = j\omega$, is realizable if and only if it is a positive real function of s, i.e, $Z(s)$ is a real rational function of s and $\mathrm{Re}(Z(s)) \geq 0$ if $\mathrm{Re}(s) \geq 0$ (Temes and Lapatra 1977). For an LC impedance this implies that all poles of $Z(s)$ are simple and lie on the $j\omega$ axis and have positive real residues. Applying these conditions to the impedances in (4-9a) and (4-9b) and performing some algebraic manipulations we get the passivity conditions of the FDEMs (see Appendix A). A FDEM is passive if the circuit elements (inductors and

capacitors) are positive and the parameters of the frequency mapping in (4-8) satisfy

$$f_i > 0,\ i = 1, ..., 4 \tag{4-10a}$$

$$\begin{vmatrix} f_1 & f_2 \\ f_3 & f_4 \end{vmatrix} > 0 \tag{4-10b}$$

Therefore, in order to insure the passivity of the FDEMs, (4-10a) and (4-10b) should be included as constraints in the optimization problem in (4-2).

4.4 MULTIVARIABLE RATIONAL FUNCTIONS

Multivariable rational functions (MRFs) Leung and Haykin (1993) are used in most of the modeling examples developed in this chapter. A multivariable rational function is the quotient of two polynomials,

$$f(\boldsymbol{x}, \boldsymbol{a}, \boldsymbol{b}) = \frac{a_0 + \sum_{i=1}^{n} a_i\, x_i + \sum_{i=1}^{n}\sum_{j \geq i}^{n} a_{ij}\, x_i\, x_j + \cdots}{1 + \sum_{i=1}^{n} b_i\, x_i + \sum_{i=1}^{n}\sum_{j \geq i}^{n} b_{ij}\, x_i\, x_j + \cdots} \tag{4-11}$$

where $\boldsymbol{x} = [x_1\ x_2 \cdots x_n]^T$ is the input vector and $\boldsymbol{a}$, $\boldsymbol{b}$ are two vectors containing the unknown a's and b's, respectively. The polynomials in the numerator and the denominator are of finite order p and q, respectively. The rational function in (4-11) is fully characterized by the number of input variables n, the numerator order p and the denominator order q, hence we refer to it as $\text{MRF}_{n,p,q}$. The number of unknown parameters in $\boldsymbol{a}$ and $\boldsymbol{b}$ can be reduced if some of the input variables are restricted to a certain order less than p or q. For example, a $\text{MRF}_{2,3,2}$ with the order of the input variable x_1 restricted to 1 is given by

$$f(\boldsymbol{x},\boldsymbol{a},\boldsymbol{b}) = \frac{a_0 + a_1x_1 + a_2x_2 + a_{12}x_1x_2 + a_{22}x_2^2 + a_{122}x_1x_2^2 + a_{222}x_2^3}{1 + b_1x_1 + b_2x_2 + b_{12}x_1x_2 + b_{22}x_2^2} \tag{4-12}$$

which has 11 unknown parameters. On the other hand, the full $MRF_{2,3,2}$ has 15 unknown parameters. The unknown parameters in $\boldsymbol{a}$ and $\boldsymbol{b}$ can be computed by two methods. First, if the values of the function f in (4-11) are explicitly available we can evaluate $\boldsymbol{a}$ and $\boldsymbol{b}$ by solving a system of linear equations. This is done by applying cross-multiplication to both sides of (4-11) and rearranging the terms to get a system of linear equations in the elements of $\boldsymbol{a}$ and $\boldsymbol{b}$. This system of linear equations can be solved by the method of least-squares or recursive least-squares (Leung and Haykin 1993). Second, if values of f are not directly available we evaluate $\boldsymbol{a}$ and $\boldsymbol{b}$ by solving a suitable optimization problem (in our case the optimization problem in (4-2)). The second method is adopted in this work since we evaluate the elements of the empirical model (inductors, capacitors and the frequency ω_c) and the only available information are the scattering parameters supplied by the EM simulators.

4.5 MODELING EXAMPLES

To display the results in a compact way we define the error in the scattering parameter S_{ij} as the modulus of the difference between the scattering parameter S_{ij}^f computed by the fine model and the scattering parameter S_{ij}^c computed by the circuit model

$$\text{error in } S_{ij} = \left|S_{ij}^f - S_{ij}^c\right| = \sqrt{(\text{Re}[S_{ij}^f] - \text{Re}[S_{ij}^c])^2 + (\text{Im}[S_{ij}^f] - \text{Im}[S_{ij}^c])^2} \tag{4-13}$$

where i = 1, 2,..., N_p and j = 1, 2,... N_p (N_p is the number of ports of the microwave device). We also define the percentage error in S_{ij} by

$$\%\ \text{error in } S_{ij} = \left| \frac{S_{ij}^f - S_{ij}^c}{S_{ij}^f} \right| \text{x } 100 \tag{4-14}$$

We will use percentage error in S_{ij} to display the results whenever $\left|S_{ij}^f\right|$ is not zero.

4.5.1 Microstrip Right Angle Bend

Here, we develop a frequency-independent and frequency-dependent empirical model for the microstrip right angle bend in Fig. 4.5(a). The fine model is analyzed by Sonnet's ***em***™ (***em*** 1997) and the circuit model is the LC circuit in Fig. 4.5(b) (Gupta, Garg and Bahl 1979). The vector of input parameters $\boldsymbol{x}_f = [W \;\; H \;\; \varepsilon_r]^T$ and the vector of the circuit elements is $\boldsymbol{y} = [L/H \;\; C/H]^T$. Applying dimensional analysis (Middendorf 1986) we can show that the elements of $\boldsymbol{y}$ are given by

$$L/H = \mu_0 \;\; f(W/H) \tag{4-15a}$$

$$C/H = \varepsilon_0 \; f(W/H, \varepsilon_r) \tag{4-15b}$$

Therefore, $\boldsymbol{y}$ is a function of $\boldsymbol{x}_d = [W/H \;\; \varepsilon_r]^T$. We first develop a FIEM in the frequency range 1 GHz to 11 GHz. The region of interest is 0.2 <W/H< 6 and 2 <ε_r< 11. The substrate height H is chosen in the range 5 mil to 30 mil. We use a three-layer perceptron ANN (with hyperbolic-tangent as nonlinear activation function) to approximate $\boldsymbol{y}$. Two hidden neurons are used for L/H and three hidden neurons for C/H. The training points are chosen according to the Central Composite Design (Montgomery 1991) in addition to 4 more points as shown in Fig. 4.6 (total 13 training points) where $\hat{x}_1$ and $\hat{x}_2$ are the scaled input variables corresponding to W/H and ε_r, respectively. The vector $\boldsymbol{y}$ is also approximated by multivariable rational functions. The inductance per unit length L/H is

approximated by a rational function $MRF_{1,2,2}$ and the capacitance per unit length C/H is approximated by a rational function $MRF_{2,3,0}$ with the order of W/H restricted to one (this gives better generalization performance than if we do not restrict the order of W/H). The parameters of the ANNs and the MRFs are obtained by the Huber optimizer in OSA90/hope™. Fig. 4.7(a) and (b) show the error in the scattering parameter S_{11} at 16 test points in the region of interest for the FIEM developed by ANN and MRF, respectively. Fig. 4.7(c) shows the corresponding error due to the model in Kirschning, Jansen and Koster (1983) at the same test points. We notice that the three models are comparable.

The results obtained by the FIEM (developed by either ANNs or MRFs) and by the empirical model (Kirschning, Jansen and Koster 1983) over broad frequency range are shown in Fig. 4.8(a), (b) and (c), respectively. It is clear that neither the FIEM nor the empirical model in Kirschning, Jansen and Koster (1983) are accurate at high frequencies. Therefore, we develop a FDEM (see Fig. 4.4), where ω_c is a function of ω and the other parameters. Applying dimensional analysis (see Appendix B) and using the odd property of ω_c we get

$$\omega_c = \omega \ \gamma(\boldsymbol{x}_d, (\omega H/c)^2) \tag{4-16}$$

where c is the speed of light and γ is an unknown function to be approximated. We use multivariable rational functions to approximate $\boldsymbol{y}$ as well as ω_c. A $MRF_{3,2,2}$ with the order of $(\omega H/c)^2$ restricted to one is used to approximate ω_c. The number of training points used to develop the FDEM is the same as that used to develop the FIEM. Fig. 4.9(a) and (b) show the errors in the scattering parameters S_{11} and S_{21} at 16 test points in the region of interest for the FDEM. Fig. 4.10 compares the results obtained by the FDEM and

those from Sonnet's ***em***™. The empirical expressions for $\boldsymbol{y}$ and ω_c are given in TABLE 4.1.

We transform the FDEM into an equivalent FIEM as follows. The frequency ω_c is given by (4-8) and, hence the impedances associated with L and C are given by (4-9a) and (4-9b), respectively. These impedances are realized by the first Foster realization synthesis (Temes and Lapatra 1977). The equivalent FIEM is shown in Fig. 4.11(b), where all elements are frequency independent and functions only of the device parameters.

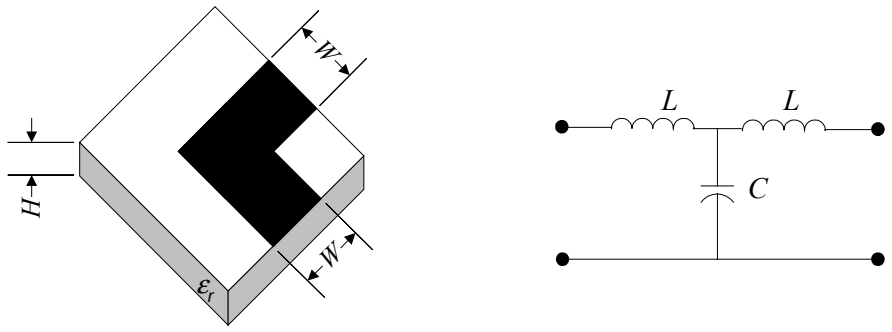

(a) (b)

Fig. 4.5 The microstrip right angle bend: (a) the fine model, (b) the circuit model.

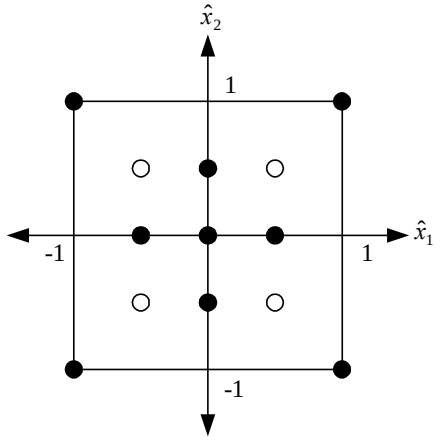

Fig. 4.6 The training points for the microstrip right angle bend.

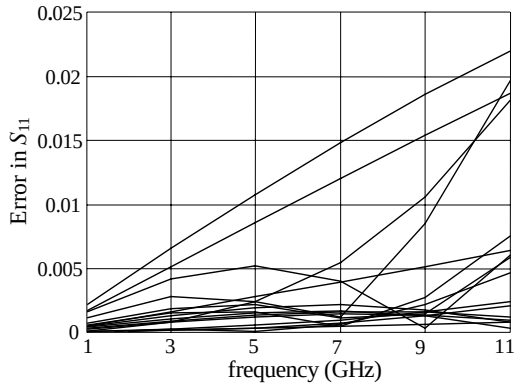

(a)

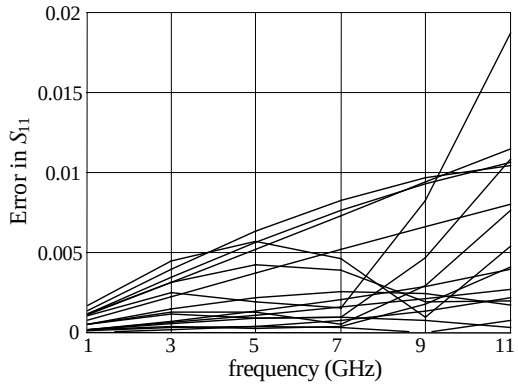

(b)

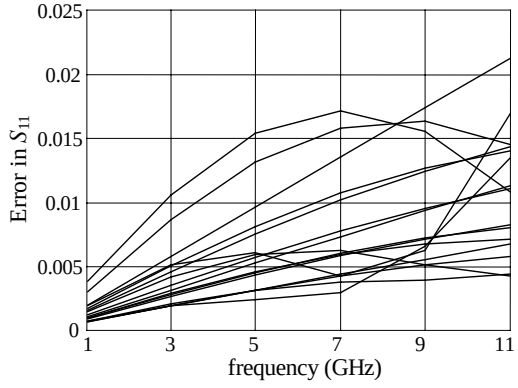

(c)

Fig. 4.7 The error in S_{11} of the microstrip right angle bend with respect to ***em***™ at the test points: (a) the FIEM developed by ANNs, (b) the FIEM developed by MRFs, (c) by the empirical model in Kirschning, Jansen and Koster (1983).

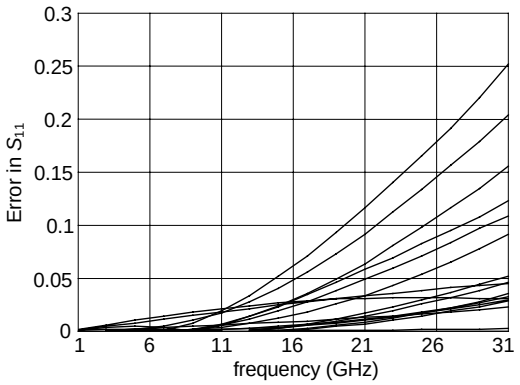

(a)

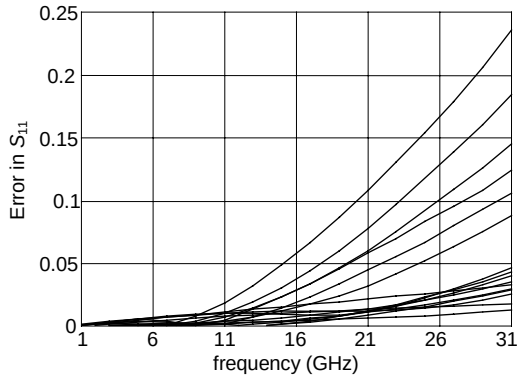

(b)

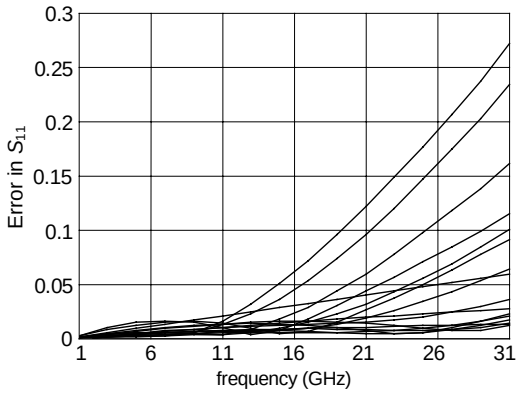

(c)

Fig. 4.8 The error in S_{11} of the microstrip right angle bend with respect to ***em***™ over a broad frequency range: (a) the FIEM developed by ANNs, (b) the FIEM developed by MRFs, (c) the empirical model in Kirschning, Jansen and Koster (1983).

TABLE 4.1

EXPRESSIONS OF THE ELEMENTS OF THE FDEM
OF THE MICROSTRIP RIGHT ANGLE BEND

Element	Expression
L/H (nH/mil)	$0.03192\,\dfrac{-0.09-0.018x_1+0.3x_1^2}{1+2.853x_1^2}$
C/H (pF/mil)	$0.000225(-0.46+0.162x_1-0.014x_2+0.275x_1^2+2.855x_1x_2+0.262x_1^2x_2)$
ω_c/ω	$\dfrac{f_1(x_1,x_2,x_3)}{f_2(x_1,x_2,x_3)}$
	$f_1(x_1,x_2,x_3)=0.759-0.0192x_1-0.0179x_2+0.0187x_3+0.0738x_1^2+0.0026x_1x_2$ $-0.1405x_1x_3+0.0079x_2x_3+0.0018x_1^3-0.0071x_1^2x_2+0.1188x_1^2x_3$ $+0.0017x_1x_2^2+0.0419x_1x_2x_3-0.0022x_2^2x_3$
	$f_2(x_1,x_2,x_3)=1+0.0282x_1-0.0086x_2-0.0175x_3+0.0051x_1^2-0.0063x_1x_2$ $+0.1674x_1x_3+0.0037x_2^2-0.0067x_2x_3+0.0055x_1^3-0.0028x_1^2x_2$ $+0.0011x_1^2x_3+0.0056x_1x_2x_3-0.0012x_2^2x_3$
	where $x_1=W/H,\ x_2=\varepsilon_r,\ x_3=1.816\text{e}-7\ (\omega(\text{GHz})H(\text{mil}))^2$

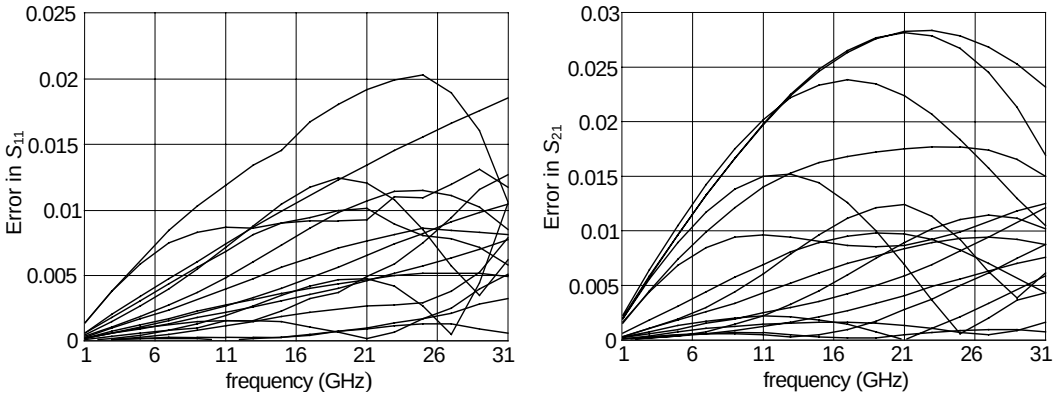

(a) (b)

Fig. 4.9 The error of the FDEM of the microstrip right angle bend (developed by MRFs) with respect to ***em***™ at the test points: (a) in S_{11}, (b) in S_{21}.

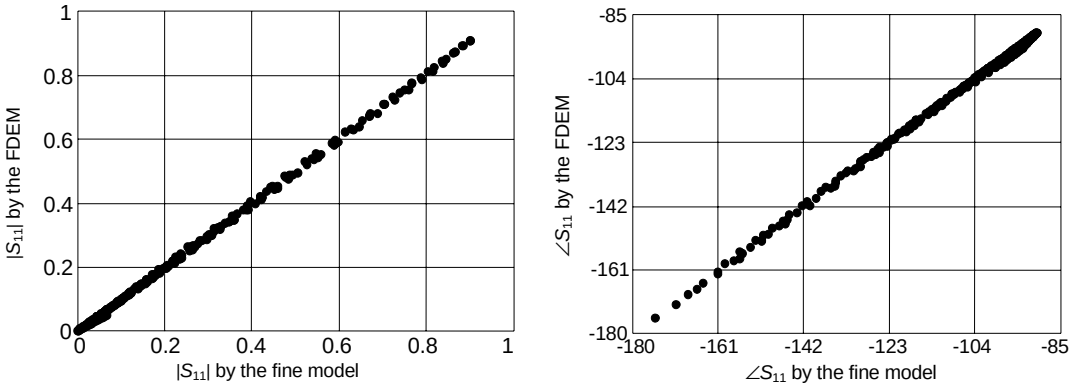

(a) (b)

Fig. 4.10 Comparison between the responses obtained by the FDEM of the microstrip right angle bend and those obtained by ***em***™ at the test points: (a) magnitude of S_{11}, (b) phase of S_{11} in degrees.

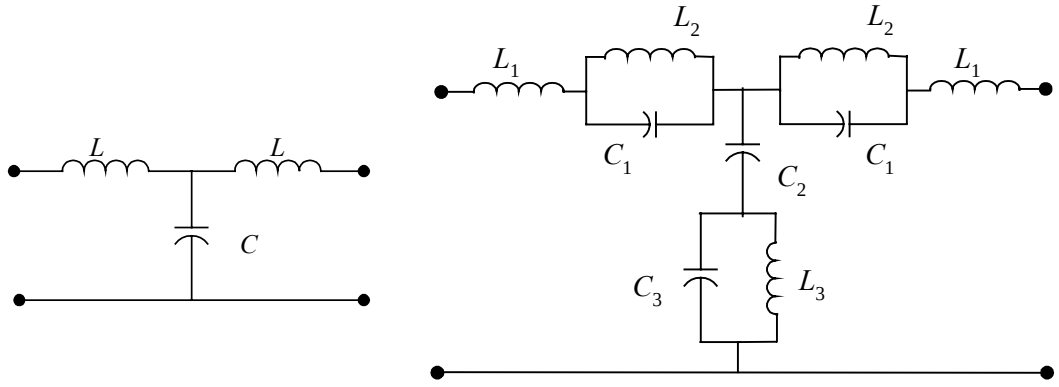

Fig. 4.11 The FDEM of the microstrip right angle bend (a), and the equivalent FIEM (b).

4.5.2 Microstrip Via

Here, we consider modeling the microstrip via in Fig. 2.3 (a). The circuit model is an inductor L to ground (Fig. 2.3 (b)). The fine model is analyzed by Sonnet's ***em***™. The reference plane is at the junction of the microstrip line and the square pad. The

vector $\boldsymbol{x}_f = [W \;\; H \;\; W_0 \;\; D]^T$, where H is the substrate height (GaAs, ε_r=12.9). Here, $\boldsymbol{y}$ = [L/H], which is given by (see Section 2.4.1)

$$L/H = \mu_0 \;\; f(W/H, W_0/W, D/W) \tag{4-17}$$

hence, $\boldsymbol{x}_d = [W/H \;\; W_0/W \;\; D/W]^T$. A FIEM was developed in the range 2 GHz to 10 GHz. The region of interest is 1 <W/H< 2.2, 0.2 <W_0/W < 1 and 0.2 <D/W< 0.8. We use a $MRF_{3,2,2}$ to approximate L/H. The training points are chosen according to the Central Composite Design (Montgomery 1991) in addition to 8 more points (total 23 training points). The parameters of the MRF are obtained by the Huber optimizer in OSA90/hope™. The percentage errors in the inductance L and in S_{11} at 30 test points are shown in Fig. 4.12. Fig. 4.13 compares the results obtained by the FIEM and those from Sonnet's ***em***™.

The results of the FIEM in the range 2 GHz to 22 GHz are shown in Fig. 4.14. We notice large errors at high frequencies. This is because the simple inductor to ground does not take into account the effect of the pad surrounding the via hole and the step junction (Swanson 1992) (see Fig. 2.3(a)). To overcome this deficiency we develop a FDEM in the range 2 GHz to 22 GHz. The circuit model frequency (applying dimensional analysis and using the odd property of the frequency mapping) takes the same form as in (4-16). We use multivariable rational functions to approximate $\boldsymbol{y}$ as well as ω_c. The number of training points used is 23. The percentage errors in L and in S_{11} at 30 test points are shown in Fig. 4.15 (a) and (b), respectively. The transformation of the FDEM into an equivalent FIEM follows the microstrip right angle bend example. The frequency ω_c is given by (4-8). The equivalent impedance of L is of the form of (4-9a). The resulting FIEM is shown in Fig. 4.16. The empirical expressions for $\boldsymbol{y}$ and ω_c are

given in TABLE 4.2.

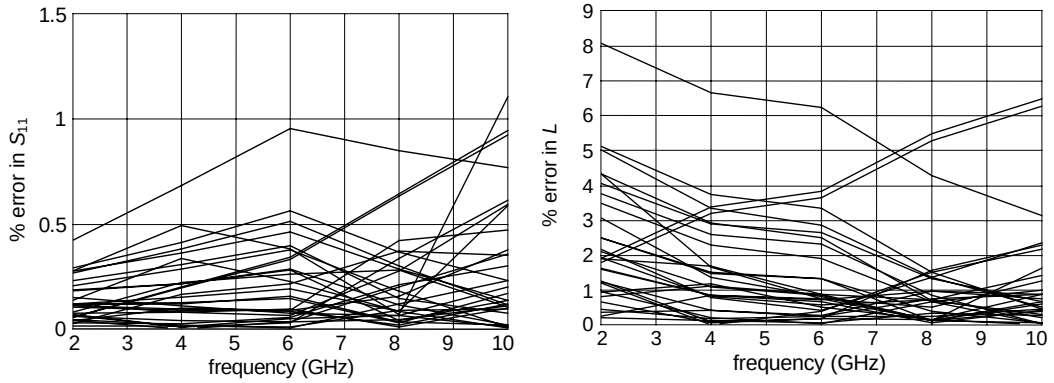

(a) (b)

Fig. 4.12 Percentage error of the FIEM of the microstrip via with respect to ***em***™ at the test points: (a) in S_{11}, (b) in L.

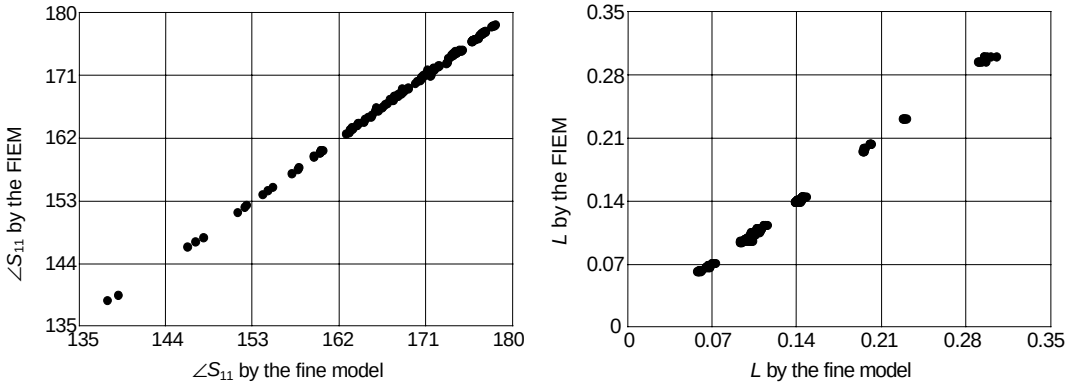

(a) (b)

Fig. 4.13 Comparison between the responses obtained by the FIEM of the microstrip via and those obtained by ***em***™ at the test points: (a) phase of S_{11}, (b) the inductance L.

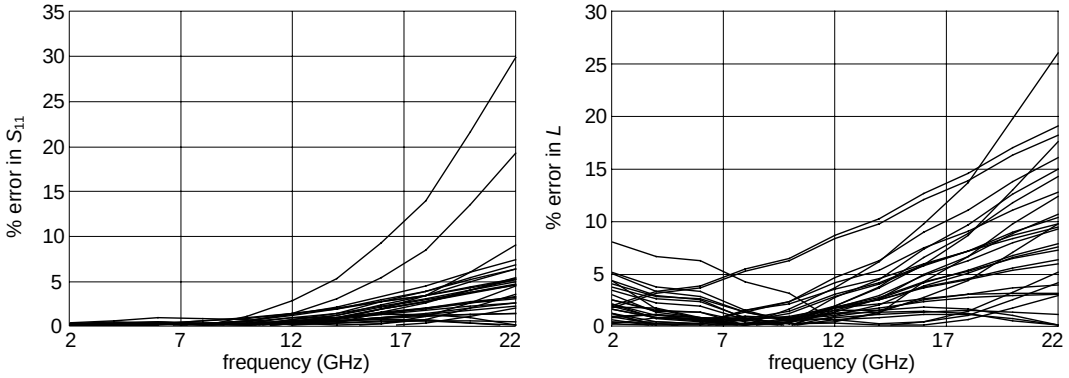

(a) (b)

Fig. 4.14 Comparison of the FIEM of the microstrip via with respect to ***em***™ over a broad frequency range at the test points: (a) % error in S_{11}, (b) % error in L.

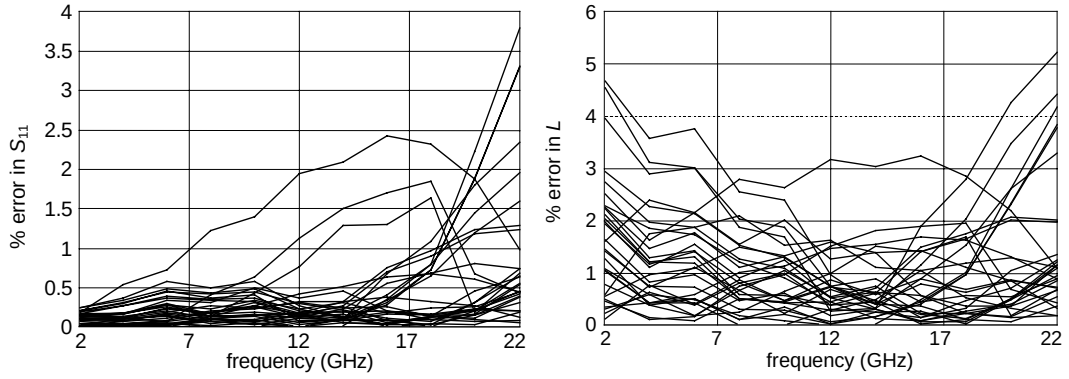

(a) (b)

Fig. 4.15 Comparison of the FDEM of the microstrip via with respect to ***em***™ over a broad frequency range at the test points: (a) % error in S_{11}, (b) % error in L.

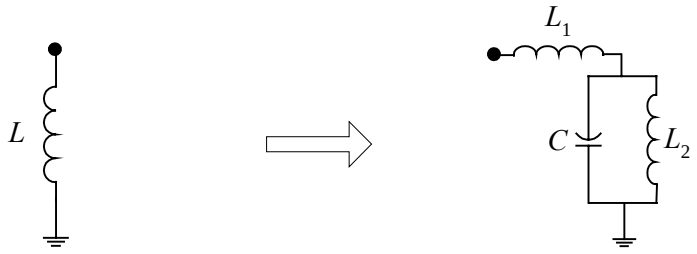

Working frequency is ω_c working frequency is ω

(a) (b)

Fig. 4.16 The FDEM of the microstrip via (a) and the corresponding FIEM (b).

TABLE 4.2

EXPRESSIONS OF THE ELEMENTS OF THE FDEM
OF THE MICROSTRIP VIA

Elemen	Expression
L/H (nH/mil)	$0.03192\,\dfrac{f_1(x_1,x_2,x_3)}{f_2(x_1,x_2,x_3)}$
	$f_1(x_1,x_2,x_3) = 0.0123 + 2.173x_1 + 14.166x_2 + 1.779x_3 + 1.875x_1^2 - 5.036x_1x_2 - 0.983x_1x_3 - 8.622x_2^2 - 2.111x_2x_3$
	$f_2(x_1,x_2,x_3) = 1 - 3.835x_1 + 30.784x_2 + 3.26x_3 + 7.161x_1^2 + 15.471x_1x_2 - 1.088x_1x_3 - 21.862x_2^2 - 7.381x_2x_3$
ω_c/ω	$\dfrac{f_3(x_1,x_2,x_3,x_4)}{f_4(x_1,x_2,x_3,x_4)}$
	$f_3(x_1,x_2,x_3,x_4) = 0.9156 - 0.0427x_1 - 0.065x_2 - 0.3837x_3 - 0.2494x_4 - 0.0948x_1^2 - 0.0979x_1x_2 + 0.0808x_1x_3 + 0.0095x_1x_4 + 0.161x_2^2 + 0.1121x_2x_3 + 0.5776x_2x_4 + 0.0962x_3^2 + 0.0108x_3x_4$
	$f_4(x_1,x_2,x_3,x_4) = 1 - 0.2841x_1 + 0.0418x_2 - 0.2042x_3 - 0.4723x_4 - 0.024x_1^2 - 0.1315x_1x_2 + 0.0649x_1x_3 + 0.0342x_1x_4 + 0.1864x_2^2 + 0.101x_2x_3 + 0.885x_2x_4 - 0.0029x_3^2 + 0.0725x_3x_4$
	where $x_1 = W/H,\quad x_2 = D/W,\quad x_3 = W_0/W, x_3 = 1.816\text{e}-07\,(\omega(\text{GHz})H(\text{mil}))^2$

4.5.3 Microstrip Double-Step

Here, we consider broadband modeling of the microstrip double-step element in Fig. 4.17(a). It can be used to model microstrip tapered lines or nonuniform (in width) microstrip lines. The circuit model consists of two shunt capacitances and one series inductance (see Fig. 4.17(b)). The fine model is analyzed by Sonnet's ***em***™. The vector of fine model parameters $\boldsymbol{x}_f = [W_1 \quad W_2 \quad W_3]^T$. The substrate height H=25 mil, the relative dielectric constant $\varepsilon_r = 9.7$ and the length l (see Fig. 4.17(a)) is 5 mil. The circuit elements vector $\boldsymbol{y} = [L_1/H \quad C_1/H \quad C_2/H]^T$. The elements of $\boldsymbol{y}$ are given by

$$L_1/H = \mu_0 \ \ f_1(\frac{W_2}{H}, \frac{W_2}{W_1}, \frac{W_3}{W_2}) \tag{4-18a}$$

$$C_1/H = \varepsilon_0 \ \ f_2(\frac{W_2}{H}, \frac{W_2}{W_1}, \frac{W_3}{W_2}) \tag{4-18b}$$

$$C_2/H = \varepsilon_0 \ \ f_3(\frac{W_2}{H}, \frac{W_2}{W_1}, \frac{W_3}{W_2}) \tag{4-18c}$$

hence, $\boldsymbol{x}_d = [W_2/H \ \ W_2/W_1 \ \ W_3/W_2]^T$. The circuit model frequency (applying dimensional analysis and using the odd property of the frequency mapping) takes the same form as in (4-16). A FDEM of the double-step element is developed in the frequency range 1 GHz 41 GHz. The region of interest is $0.1<W_2/H<1$, $0.5<W_2/W_1<0.9$ and $0.5<W_3/W_2<0.9$. We use a $MRF_{3,2,2}$ to approximate each element of the vector $\boldsymbol{y}$ and a $MRF_{4,2,2}$ to approximate ω_c with the order of $(\omega H/c)^2$ restricted to 1. The number of training points is 23. The parameters of the MRFs are obtained by the Huber optimizer in OSA90/hope™. The empirical expressions for $\boldsymbol{y}$ and ω_c are given in TABLE 4.3. The errors in S_{11} and S_{21} of the FDEM with respect to Sonnet's ***em***™ at 27 testing points in the region of interest are shown in Fig. 4.18(a) and (b), respectively. To evaluate the FDEM of the double-step we consider an alternative model for the double-step element. This model is composed of a microstrip transmission line and 2 step junctions as shown in Fig. 4.19. The empirical models for the microstrip line and the 2 step junctions are taken from OSA90/hope™. Fig. 4.20(a) and (b) show the errors in S_{11} and S_{21} of this model with respect to Sonnet's ***em***™ at 27 testing points in the region of interest. It is clear from Fig. 4.18 and Fig. 4.20 that the FDEM outperforms the double-step model in Fig. 4.19.

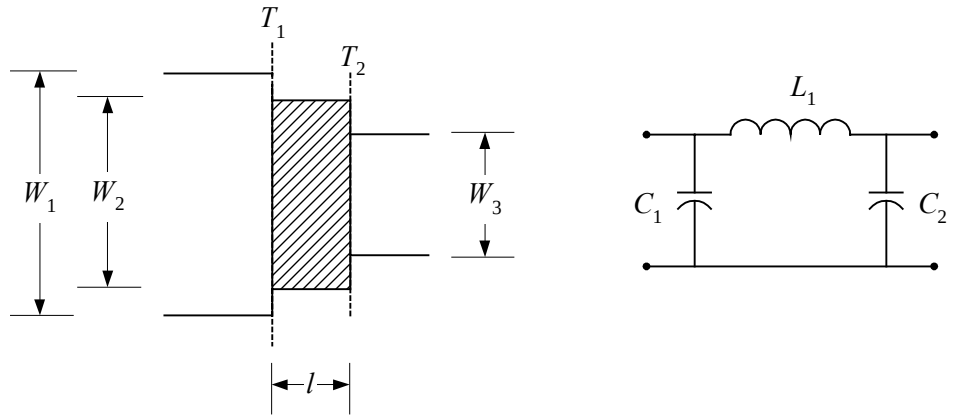

Fig. 4.17 The microstrip double-step: (a) the physical structure where T_1 and T_2 are the reference planes, (b) the circuit model.

The FDEM of the double-step element is used to model the linear tapered microstrip line in Fig. 4.21. The parameters of the tapered line are L= 150 mil, W_{in}=18 mil, W_{out}=2 mil, H= 25 mil and $\varepsilon_r = 9.7$. The input microstrip line has a characteristic impedance of 50 ohm and the output line has a characteristic impedance of 100 ohm. The linear tapered microstrip line can be modeled by cascading 30 double-step elements (each of length l= 5 mil). The ABCD matrix of the tapered line is related to the ABCD matrices of the double-step elements by

$$\begin{bmatrix} A & B \\ C & D \end{bmatrix} = \prod_{i=1}^{30} \begin{bmatrix} A_i & B_i \\ C_i & D_i \end{bmatrix} \tag{4-19}$$

We analyze the tapered line by three methods: by Sonnet's ***em***™ (the fine model), by cascading 30 double-step elements, where the FDEM is used to model each element and by cascading 30 elements where the alternative model of the double-step element in Fig. 4.19 is used. Fig. 4.22 compares the results obtained by the three methods.

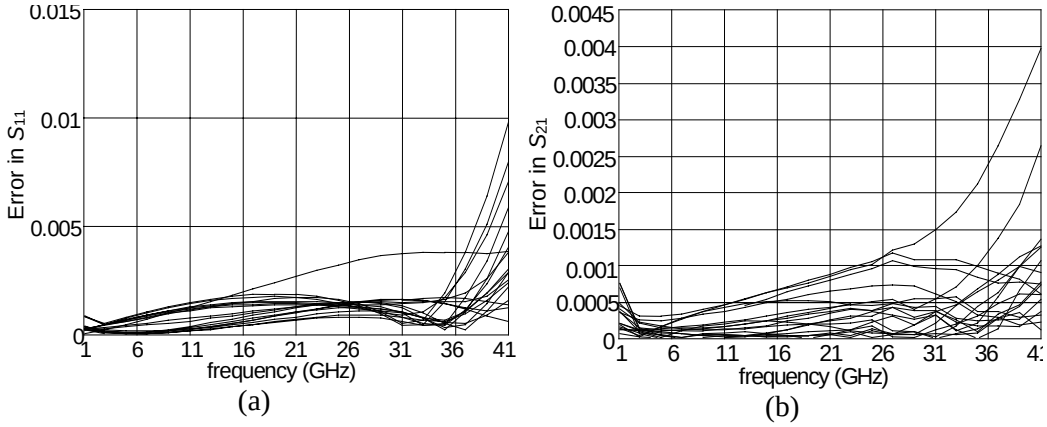

Fig. 4.18 Comparison between the FDEM of the double-step element and ***em***™ at the test points in the region of interest: (a) error in S_{11}, (b) error in S_{21}.

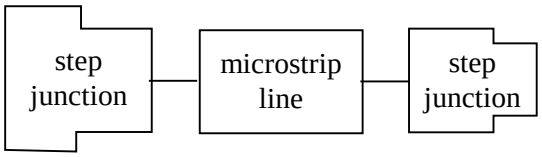

Fig. 4.19 An alternative model for the microstrip double-step element.

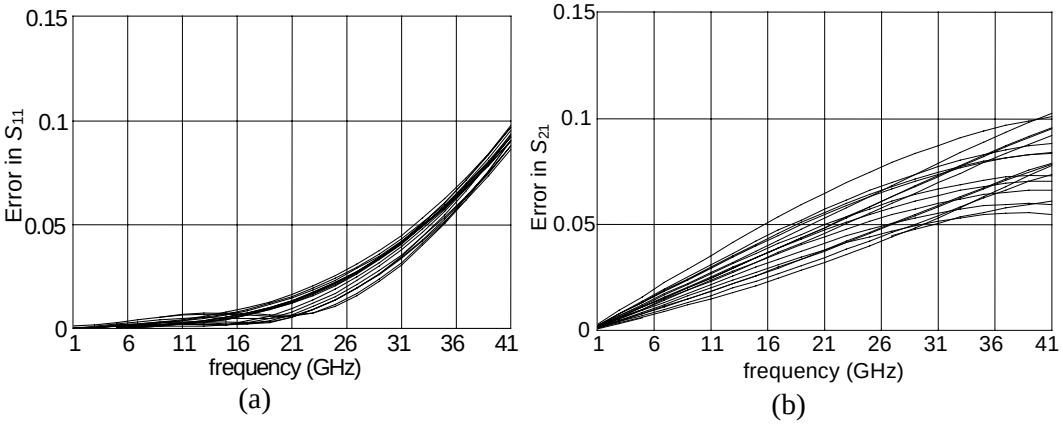

Fig. 4.20 Comparison between the double-step model in Fig. 4.19 and ***em***™ at the test points in the region of interest: (a) error in S_{11}, (b) error in S_{21}.

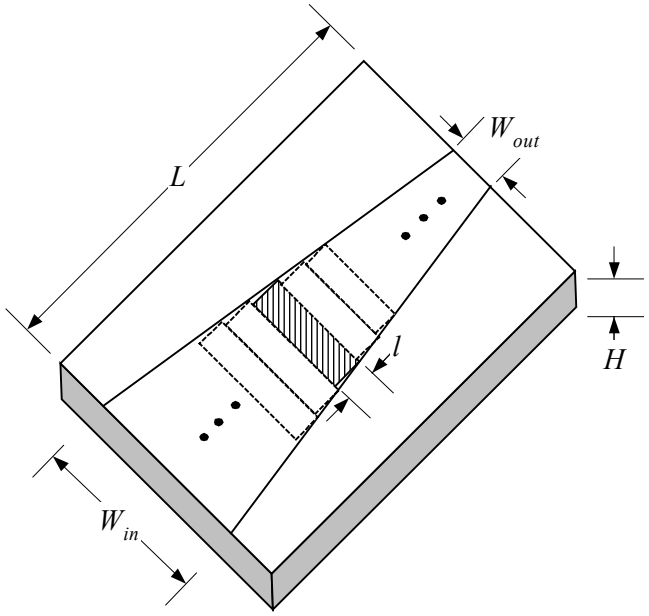

Fig. 4.21 Linear tapered microstrip line.

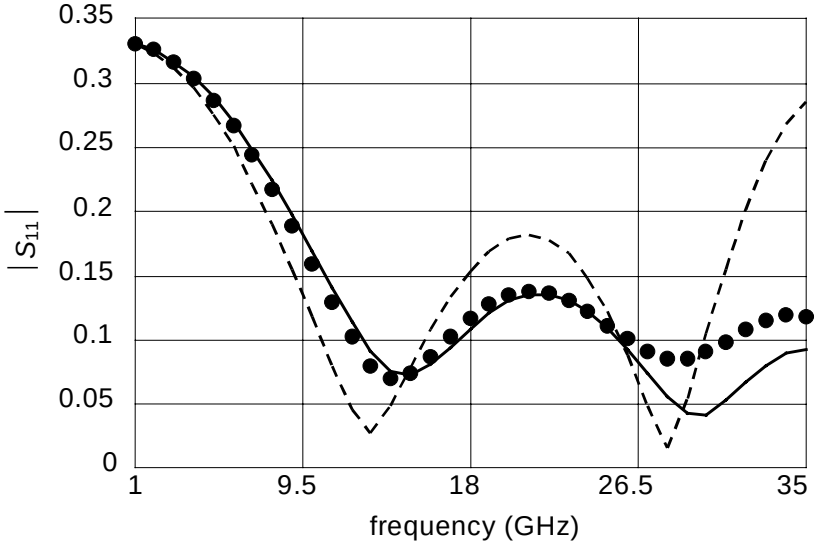

Fig. 4.22 The response of the linear tapered microstrip line by ***em***™ (•), by the FDEM of the double-step element (—), by the model in Fig. 4.19 of the double-step element (----).

TABLE 4.3

EXPRESSIONS OF THE ELEMENTS OF
THE FDEM OF THE MICROSTRIP DOUBLE-STEP

Element	Expression
C_1/H (pF/mil)	$0.0002246\,\dfrac{f_1(x_1,x_2,x_3)}{f_2(x_1,x_2,x_3)}$ $f_1(x_1,x_2,x_3) = 0.6433 + 0.6697x_1 - 0.4604x_2 + 0.0088x_3 - 0.7741x_1^2 + 0.099x_1x_2 + 0.3921x_1x_3 - 0.2749x_2^2 + 0.1779x_2x_3 - 0.0642x_3^2$ $f_2(x_1,x_2,x_3) = 1 + 0.5641x_1 - 0.3232x_2 - 0.0211x_3 - 0.6742x_1^2 + 0.0499x_1x_2 + 0.4428x_1x_3 - 0.5845x_2^2 + 0.0087x_2x_3 - 0.2907x_3^2$
C_2/H (pF/mil)	$0.0002246\,\dfrac{f_3(x_1,x_2,x_3)}{f_4(x_1,x_2,x_3)}$ $f_1(x_1,x_2,x_3) = 0.7485 + 3.0972x_1 + 0.1092x_2 - 0.3263x_3 - 0.0003x_1^2 + 0.2666x_1x_2 + 1.0371x_1x_3 + 0.2595x_2^2 + 0.3725x_2x_3 - 0.5347x_3^2$ $f_2(x_1,x_2,x_3) = 1 - 0.6556x_1 - 0.1716x_2 - 1.1229x_3 - 0.025x_1^2 + 0.4179x_1x_2 + 0.4398x_1x_3 + 0.0063x_2^2 + 1.897x_2x_3 + 0.0122x_3^2$
L/H (nH/mil)	$0.03192\,\dfrac{f_5(x_1,x_2,x_3)}{f_6(x_1,x_2,x_3)}$ $f_5(x_1,x_2,x_3) = 0.2934 + 0.2522x_1 - 0.2209x_2 - 0.1631x_3 - 0.0737x_1^2 - 0.0891x_1x_2 - 0.1021x_1x_3 + 0.1401x_2^2 - 0.0169x_2x_3 + 0.117x_3^2$ $f_2(x_1,x_2,x_3) = 1 + 2.5332x_1 + 0.066x_2 + 0.6713x_3 - 1.111x_1^2 + 0.7775x_1x_2 - 0.1045x_1x_3 - 0.1237x_2^2 - 0.8642x_2x_3 - 0.3023x_3^2$
ω_c/ω	$\dfrac{f_5(x_1,x_2,x_3,x_4)}{f_6(x_1,x_2,x_3,x_4)}$ $f_3(x_1,x_2,x_3,x_4) = 0.8955 - 0.2519x_1 + 0.0699x_2 + 0.2416x_3 - 0.076x_4 - 0.1473x_1^2 + 0.2027x_1x_2 - 0.3735x_1x_3 + 0.0583x_1x_4 - 0.0602x_2^2 - 0.0456x_2x_3 + 0.0499x_2x_4 + 0.1394x_3^2 - 0.0257x_3x_4$ $f_6(x_1,x_2,x_3,x_4) = 1 + 0.0524x_1 - 0.1599x_2 + 0.0579x_3 - 0.0748x_4 - 0.1895x_1^2 - 0.0577x_1x_2 - 0.5079x_1x_3 + 0.064x_1x_4 + 0.1261x_2^2 + 0.1076x_2x_3 + 0.0389x_2x_4 + 0.2899x_3^2 - 0.0373x_3x_4$ where $x_1 = W_2/H, \quad x_2 = W_2/W_1, \quad x_3 = W_3/W_2, x_4 = 1.816\text{e}-07\,(\omega(\text{GHz})H(\text{mil}))^2$

4.5.4 CPW Step Junction

Here, we develop a FIEM for the CPW step junction in Fig. 4.23(a). The fine model is analyzed by Sonnet's ***em***™ and the circuit model is the LC circuit in Fig. 4.24(b) (Gupta, Garg and Bahl 1979). The vector of input parameters $\boldsymbol{x}_f = [W_1 \;\; W_2 \;\; G]^T$ and the vector of the circuit elements is $\boldsymbol{y} = [L_1/H \;\; L_2/H \;\; C/H]^T$, where

$$L_1 / H = \mu_0 \;\; f_1(W_1/H, W_2/W_1, G/W_1) \tag{4-20a}$$

$$L_2 / H = \mu_0 \;\; f_2(W_1/H, W_2/W_1, G/W_1) \tag{4-20b}$$

$$C / H = \varepsilon_0 \;\; f_3(W_1/H, W_2/W_1, G/W_1) \tag{4-20c}$$

Therefore, $\boldsymbol{y}$ is a function of $\boldsymbol{x}_d = [W_1/H \;\; W_2/W_1 \;\; G/W_1]^T$. The region of interest is 40 μm $< W_1 <$ 120 μm, $0.2 < W_2/W_1 < 0.8$ and $0.2 < G/W_1 < 1$ and the frequency range is 5 GHz 50 GHz. The substrate height H is 635 μm and the relative dielectric constant is $\varepsilon_r = 12.9$ (GaAs). The number of training points is 23. Each element of the vector $\boldsymbol{y}$ is approximated by a rational function $MRF_{3,2,2}$. The parameters of the MRFs are obtained by the Huber optimizer in OSA90/hope™. The expressions for the elements of $\boldsymbol{y}$ are given in TABLE 4.4. Fig. 4.24(a) and (b) compares between the results obtained by Sonnet's ***em***™ and those by the CPW step junction FIEM at 27 test points in the region of interest. We notice that the CPW step junction FIEM gives good results in broad frequency range 5 GHz to 50 GHz. Therefore, we do not need to develop a FDEM for the CPW step junction. This means that the elements of the CPW step junction empirical model are frequency independent. Fig. 4.25 compares between the capacitance C extracted from the Z-parameters obtained by Sonnet's ***em***™ and that predicted by the FIEM at 6 test points in the region of interest.

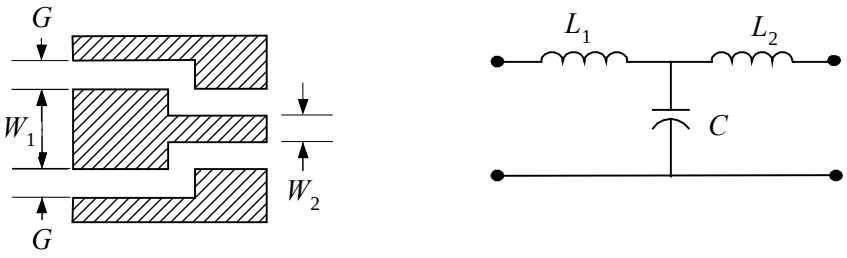

(a) (b)

Fig. 4.23 The CPW step junction: (a) the physical structure, (b) the circuit model.

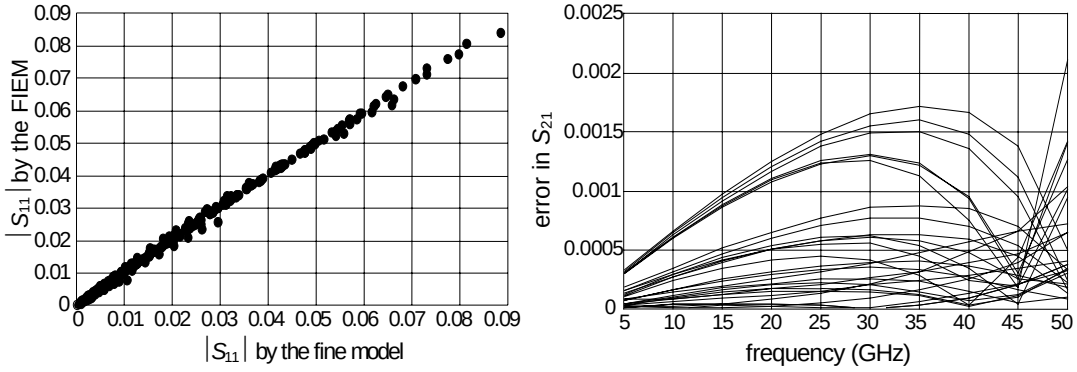

(a) (b)

Fig. 4.24 Comparison between the results obtained by ***em***™ and by the FIEM of the CPW step junction: (a) $|S_{11}|$ by ***em***™ versus that of the FIEM, (b) the error in S_{21}.

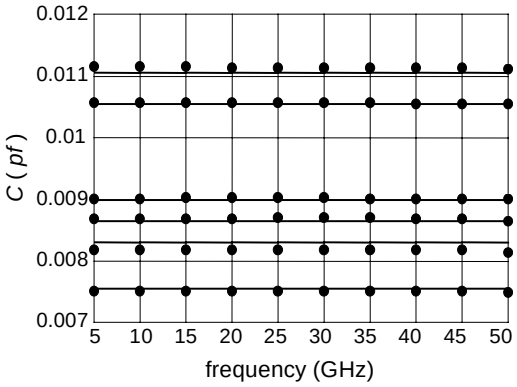

Fig. 4.25 The capacitance of the CPW step junction: (a) extracted from the fine model (•); (b) predicted by the FIEM of the CPW step junction (—).

TABLE 4.4

EXPRESSIONS OF THE ELEMENTS OF
THE FIEM OF THE CPW STEP JUNCTION

Element	Expression
	$$0.00126\,\frac{f_1(x_1,x_2,x_3)}{f_2(x_1,x_2,x_3)}$$
L_1/H (nH/μm)	$f_1(x_1,x_2,x_3) = 0.0236 - 0.0222x_1 - 0.0013x_2 - 0.0114x_3 + 0.1257x_1^2 + 0.0045x_1x_2 - 0.0131x_1x_3 - 0.0099x_2^2 + 0.0147x_2x_3 - 0.0092x_3^2$
	$f_2(x_1,x_2,x_3) = 1 + 0.0909x_1 + 0.4219x_2 - 0.9638x_3 + 0.1791x_1^2 + 0.0011x_1x_2 + 0.5169x_1x_3 - 0.0372x_2^2 - 0.1109x_2x_3 - 0.0045x_3^2$
	$$0.00126\,\frac{f_3(x_1,x_2,x_3)}{f_4(x_1,x_2,x_3)}$$
L_2/H (nH/μm)	$f_3(x_1,x_2,x_3) = 0.0246 + 0.0782x_1 - 0.0496x_2 + 0.0175x_3 - 0.3558x_1^2 - 0.0523x_1x_2 + 0.1423x_1x_3 + 0.0415x_2^2 + 0.0192x_2x_3 - 0.0122x_3^2$
	$f_4(x_1,x_2,x_3) = 1 - 1.3664x_1 + 0.2942x_2 + 0.2462x_3 - 0.511x_1^2 - 0.0126x_1x_2 - 0.1033x_1x_3 + 0.1729x_2^2 + 1.0585x_2x_3 - 0.4105x_3^2$
	$$8.842\text{e}-06\,\frac{f_5(x_1,x_2,x_3)}{f_6(x_1,x_2,x_3)}$$
C/H (pF/μm)	$f_5(x_1,x_2,x_3) = 1.7 - 1.8175x_1 + 0.0193x_2 - 0.0039x_3 + 0.1988x_1^2 - 2.5228x_1x_2 + 0.5604x_1x_3 + 0.0358x_2^2 + 2.3426x_2x_3 + 0.873x_3^2$
	$f_6(x_1,x_2,x_3) = 1 - 2.9222x_1 - 0.5578x_2 + 0.7102x_3 - 1.2069x_1^2 + 1.6552x_1x_2 + 1.0808x_1x_3 + 0.0459x_2^2 + 0.9144x_2x_3 + 0.8377x_3^2$
	where $x_1 = W_1/H, \quad x_2 = W_2/W_1, \quad x_3 = G/W_1$

4.6 CONCLUDING REMARKS

We present a unified computer-aided modeling methodology for developing broadband models of microwave passive components. Our approach integrates in a coherent way full-wave EM simulations, artificial neural networks, multivariable rational functions, dimensional analysis and frequency mapping. Two types of models are considered: frequency-independent and frequency-dependent empirical models. The latter can be transformed to the former if we use a rational function to approximate the frequency mapping. This is important since the frequency-independent empirical models are readily implementable in conventional circuit simulators. We have also discussed the passivity condition of the frequency-dependent empirical models. We have applied our modeling methodology to develop broadband models for several microwave components, including a microstrip right angle bend, a microstrip via, a microstrip double-step and a CPW step junction.

Chapter 5

EXPANDED SPACE MAPPING EXPLOITING PREASSIGNED PARAMETERS

5.1 INTRODUCTION

We present a novel design framework for microwave circuits. We expand the original space mapping technique by allowing some preassigned parameters (which are not used in optimization) to change in some components of the coarse model (Bandler, Ismail and Rayas-Sánchez 2001b and 2001c). We refer to those components as "relevant" components and we present a method based on sensitivity analysis to identify them. As a result, the coarse model can be calibrated to align with the fine model.

The concept of calibrating coarse models (circuit based models) to align with fine models (typically an EM simulator) in microwave circuit design has been exploited by several authors (Bandler, Biernacki, Chen, Grobelny and Hemmers 1994, Bandler, Georgieva, Ismail, Rayas-Sánchez and Zhang 1999 and Ye and Mansour 1997). In Bandler, Biernacki, Chen, Grobelny and Hemmers (1994) and Bandler, Georgieva, Ismail, Rayas-Sánchez and Zhang (1999), this calibration is performed by means of

optimizable parameter space transformation known as space mapping. In Ye and Mansour (1997), this is done by adding circuit components to nonadjacent individual coarse model elements. Here, we expand the space mapping technique. We calibrate the coarse model by allowing some preassigned parameters (we call them key preassigned parameters (KPP)) to change in certain coarse model components.

Examples of KPP are dielectric constant and substrate height in microstrip structures. We assume that the coarse model consists of several components such as transmission lines, junctions, etc. We decompose the coarse model into two sets of components. We allow the KPP to change in the first set and keep them intact in the second set. In Section 5.3 we present a method based on sensitivity analysis to perform this decomposition.

At each iteration, the Expanded Space Mapping Design Framework (ESMDF) algorithm calibrates the coarse model by extracting the KPP such that the coarse model matches the fine model. Then it establishes a mapping from some of the optimizable parameters to the KPP. The mapped coarse model (the coarse model with the mapped KPP) is then optimized subject to a trust region size. The optimization step is accepted only if it results in an improvement in the fine model objective function. The trust region size is updated (Bakr, Bandler, Biernacki, Chen and Madsen 1998, Alexandrov, Dennis, Lewis and Torczon 1998 and Søndergaard 1999) according to the agreement between the fine and mapped coarse model. Therefore, the algorithm enhances the coarse model at each iteration either by extracting the KPP and updating the mapping or by reducing the region in which the mapped coarse model is to be optimized. The algorithm terminates if one of certain relevant stopping criteria is satisfied. We elaborate on possible practical stopping criteria. We also present some solutions to overcome the problems associated

with the KPP extraction process.

We start the chapter by introducing some notation to be used throughout the chapter. Then we present a coarse model decomposition technique. Next, we explain the ESMDF algorithm in details. We also consider a software implementation emphasizing an interface to commercial EM simulators. Finally, we present several design problems, including a microstrip transformer, an HTS filter and a microstrip bandstop filter with open stubs.

5.2 BASIC CONCEPTS AND NOTATION

Consider a microwave circuit with two kinds of models: a fine model and a coarse model. We decompose the coarse model into two sets of components: Set A and Set B. In Set A, we allow the KPP of each component to change throughout the design process such that the coarse model matches the fine model. In Set B, we keep the KPP intact. The coarse model components in Set A are referred to as the relevant components. The vector $\boldsymbol{x}_0 \in \Re^{n_0}$ represents the original values of the KPP. Assume that the total number of coarse model components is N_c, the number of components in the Set A is $m \leq N_c$ and the set I is defined by

$$I = \{1, 2, \cdots, N_c\} \tag{5-1}$$

The vector of the KPP of the components in Set A (the relevant components) is given by

$$\boldsymbol{x} = [\boldsymbol{x}_{j_1}^T \ \boldsymbol{x}_{j_2}^T \ \ldots \ \boldsymbol{x}_{j_m}^T]^T \in \Re^{mn_0} \tag{5-2}$$

where $\boldsymbol{x}_{j_i} \in \Re^{n_0}$ is a vector containing the KPP of the ith relevant component and j_1, j_2,

$\ldots, j_m \in I$. The vector $\boldsymbol{x}_f \in \Re^n$ represents the optimization variables.

The vector $\boldsymbol{R}_f(\boldsymbol{x}_f, \Omega) \in \Re^{FL}$ represents a complete set of basic responses of the fine model (such as the real and imaginary parts of S-parameters) at the point $\boldsymbol{x}_f$ and over a set of discrete frequencies Ω

$$\boldsymbol{R}_f(\boldsymbol{x}_f, \Omega) = [\boldsymbol{R}_f^T(\boldsymbol{x}_f, \omega_1) \;\; \boldsymbol{R}_f^T(\boldsymbol{x}_f, \omega_2) \cdots \boldsymbol{R}_f^T(\boldsymbol{x}_f, \omega_F)]^T \tag{5-3}$$

$$\Omega = \{\omega_1, \omega_2, \cdots, \omega_F\} \tag{5-4}$$

The number of basic responses at one frequency point is L and the number of discrete frequencies in the set Ω is F. Similarly, the vector $\boldsymbol{R}_c(\boldsymbol{x}_f, \boldsymbol{x}, \Omega) \in \Re^{FL}$ represents a complete set of basic responses for the coarse model at the point $\boldsymbol{x}_f$, at the KPP vector $\boldsymbol{x}$ and over the set Ω. The vectors $\boldsymbol{R}_{fs}(\boldsymbol{x}_f, \Omega)$, $\boldsymbol{R}_{cs}(\boldsymbol{x}_f, \boldsymbol{x}, \Omega) \in \Re^{FM}$ represent some specific responses (such as the magnitude of S_{11}, S_{21}, etc.) of the fine and coarse model, respectively. The design specifications and hence the objective function of the fine and coarse model are given in terms of those responses. In this work, we have two sets of frequencies. The first set Ω_p contains F_p discrete frequency points and is used in the KPP extraction process. The coarse and fine models are both simulated over this set. The second set Ω_s contains F_s frequency points and is used only in optimizing the mapped coarse model. Typically we choose $F_s > F_p$ since we wish to simulate the fine model over the least possible number of frequencies.

We assume that we can establish a mapping from some of the optimization variables to the vector $\boldsymbol{x}$. This mapping is established such that the coarse model aligns with the fine model. The mapping is given by

$$\boldsymbol{x} = \boldsymbol{P}(\boldsymbol{x}_r) : \Re^{n_r} \mapsto \Re^{mn_0} \tag{5-5}$$

$$\boldsymbol{x}_f = [\boldsymbol{x}_r^T \quad \boldsymbol{x}_s^T]^T \tag{5-6}$$

In this work, we assume that the mapping given by (5-5) is linear, i.e.,

$$\Delta\boldsymbol{x} = \boldsymbol{B}_r \, \Delta\boldsymbol{x}_r \tag{5-7}$$

where $\boldsymbol{B}_r \in \Re^{(mn_0) \times n_r}$ is a matrix to be determined. In (5-7) we express the mapping in a difference form for convenience. Fig. 5.1 illustrates these concepts. The matrix $\boldsymbol{B}_r$ may be sparse as we will see in the examples.

5.3 COARSE MODEL DECOMPOSITION

In this section, we present a method based on sensitivity analysis to decompose

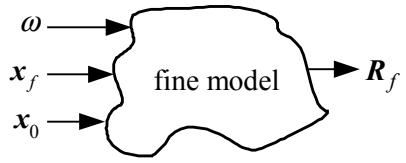

(a)

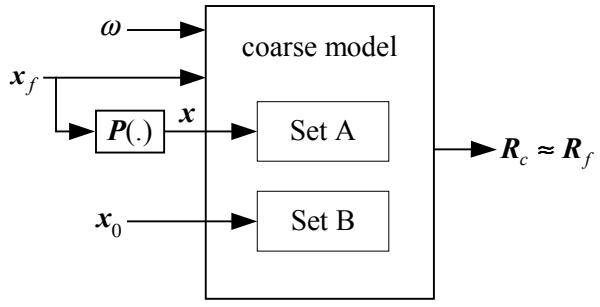

(b)

Fig. 5.1 Changing the KPP in some of the coarse model components (the components in Set A) results in aligning the coarse model (b) with the fine model (a).

the coarse model components into two sets of components. The first set (Set A) contains those components that the coarse model response is very sensitive to any small change in their KPP. The second set (Set B) contains those components for which the coarse model response is insensitive to any change in their KPP. The method is summarized in the following steps.

Step 1 for all $i \in I$ in (5-1) evaluate

$$S_i = \left\| \left(\frac{\partial \boldsymbol{R}_{cs}^T}{\partial \boldsymbol{x}_i} \boldsymbol{D} \right)^T \right\|_F \tag{5-8}$$

where S_i represents the sensitivity of the coarse model response to any change in the KPP of the ith component, the matrix $\boldsymbol{D}$ is for scaling and $\| \ \|_F$ denotes the Frobenius norm.

Step 2 Evaluate

$$\hat{S}_i = \frac{S_i}{\max\limits_{j \in I} \{S_j\}}, \ i \in I \tag{5-9}$$

Step 3 Put the ith component in Set A if $\hat{S}_i \geq \alpha$ otherwise put it in Set B.

The Jacobian of $\boldsymbol{R}_{cs}$ with respect to $\boldsymbol{x}_i$ in (5-8) is evaluated by perturbation at the original preassigned parameters $\boldsymbol{x}_i = \boldsymbol{x}_0, i \in I$ and at the optimal coarse model solution $\boldsymbol{x}_f = \boldsymbol{x}_f^{(0)}$. The matrix $\boldsymbol{D}$ is a diagonal matrix whose elements are the values of the original KPP (that is the elements of the vector $\boldsymbol{x}_0$). The scalar α is a small positive number less than 1. In the examples presented here we set $\alpha = 0.2$.

5.4 THE ESMDF ALGORITHM

The ESMDF algorithm starts by decomposing the coarse model into two sets of components as shown in Section 5.3. Then it obtains the optimal solution of the coarse model. If the fine model response at that solution satisfies the specifications and (or) is very close to the optimal coarse model response (the coarse model is already very good) the algorithm terminates. Otherwise, the algorithm iteratively calibrates the coarse model by extracting the KPP at the optimal coarse model solution and updating the matrix $\boldsymbol{B}_r$. At each iteration, the algorithm obtains the optimal solution of the mapped coarse model subject to a certain trust region (Bakr, Bandler, Biernacki, Chen and Madsen 1998 and Søndergaard 1999). This solution is accepted if it results in a reduction in the fine model objective function. The trust region size is adaptively updated according to the relative improvement of the fine model objective function to that of the coarse model. The algorithm terminates if any one of certain stopping criteria is satisfied. The algorithm performs four main tasks: mapped coarse model optimization, KPP extraction, checking the stopping criteria and updating the mapping parameters and the trust region size. The following subsections explain those tasks in detail.

5.4.1 Mapped Coarse Model Optimization

The ESMDF algorithm obtains the optimal solution of the mapped coarse model at every iteration. It uses trust region methodology to control the amount of optimization done to the mapped coarse model to ensure improvement in the fine model objective function. Let $\boldsymbol{h}$ denote the prospective step $\Delta\boldsymbol{x}_f$ and $\boldsymbol{h}_r$ denote the corresponding step $\Delta\boldsymbol{x}_r$. At the ith iteration the algorithm obtains the step $\boldsymbol{h}^{(i)}$ by solving the optimization

problem

$$\begin{aligned} \boldsymbol{h}^{(i)} &= \arg\min_{\boldsymbol{h}} U(\boldsymbol{R}_{cs}(\boldsymbol{x}_f^{(i)} + \boldsymbol{h}, \boldsymbol{x}^{(i)} + \boldsymbol{B}_r^{(i)}\, \boldsymbol{h}_r)) \\ &\text{subject to } \left\| \boldsymbol{\Lambda}_i \boldsymbol{h} \right\| \le \delta_i \end{aligned} \tag{5-10}$$

where U is a suitable objective function (see Section 2.2.2), δ_i is the trust region radius and the matrix $\boldsymbol{\Lambda}_i$ is for scaling (Alexandrov, Dennis, Lewis and Torczon 1998). In this work, we set $\boldsymbol{\Lambda}_i$ as a diagonal matrix whose elements are the reciprocal of the elements of $\boldsymbol{x}_f^{(i)}$. Therefore, the trust region radius δ_i represents the maximum allowable percentage change in the design variables at the ith iteration. The norm used in (5-10) is the ℓ_∞ norm. Other choices of norm are possible to define the trust region as well. The algorithm decides whether to accept the prospective step $\boldsymbol{h}^{(i)}$:

$$\boldsymbol{x}_f^{(i+1)} = \begin{cases} \boldsymbol{x}_f^{(i)} + \boldsymbol{h}^{(i)} & \text{if } U(\boldsymbol{R}_{fs}(\boldsymbol{x}_f^{(i)} + \boldsymbol{h}^{(i)}, \Omega_p)) < U(\boldsymbol{R}_{fs}(\boldsymbol{x}_f^{(i)}, \Omega_p)) \\ \boldsymbol{x}_f^{(i)} & \text{otherwise} \end{cases} \tag{5-11}$$

The ith iteration is called successful if the prospective step $\boldsymbol{h}^{(i)}$ results in an improvement in the fine model objective function.

The algorithm updates the trust region radius according to the criteria in Alexandrov, Dennis, Lewis and Torczon (1998) and Søndergaard (1999):

(1) If the decrease in the fine model objective function is the same as or better than that of the mapped coarse model we enlarge the trust region.

(2) However, if the fine model objective function increases or decreases but not as much as predicted by the mapped coarse model we shrink the trust region.

(3) Otherwise we leave the trust region unchanged.

Mathematically, we evaluate the relative reduction in the fine model objective function

with respect to the corresponding reduction in the mapped coarse model objective function

$$r = \frac{U(\boldsymbol{R}_{fs}(\boldsymbol{x}_f^{(i)}, \Omega_p)) - U(\boldsymbol{R}_{fs}(\boldsymbol{x}_f^{(i+1)}, \Omega_p))}{U(\boldsymbol{R}_{cs}(\boldsymbol{x}_f^{(i)}, \boldsymbol{x}^{(i)}, \Omega_p)) - U(\boldsymbol{R}_{cs}(\boldsymbol{x}_f^{(i+1)}, \boldsymbol{x}^{(i)} + \boldsymbol{B}_r^{(i)}\boldsymbol{h}_r^{(i)}, \Omega_p))} \tag{5-12}$$

Then we update the trust region radius as follows

$$\delta_{i+1} = \begin{cases} 2\delta_i & \text{if } r > r_1 \\ \delta_i / 3 & \text{if } r < r_2 \\ \delta_i & \text{otherwise} \end{cases} \tag{5-13}$$

where r_1 and r_2 take the values 0.75 and 0.25 (Søndergaard 1999).

5.4.2 Stopping Criteria

At the *i*th iteration, the ESMDF algorithm simulates the fine model at the optimal mapped coarse model solution and stops if one of the following stopping criteria is satisfied

1. The algorithm performs a predefined maximum number of iterations $i_{\max}$.
2. The algorithm reaches a solution that satisfies the specifications.
3. The mapped coarse model response is very close to the fine model response

$$\left\| \boldsymbol{R}_{fs}(\boldsymbol{x}_f^{(i)}, \Omega_p) - \boldsymbol{R}_{cs}(\boldsymbol{x}_f^{(i)}, \boldsymbol{x}^{(i\text{-}1)} + \boldsymbol{B}_r^{(i-1)}\boldsymbol{h}_r^{(i)}, \Omega_p) \right\| \le \varepsilon_1 \tag{5-14}$$

4. The solutions obtained in two successive successful iterations are very close (Bakr, Bandler, Madsen, Rayas-Sánchez and Søndergaard 2000)

$$\left\| \boldsymbol{x}_f^{(i)} - \boldsymbol{x}_f^{(i\text{-}1)} \right\|_\infty \le \varepsilon_2 \tag{5-15}$$

5. The radius of the trust region is very small

$$\delta_i < \delta_{\min} \tag{5-16}$$

where $\delta_{\min}$ is the smallest allowable trust region radius.

The first stopping criterion puts a limit on the number of fine model evaluations the designer can afford. The second stopping criterion indicates that the designer is interested in a feasible solution (a solution which just satisfies the specifications) not the optimal one. This can be the case if the fine model is very time intensive to simulate. In the current implementation of the algorithm, the designer should set a flag which indicates that the algorithm should stop at a feasible solution. The third stopping criterion indicates that the mapped coarse model is doing an excellent job in predicting the improvement in the fine model within certain accuracy. The fifth stopping criterion prevents the algorithm from performing unnecessary fine model simulations if it is not able to predict a better solution than the current one. If none of those criteria is satisfied and the solution obtained in (5-11) is successful the algorithm extracts the KPP at the optimal coarse model solution.

5.4.3 KPP Extraction

At the *i*th iteration, if the ESMDF algorithm accepts the prospective step $\boldsymbol{h}^{(i)}$ (5-11) and the stopping criteria are not satisfied, it extracts the vector of the KPP $\boldsymbol{x}^{(i+1)}$ corresponding to $\boldsymbol{x}_f^{(i+1)}$

$$\boldsymbol{x}^{(i+1)} = \arg\min_{\boldsymbol{x}} \left\| \boldsymbol{R}_f(\boldsymbol{x}_f^{(i+1)}, \Omega_p) - \boldsymbol{R}_c(\boldsymbol{x}_f^{(i+1)}, \boldsymbol{x}, \Omega_p) \right\| \tag{5-17}$$

where the norm used in (5-17) is the Huber norm (see Section 2.2.2). The optimization problem in (5-17) may get trapped in a poor local minimum if the coarse and fine model responses are severely misaligned. Possible ways to overcome this problem is to use the

frequency mapping approach (Bandler, Biernacki, Chen, Hemmers and Madsen 1995) or statistical parameter extraction (Bandler, Biernacki, Chen and Omeragić 1997 and 1999).

Here, we present another technique to overcome this problem. Instead of solving (5-17) directly we try to roughly align the responses first. We do that by minimizing the differences between the center frequencies and the bandwidths of the coarse and fine model responses

$$\bar{\boldsymbol{x}} = \arg\min_{\boldsymbol{x}} \left|\mu_f(\boldsymbol{x}_f^{(i+1)}) - \mu_c(\boldsymbol{x}_f^{(i+1)}, \boldsymbol{x})\right| + \left|\sigma_f(\boldsymbol{x}_f^{(i+1)}) - \sigma_c(\boldsymbol{x}_f^{(i+1)}, \boldsymbol{x})\right| \tag{5-18}$$

where μ_f, μ_c are rough estimates of the center frequencies of the fine and coarse model responses, respectively, and σ_f, σ_c are estimates for the bandwidths of the fine and coarse model responses, respectively. The reader is referred to Appendix C for details on estimating center frequencies and bandwidths of the fine and coarse model responses.

We use this solution as a starting point to solve (5-17). If this procedure fails to produce a good match the algorithm uses the statistical parameter extraction approach in Bandler, Biernacki, Chen and Omeragić (1997 and 1999). That is it tries to solve (5-17) from different random starting points until it obtains a good match. We have to emphasize that we do not need to perform this procedure at every iteration. From our experience we notice that we need only to perform this procedure in the first iteration. For later iterations it is enough to use the solution obtained in the previous iteration as a starting point to solve (5-17). This is observed in all the examples we solved.

5.4.4 Updating the Mapping Parameters

After extracting the KPP at the *i*th iteration the ESMDF algorithm updates the matrix $\boldsymbol{B}_r$ in (5-7). During the first few iterations we have an underdetermined system of

linear equations which has an infinite number of solutions. We choose the minimum norm solution which makes the KPP as close as possible to their original value. That is, we choose $\boldsymbol{B}_r$ as close as possible to $\mathbf{0}$. At the ith iteration, we have

$$[\Delta\boldsymbol{x}^{(1)}\ \Delta\boldsymbol{x}^{(2)}\cdots\Delta\boldsymbol{x}^{(i)}] = \boldsymbol{B}_r\ [\Delta\boldsymbol{x}_r^{(1)}\ \Delta\boldsymbol{x}_r^{(2)}\cdots\Delta\boldsymbol{x}_r^{(i)}] \tag{5-19}$$

where

$$\Delta\boldsymbol{x}^{(j)} = \boldsymbol{x}^{(j)} - \boldsymbol{x}^{(j-1)},\ j \in 1,2,...,i \tag{5-20a}$$

$$\Delta\boldsymbol{x}_r^{(j)} = \boldsymbol{x}_r^{(j)} - \boldsymbol{x}_r^{(j-1)},\ j \in 1,2,...,i \tag{5-20b}$$

The vector $\boldsymbol{x}^{(0)}$ contains the original value of the KPP. When solving (5-19) for $\boldsymbol{B}_r$ the sparsity of the matrix $\boldsymbol{B}_r$ should be taken into consideration. Let the vector $\boldsymbol{b} \in \Re^p$ contain the nonezero elements of the matrix $\boldsymbol{B}_r$. By rearranging (5-19) we can write the linear system in the form

$$\boldsymbol{y} = \boldsymbol{X}_r\ \boldsymbol{b} \tag{5-21}$$

where $\boldsymbol{y} = [(\Delta\boldsymbol{x}^{(1)})^T\ (\Delta\boldsymbol{x}^{(2)})^T\cdots(\Delta\boldsymbol{x}^{(i)})^T]^T \in \Re^{m n_0 i}$ and $\boldsymbol{X}_r \in \Re^{m n_0 i \times p}$ is a sparse matrix whose nonezero elements are the elements of the vectors $\Delta\boldsymbol{x}_r^{(1)}, \Delta\boldsymbol{x}_r^{(2)}, \cdots \Delta\boldsymbol{x}_r^{(i)}$. The structure of the matrix $\boldsymbol{X}_r$ depends on the sparsity of $\boldsymbol{B}_r$. The solution of (5-21) is given by

$$\boldsymbol{b} = \boldsymbol{X}_r^+\ \boldsymbol{y} \tag{5-22}$$

where $\boldsymbol{X}_r^+$ is the pseudoinverse of $\boldsymbol{X}_r$. A Matlab (Matlab™ 1999) function is written to construct the matrix $\boldsymbol{X}_r$ and the Matlab function pinv is used to evaluate $\boldsymbol{X}_r^+$. The advantage of using the pseudoinverse is that it gives us the minimum norm solution in the case of underdetermined systems of equations.

5.4.5 Summary of the ESMDF Algorithm

Given δ_0, $\delta_{\min}$, $i_{\max}$, ε_1, ε_2 the algorithm performs the following steps.

Step 1 Decompose the coarse model components into two sets of components as mentioned in Section 5.3 and initialize $i = 0$, $\delta = \delta_0$, $\boldsymbol{B}_r$=0.

Step 2 Get the optimal solution $\boldsymbol{x}_f^{(0)}$ of the coarse model.

Step 3 Simulate the fine model at $\boldsymbol{x}_f^{(0)}$ and terminate if a stopping criterion is satisfied, otherwise continue.

Step 4 Extract the KPP vector $\boldsymbol{x}^{(i)}$ by solving (5-17) and update $\boldsymbol{B}_r$ from (5-22).

Step 5 Evaluate the prospective step $\boldsymbol{h}^{(i)}$ by optimizing the mapped coarse model (5-10), mark *i* as a successful iteration if $U(\boldsymbol{R}_{fs}(\boldsymbol{x}_f^{(i)} + \boldsymbol{h}, \Omega_p)) < U(\boldsymbol{R}_{fs}(\boldsymbol{x}_f^{(i)}, \Omega_p))$ and set $\boldsymbol{x}_f^{(i+1)}$ according to (5-11).

Step 6 Evaluate *r* in (5-12), update δ from (5-13) and increment *i*.

Step 7 If a stopping criterion is satisfied terminate, otherwise continue.

Step 8 If the *i*th iteration is successful go to Step 4, otherwise go to Step 5.

Notice that the algorithm extracts the KPP in Step 4 only if no stopping criterion is satisfied and if the current iteration is successful. In the first iteration of the algorithm (*i*=1), we do not restrict the optimization problem in (5-10) to any trust region. This enables us to use a small value for the initial trust region radius. For example, an initial trust region radius of 0.05 is used in all the design problems presented here.

5.5 SOFTWARE IMPLEMENTATION

The ESMDF algorithm is currently implemented in Matlab™ (Matlab 1999).

The user should write a text input file which includes the coarse and fine model names and directories, the frequency ranges and the design specifications. It also includes the starting point for the optimization variables and other parameters such as the maximum allowable number of fine model simulations and the initial trust region radius. The output of the algorithm includes plots of the mapped coarse and fine model responses at each iteration as well as a trace of the fine model objective function. It also includes a text output file containing the optimal coarse model solution and the numerical value of the matrix $\boldsymbol{B}_r$ at each iteration. It contains a trace of the trust region radius and the fine model objective function as well as the time taken by the algorithm to solve the problem.

The current implementation drives OSA90/hope™ as a circuit simulator and Sonnet's ***em***™ through OSA90/hope. It uses the optimizers in OSA90/hope™. Driving other EM simulators (with structure parameterization capability such as in Bandler, Biernacki and Chen (1996 and 1999)) in an automatic way is not trivial from inside a programming environment such as Matlab™. We have developed a tool to drive such simulators. This tool is a Windows based program written in Microsoft visual C++. It can be called from any Windows based programming environment such as C++, Matlab, etc. We call this tool Simulator_Driver. Fig. 5.2 illustrates the operation of such a tool. First Matlab runs the executable file "Simulator_Driver.exe" which opens the input file "Input.dat". This input file contains the necessary information to simulate the microwave structure such as the project directory, the design parameters and the frequency ranges. Simulator_Driver.exe then calls the EM simulator, opens the proper windows and fills in the necessary information required for simulating the microwave structure. The Simulator_Driver.exe commands the EM simulator to export the simulated results (S-

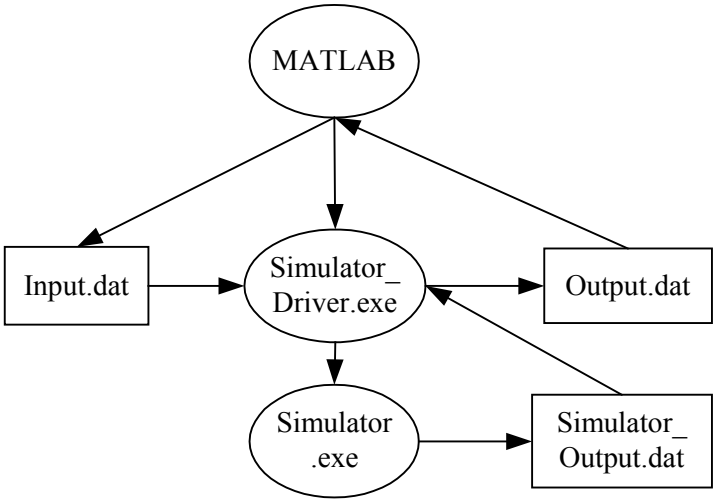

Fig. 5.2 Driving EM/circuit simulators from inside Matlab.

parameters) to the file "Simulator_Output.dat". Then, it reads this output file and saves its contents in a certain format in the file "Output.dat". We have created such a tool (Momentum_Driver) for driving Momentum™ (Momentum 1999). The reader is referred to Appendix D for a detailed description of the Momentum_Driver program.

5.6 EXAMPLES

The ESMDF algorithm is tested on three typical design problems. In all these problems $\delta_0 = 0.05$, $\delta_{\min} = 0.005$, $i_{\max} = 10$, and $\varepsilon_1 = 0.005$. The computer used is an IBM Aptiva (AMD Athlon 650 MHz, 384 MB).

5.6.1 Three-Section Microstrip Transformer

In this example, we consider a 3:1 impedance microstrip transformer (Fig. 5.3(a)). The source and load impedances are 50 and 150 Ω, respectively. The design

specifications are

$$|S_{11}| \le -20 \text{ dB}, \text{ for } 5 \text{ GHz} \le \omega \le 15 \text{ GHz}$$

The fine model is parameterized by Empipe™ (Empipe 1997) and is simulated by Sonnet' ***em***™. The cell size used is 1 mil by 1 mil. Linear interpolation is used to approximate the response at off grid parameters. The coarse model in Fig. 5.3(b) is analyzed by OSA90/hope™. The optimization variables are the widths and lengths of the microstrip transmission lines in Fig. 5.3(a). That is,

$$\boldsymbol{x}_f = [W_1 \; W_2 \; W_3 \; L_1 \; L_2 \; L_3 \;]^T$$

The KPP are the dielectric constant ε_r = 9.7 and the substrate height H = 25 mil. The substrate dielectric loss tangent is 0.002. Therefore, the vector $\boldsymbol{x}_0$=[25 mil 9.7]^T.

The coarse model consists of five components as shown in Fig. 5.3(b). The algorithm applies the coarse model decomposition technique in Section 5.3. The sensitivity of the coarse model response to any change in the KPP of the *i*th component is shown in TABLE 5.1. Therefore, the algorithm chooses components # 1, 3 and 5 as the relevant components. The vector of the KPP of those components is given by

$$\boldsymbol{x} = [\boldsymbol{x}_1^T \;\; \boldsymbol{x}_3^T \;\; \boldsymbol{x}_5^T \;]^T$$

where $\boldsymbol{x}_i = [\varepsilon_{ri} \quad H_i]^T$, i=1, 3, 5. The vector $\boldsymbol{x}_r$ in (5-5) is given by

$$\boldsymbol{x}_r = [W_1 \; W_2 \; W_3 \;]^T$$

We notice that $\boldsymbol{x}_r$ does not include the transmission lines lengths. This is because the reason for changing the KPP is to adjust the characterizing parameters of each transmission line (the characteristic impedance and the propagation constant) such that the coarse model matches the fine model. The characterizing parameters of a

transmission line do not depend on its length. The matrix $\boldsymbol{B}_r$ is sparse

$$\boldsymbol{B}_r = \begin{bmatrix} \text{x} & 0 & 0 \\ \text{x} & 0 & 0 \\ 0 & \text{x} & 0 \\ 0 & \text{x} & 0 \\ 0 & 0 & \text{x} \\ 0 & 0 & \text{x} \end{bmatrix}$$

where x denotes a nonzero entry. The structure of $\boldsymbol{B}_r$ indicates that the KPP of each component is a function only of the design parameters of this component. For example, the KPP of the first component are functions only of W_1. The frequency set Ω_s contains 21 evenly spaced frequencies while Ω_p contains 11 frequencies.

The ESMDF algorithm takes 2 iterations (three fine model simulations) to reach the optimal solution in TABLE 5.2. The time taken by the algorithm to reach this solution is 17 min. The fine model objective function is shown in Fig. 5.4. The stopping

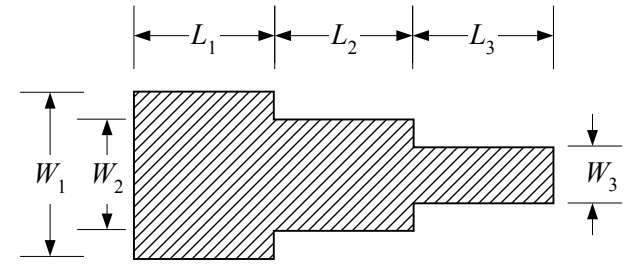

(a)

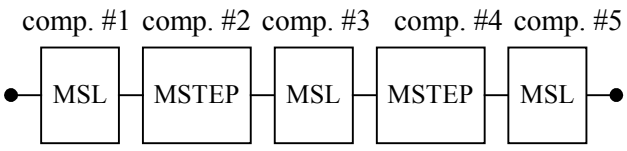

(b)

Fig. 5.3 The 3:1 microstrip transformer (a); the coarse model (b).

criterion (5-14) causes the algorithm to terminate, which means that the agreement between the mapped coarse model and fine model at the second iteration is excellent. The results at the initial solution $\boldsymbol{x}_f^{(0)}$ and the final solution obtained by the algorithm are shown in Fig. 5.5 and Fig. 5.6, respectively. TABLE 5.3 shows the KPP at the final iteration in contrast with the original KPP.

The mapped coarse model obtained at the final iteration can be utilized in statistical analysis such as yield estimation. For Monte Carlo estimation we assume a uniform distribution with 0.25 mil tolerance on all six geometrical parameters. The yield estimated at the solution obtained by the ESMDF algorithm exploiting the mapped coarse model is 78 %. The yield obtained by the fine model at the same solution is 79%. The yield estimation is based on 250 outcomes.

5.6.2 Direct Optimization of the Three-Section Microstrip Transformer

In this section, we optimize the three-section microstrip transformer fine model (see Fig. 5.3) directly using the minimax optimizer in OSA90/hope™. The design specifications as well as the optimization variables are the same as in the previous section. The number of discrete frequency points in the frequency range of interest is 21 frequencies. The optimal solution of the coarse model (see TABLE 5.2) is taken as a starting point for direct optimization. Direct optimization converges to the solution in TABLE 5.2. It takes 153 min in contrast with the ESMDF algorithm, which takes 17 min. We notice that the solution obtained by the ESMDF algorithm is different from that obtained by direct optimization (see TABLE 5.2). However, the fine model responses at both solutions are practically the same (see Fig. 5.7).

TABLE 5.1

COARSE MODEL SENSITIVITIES TO ANY CHANGE IN THE KPP OF THE MICROSTRIP TRANSFORMER COARSE MODEL COMPONENTS

Component #	$\hat{S}_i$
1	1.00
2	0.05
3	0.39
4	0.04
5	0.77

TABLE 5.2

VALUES OF THE DESIGN PARAMETERS FOR THE THREE-SECTION MICROSTRIP TRANSFORMER

Parameter (mm)	Starting point	Optimal coarse model solution	Solution obtained by the ESMDF algorithm	Solution obtained by direct optimization
W_1	0.40	0.381	0.335	0.354
W_2	0.15	0.151	0.136	0.144
W_3	0.05	0.042	0.039	0.044
L_1	3.00	2.783	2.990	2.964
L_2	3.00	3.003	3.079	3.066
L_3	3.00	3.085	3.139	3.162

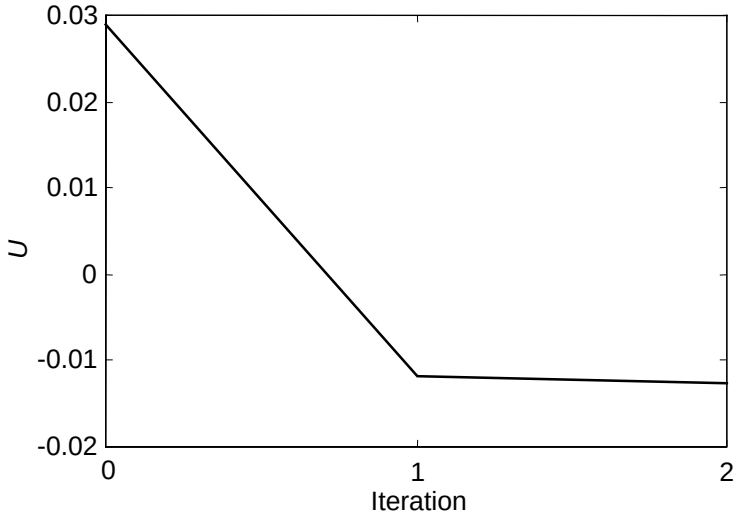

Fig. 5.4 The objective function of the microstrip transformer fine model.

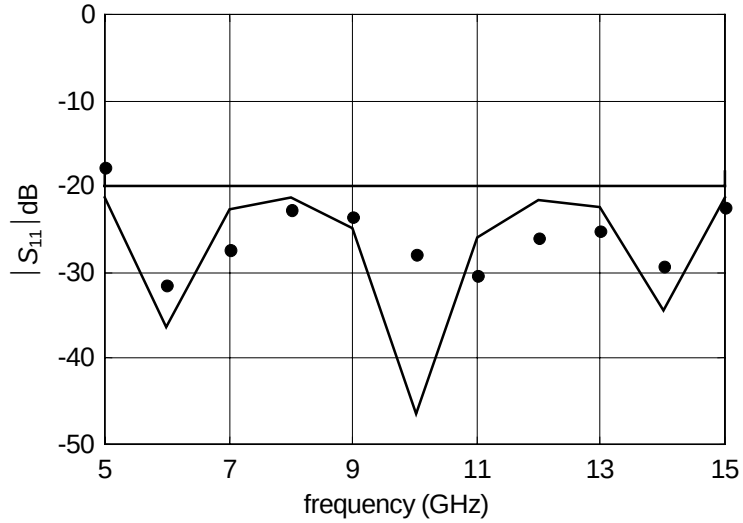

Fig. 5.5 The fine (•) and mapped coarse model (—) responses of the microstrip transformer at the initial solution.

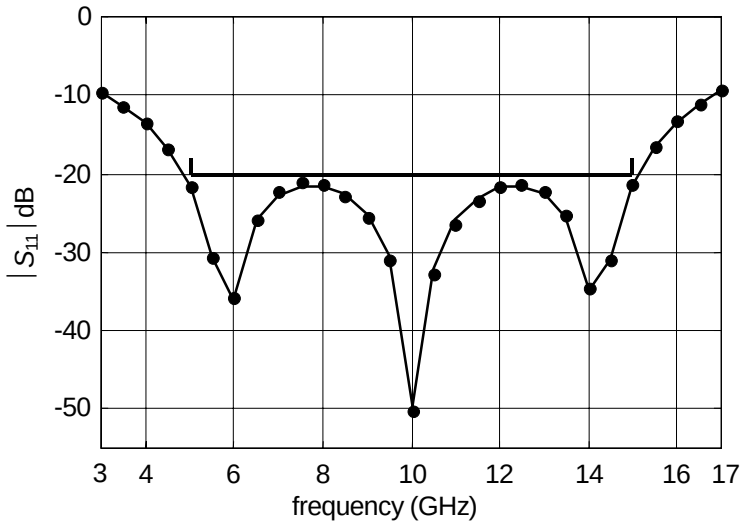

Fig. 5.6 The fine (•) and mapped coarse model (—) responses of the microstrip transformer at the final solution (detailed frequency sweep).

TABLE 5.3

VALUES OF THE KPP OF THE MICROSTRIP TRANSFORMER COARSE MODEL RELEVANT COMPONENTS AT THE INITIAL AND FINAL ITERATIONS

KPP	Original value of the KPP	KPP at the final iteration
H_1	25 mil	19.36 mil
H_3	25 mil	20.97 mil
H_5	25 mil	21.48 mil
ε_{r1}	9.7	8.57
ε_{r3}	9.7	9.17
ε_{r5}	9.7	9.31

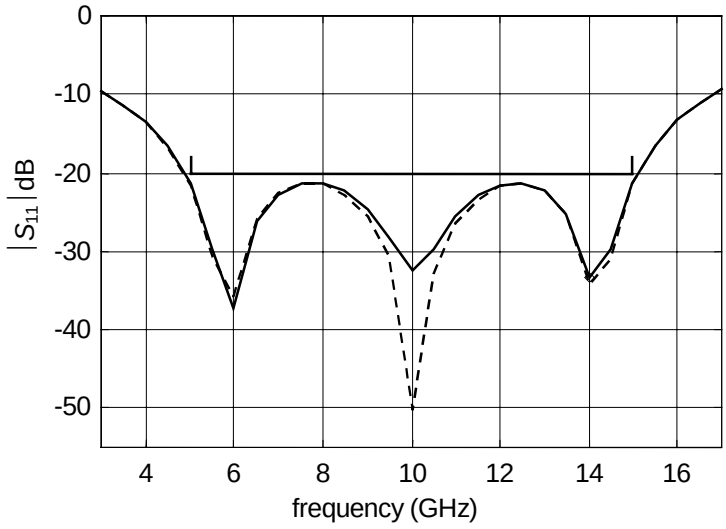

Fig. 5.7 The fine model responses of the microstrip three section transformer at the solution obtained by direct optimization (—) and the ESMDF algorithm (----).

5.6.3 HTS Filter

In this example, we consider the HTS bandpass filter in Fig. 5.8(a) (Bandler, Biernacki, Chen, Getsinger, Grobelny, Moskowitz and Talisa 1995). The design variables are the lengths of the coupled lines and the separation between them

$$\boldsymbol{x}_f = [S_1\ S_2\ S_3\ L_1\ L_2\ L_3\ ]^T,\ \boldsymbol{x}_r = [S_1\ S_2\ S_3]^T$$

The substrate used is lanthanum aluminate with ε_r= 23.425, H= 20 mil and substrate dielectric loss tangent of 0.00003. The length of the input and output lines is L_0=50 mil and the lines width W= 7 mil. We choose the dielectric constant and the substrate height as the KPP, $\boldsymbol{x}_0$=[20 mil 23.425]^T. The design specifications are

$$|S_{21}| \le 0.05 \quad \text{for } \omega \ge 4.099 \text{ GHz and for } \omega \le 3.967 \text{ GHz}$$

$$|S_{21}| \ge 0.95 \quad \text{for } 4.008 \text{ GHz} \le \omega \le 4.058 \text{ GHz}$$

This corresponds to a 1.25% bandwidth. The coarse model consists of empirical models

for single and coupled microstrip transmission lines (see Fig. 5.8(b)). All open circuits are considered ideally open and are not modeled by any empirical model. Because of symmetry we can see that there are only three relevant components in the coarse model: components # 1, 2 and 3. The input and output lines as well as the ideal open circuits are not taken into account. TABLE 5.4 shows the sensitivity of the coarse model response to any change in the KPP of these components. Fig. 5.9 shows the coarse model responses due to 2% perturbation in the KPP of each component (the coarse model is simulated at the optimal solution $\boldsymbol{x}_f^{(0)}$). The vector of KPP is given by $\boldsymbol{x} = [\boldsymbol{x}_1^T \ \boldsymbol{x}_2^T \ \boldsymbol{x}_3^T]^T$, where $\boldsymbol{x}_i = [\varepsilon_{ri} \quad H_i]^T$ is the KPP of the ith component, i=1,2,3. The matrix $\boldsymbol{B}_r$ is sparse and takes the form

$$\boldsymbol{B}_r = \begin{bmatrix} \text{x} & 0 & 0 \\ \text{x} & 0 & 0 \\ 0 & \text{x} & 0 \\ 0 & \text{x} & 0 \\ 0 & 0 & \text{x} \\ 0 & 0 & \text{x} \end{bmatrix}$$

We will consider two cases with different fine models.

5.6.3.1 Case 1: OSA90 as a "Fine" Model

In this case we consider that the "fine" model is exactly the same as the coarse model but with the open circuits modeled by an empirical model for the open circuit stub (with zero length). Therefore, the coarse and fine models are very fast to simulate. This case is recommended during software development and testing of any space mapping based algorithm. The algorithm takes four iterations to converge. The time taken by the algorithm to converge is 1.4 min. The objective function of the fine model is shown in

Fig. 5.10. We notice that the objective function does not change in the second iteration, which means that the second iteration is not successful. The fine model response at the initial and final iterations is shown in Fig. 5.11. TABLE 5.5 shows the design parameter values at the starting point, the optimal coarse model solution $\boldsymbol{x}_f^{(0)}$ and the solution obtained by the algorithm.

5.6.3.2 Case 2: Sonnet's *em* as a Fine Model

The fine model is parameterized by Empipe™ and is simulated by Sonnet ***em***™. The cell size used is 0.5 mil by 1 mil. All parameter values are rounded to the nearest grid point. The frequency set Ω_s contains 25 frequencies while Ω_p contains 17 frequencies. The coarse and fine model responses at the initial solution $\boldsymbol{x}_f^{(0)}$ are shown in Fig. 5.12. We notice that we have severe misalignment between the coarse and fine model, which causes a problem in the KPP extraction. The procedure suggested in Section 5.4.3 managed to yield a good solution of (5-17).

The algorithm takes 4 iterations (five fine model simulations) to terminate. The time taken by the algorithm is 6.2 hr (one fine model simulation takes 1.2 hr). The fine model objective function is shown in Fig. 5.13. TABLE 5.6 shows the design parameter values at the starting point, the optimal coarse model solution $\boldsymbol{x}_f^{(0)}$ and the solution obtained by the algorithm. The detailed coarse and fine model responses at the final iteration are shown in Fig. 5.14. TABLE 5.7 shows the KPP at the final iteration in contrast with the original KPP.

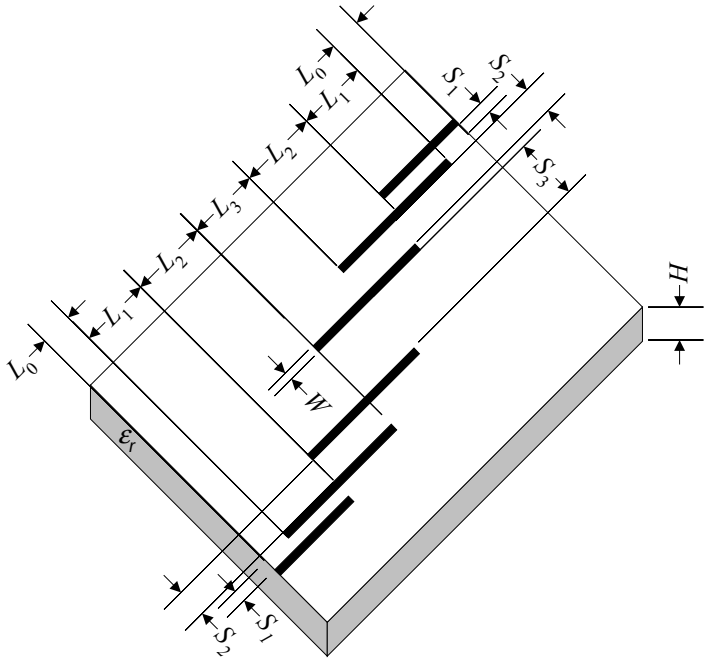

(a)

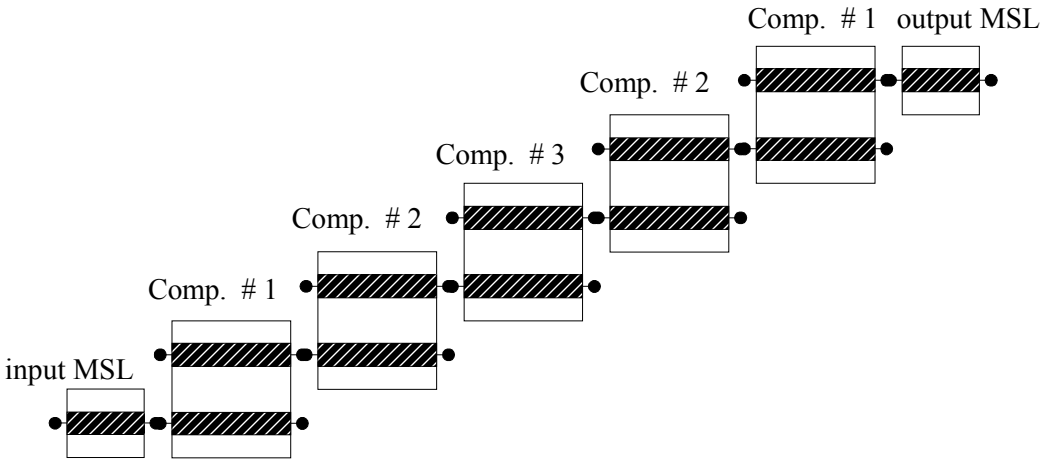

(b)

Fig. 5.8 The HTS filter: (a) the physical structure; (b) the coarse model.

TABLE 5.4

COARSE MODEL SENSITIVITIES TO ANY CHANGE IN THE KPP OF THE HTS COARSE MODEL COMPONENTS

Component #	$\hat{S}_i$
1	0.69
2	1.00
3	0.30

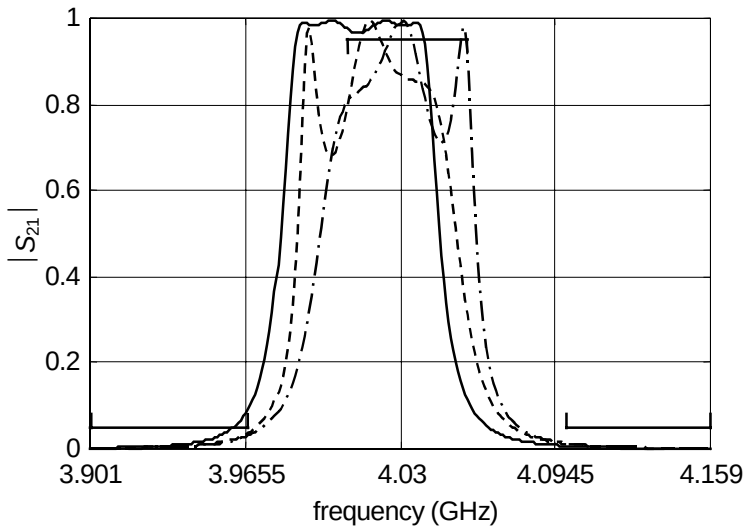

Fig. 5.9 The coarse model response resulting from 2% perturbation in the KPP of: (a) the first component (–·–·–); (b) the second component (—); (c) the third component (----).

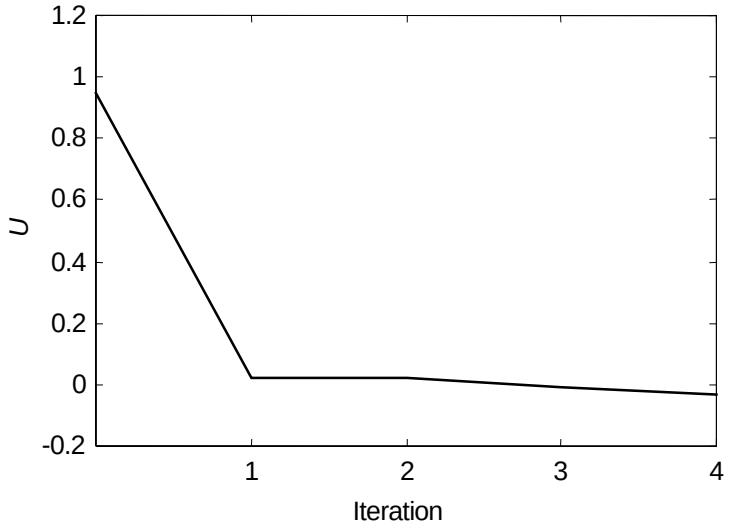

Fig. 5.10 The objective function of the HTS filter fine model (Case 1).

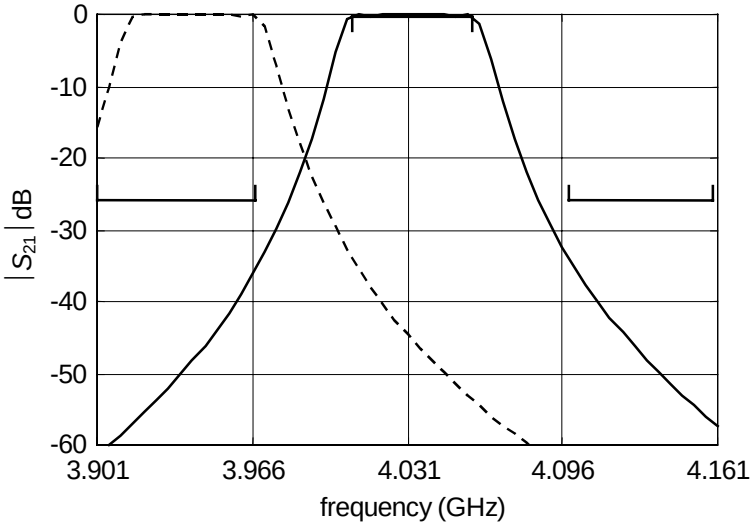

Fig. 5.11 The OSA90 "fine" model response of the HTS filter (Case 1) at the initial solution (---) and at the final solution (—).

TABLE 5.5

VALUES OF THE DESIGN PARAMETERS FOR THE HTS FILTER (CASE 1)

Parameter (mil)	Starting point	Optimal coarse model solution	Solution reached by the ESMDF algorithm
S_1	20.0	20.76	21.55
S_2	100	108.46	107.91
S_3	100	101.80	108.38
L_1	190	172.27	173.77
L_2	190	213.83	203.37
L_3	190	172.74	174.17

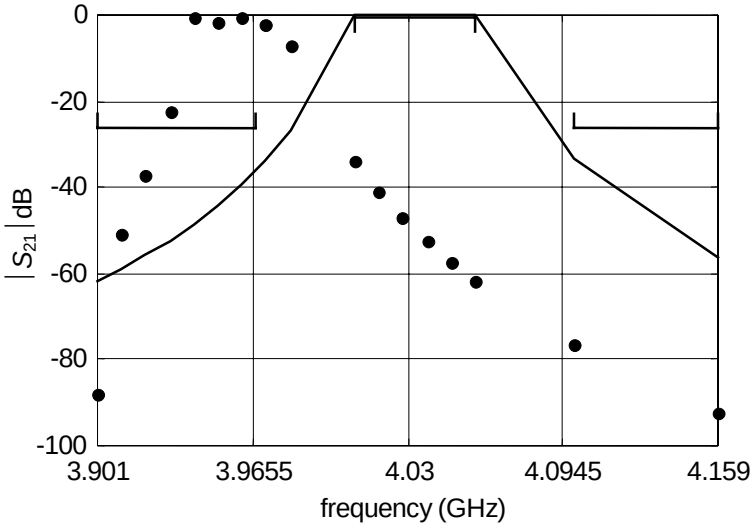

Fig. 5.12 The Sonnet ***em*** fine model response (•) and the coarse model response (—) of the HTS filter (Case 2) at the initial solution.

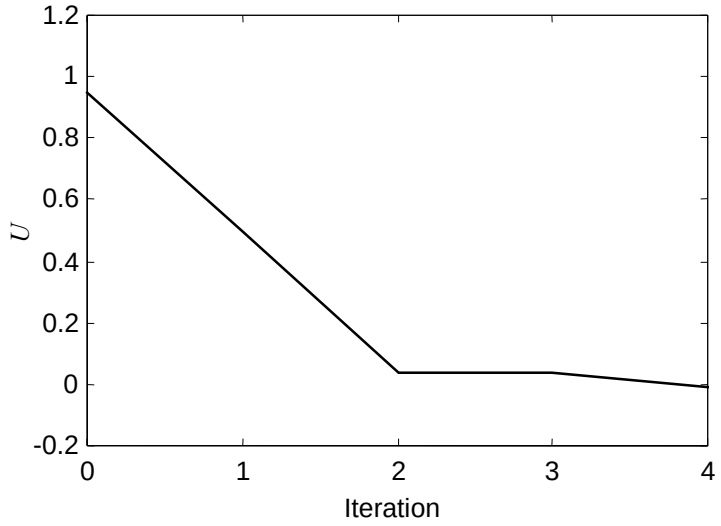

Fig. 5.13 The objective function U of the HTS filter fine model (Case 2).

TABLE 5.6

VALUES OF THE DESIGN PARAMETERS FOR THE HTS FILTER (CASE 2)

Parameter (mil)	Starting point	Optimal coarse model solution	Solution reached by the ESMDF algorithm
S_1	20.0	20.76	19
S_2	100	108.46	78
S_3	100	101.80	80
L_1	190	172.27	178.5
L_2	190	213.83	201.5
L_3	190	172.74	177.5

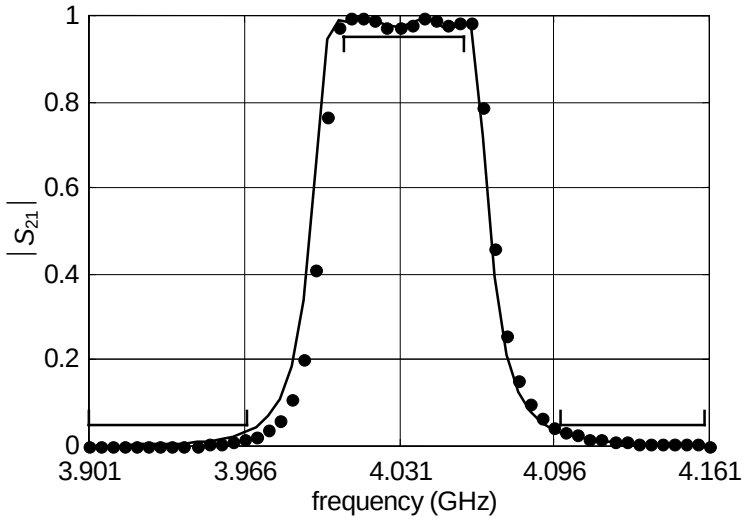

(a)

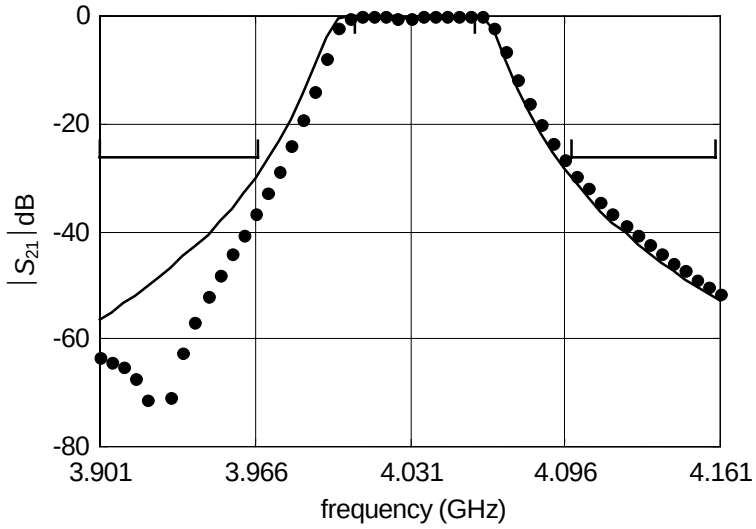

(b)

Fig. 5.14 Detailed frequency sweep of the fine and coarse model responses of the HTS filter (Case 2) at the final solution: (a) $|S_{21}|$; (b) $|S_{21}|$ in decibels.

TABLE 5.7

VALUES OF THE KPP OF THE HTS FILTER (CASE 2) COARSE MODEL RELEVANT COMPONENTS AT THE INITIAL AND FINAL ITERATIONS

KPP	Original value of the KPP	KPP at the final iteration
H_1	20 mil	18.607 mil
H_2	20 mil	16.242 mil
H_3	20 mil	16.298 mil
ε_{r1}	23.425	23.746
ε_{r2}	23.425	24.625
ε_{r3}	23.425	23.809

5.6.4 Microstrip Bandstop Filter with Open Stubs

The structure of the filter is shown in Fig. 5.15(a). The optimization parameters are given by

$$\boldsymbol{x}_f = [W_1\ W_2\ L_0\ L_1\ L_2\ ]^T,\ \boldsymbol{x}_r = [W_1\ W_2]^T$$

The width of the middle microstrip line is fixed at W_0= 25 mil. The KPP are the dielectric constant ε_r= 9.4 and the substrate height H= 25 mil, $\boldsymbol{x}_0$=[25 mil 9.4]^T. The dielectric loss tangent is 0.002. The coarse model consists of empirical models for microstrip lines, T-junctions and ideal open circuits (see Fig. 5.15(b)). The design specifications are

$$|S_{21}| \geq -1 \text{ dB} \quad \text{for } \omega \geq 12 \text{ GHz and for } \omega \leq 8 \text{ GHz}$$

$$|S_{21}| \leq -25 \text{ dB} \quad \text{for } 9 \text{ GHz} \leq \omega \leq 11 \text{ GHz}$$

Because of symmetry we have five components as shown in Fig. 5.15(b). The sensitivities of the coarse model response to the KPP of the coarse model components are given in TABLE 5.8. Therefore, the relevant components are components # 2, 3, 5. The KPP vector is given by

$$\boldsymbol{x} = [\boldsymbol{x}_2^T \;\; \boldsymbol{x}_3^T \;\; \boldsymbol{x}_5^T]^T$$

where $\boldsymbol{x}_i = [\varepsilon_{ri} \quad H_i]^T$ is the KPP of the ith component. The structure of the matrix $\boldsymbol{B}_r$ is given by

$$\boldsymbol{B}_r = \begin{bmatrix} 0 & 0 \\ 0 & 0 \\ \text{x} & 0 \\ \text{x} & 0 \\ 0 & \text{x} \\ 0 & \text{x} \end{bmatrix}$$

Notice that the KPP of component # 2 is not function of $\boldsymbol{x}_r$ and this is reflected in the structure of $\boldsymbol{B}_r$ where the first two rows are zeros. The fine model is analyzed by Momentum™ (Momentum 1999) and the coarse model is simulated by OSA90/hope™. The algorithm uses Momentum_Driver (see Section 5.5 and Appendix D) to drive Momentum™ from Matlab™. The frequency set Ω_s contains 35 frequencies while Ω_p contains 17 frequencies.

The algorithm takes 5 iterations to converge. The time taken by the algorithm is 1.5 hr. The trace of the objective function is shown in Fig. 5.16. The algorithm terminates because the trust region radius reaches its minimum value. The fine and coarse model responses at the initial solution are shown in Fig. 5.17. Fig. 5.18 shows a detailed frequency sweep of the coarse and fine model responses at the solution reached

by the algorithm. The values of the design parameters at the starting point, the optimal coarse model solution and the solution obtained by the algorithm are given in TABLE 5.9. TABLE 5.10 shows the KPP at the final iteration in contrast with the original KPP.

5.6.5 Direct Optimization of the Microstrip Bandstop Filter with Open Stubs

In this section, we optimize the microstrip open stub filters in Fig. 5.15(a) directly using the Momentum minimax optimizer. The design specifications as well as the optimization variables are the same as in the previous section. The number of discrete frequency points in the frequency range of interest is 17. The optimal solution of the coarse model (see TABLE 5.9) is taken as a starting point for direct optimization. Direct optimization converges to the solution in TABLE 5.9. Momentum optimization takes 10 hr (quadratic interpolation was used) in contrast with the ESMDF algorithm which takes 1.5 hr. The optimal response obtained by the algorithm and by direct optimization are shown in Fig. 5.18.

TABLE 5.8

COARSE MODEL SENSITIVITIES TO ANY CHANGE IN THE KPP OF THE MICROSTRIP OPEN STUB FILTER COARSE MODEL COMPONENTS

Component #	$\hat{S}_i$
1	0.14
2	0.64
3	0.84
4	0.19
5	1.00

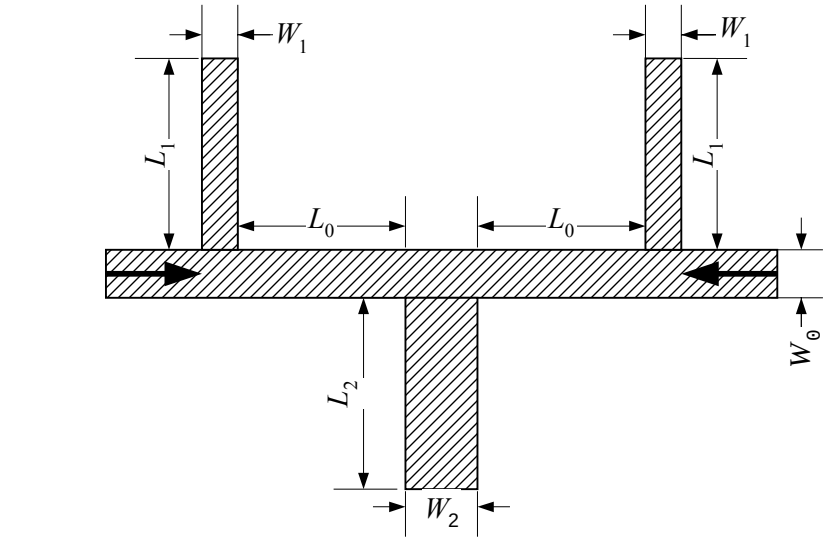

(a)

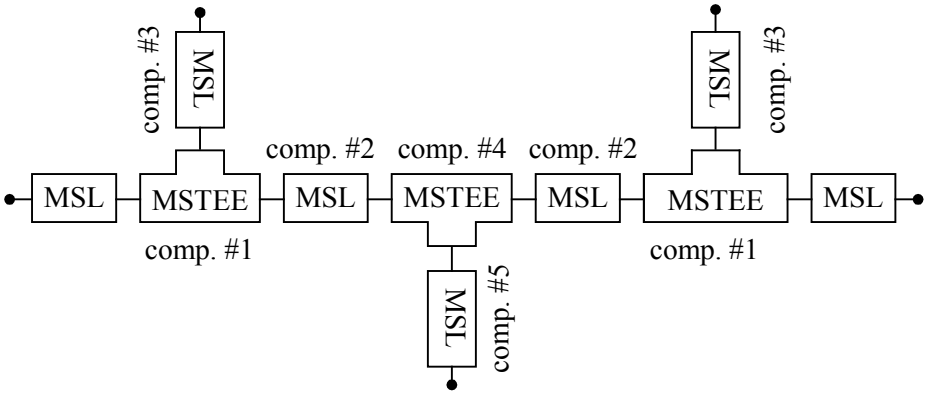

(b)

Fig. 5.15 Microstrip bandstop filter with open stubs: (a) the physical structure; (b) the coarse model.

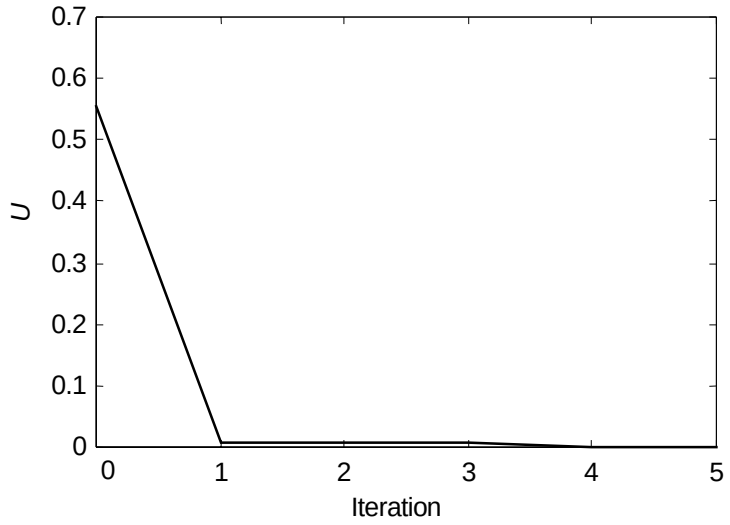

Fig. 5.16 The objective function U of the open stub filter fine model.

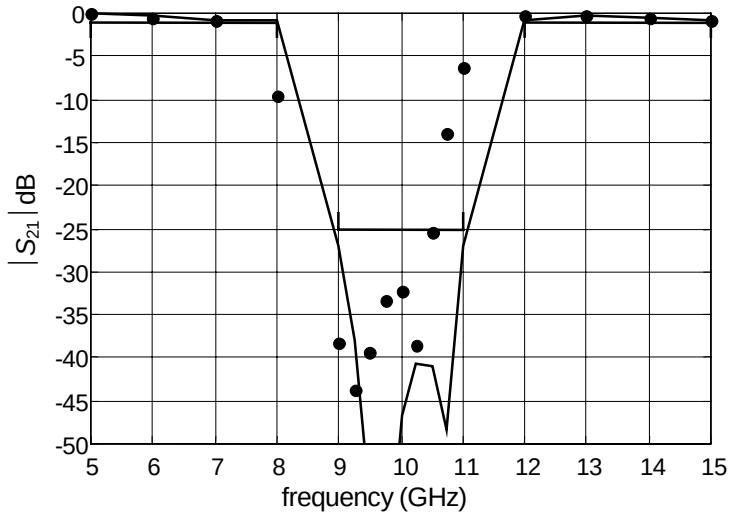

Fig. 5.17 The fine model response (•) versus the coarse model response (—) of the open stub filter at the initial solution.

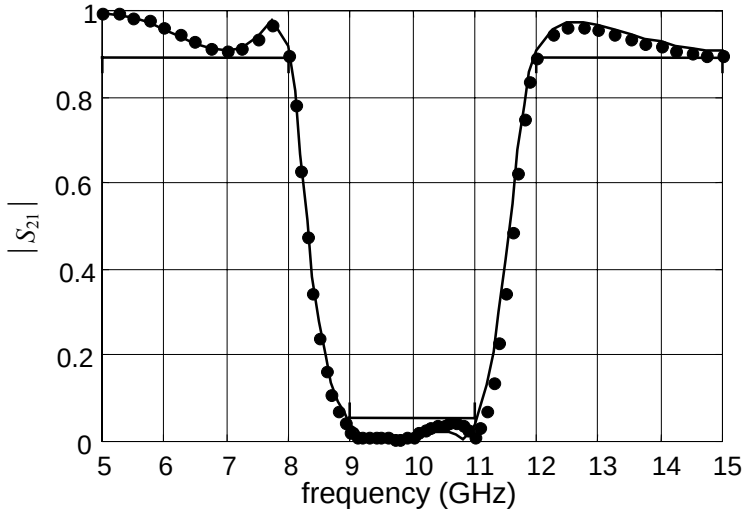

(a)

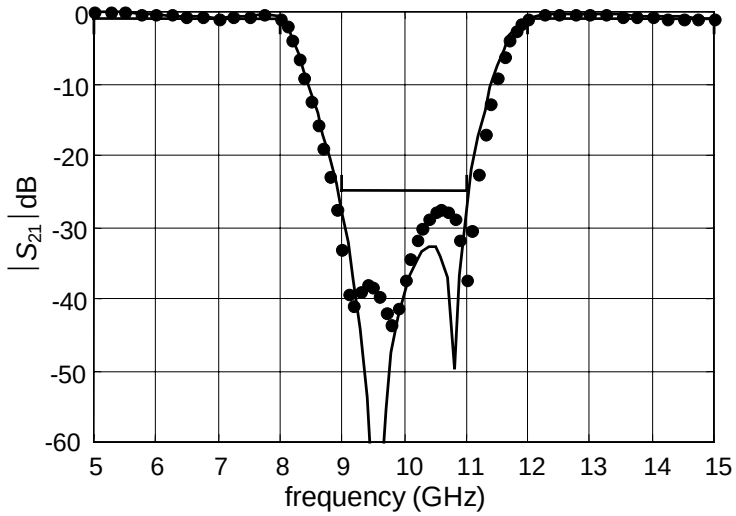

(b)

Fig. 5.18 Detailed frequency sweep of the fine (•) and coarse model (—) responses of the open stub filter at the final solution: (a) $|S_{21}|$; (b) $|S_{21}|$ in decibels.

TABLE 5.9

VALUES OF THE DESIGN PARAMETERS FOR THE MICROSTRIP OPEN STUB FILTER

Parameter (mil)	Starting point	Optimal coarse model solution	Solution reached by the ESMDF algorithm	Solution obtained by direct optimization
W_1	5.00	3.79	3.80	3.70
W_3	10.0	10.25	10.16	9.89
L_0	120	124.23	124.78	117.50
L_1	120	131.60	124.61	125.05
L_2	120	115.89	107.48	110.03

TABLE 5.10

VALUES OF THE KPP OF THE MICROSTRIP OPEN STUB FILTER COARSE MODEL RELEVANT COMPONENTS AT THE INITIAL AND FINAL ITERATIONS

KPP	Original value of the KPP	KPP at the final iteration
H_2	25 mil	28.74 mil
H_3	25 mil	40.60 mil
H_5	25 mil	38.53 mil
ε_{r2}	9.4	9.99
ε_{r3}	9.4	10.56
ε_{r5}	9.4	10.60

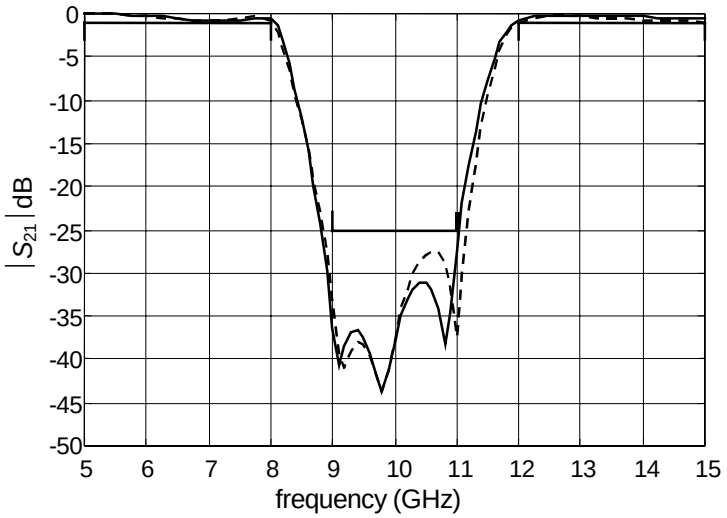

Fig. 5.19 The fine model responses of the microstrip bandstop filter at the solution obtained by direct Momentum optimization (—) and the ESMDF algorithm (- - -).

5.7 CONCLUDING REMARKS

We have presented an expanded space mapping algorithm for circuit design. We deliberately change the key preassigned parameters in some of the coarse model components to align (calibrate) the coarse model with the fine model.

First the algorithm decomposes the coarse model components into two sets. The KPP are allowed to change in one set and are kept intact in the other. A mapping is established from the optimization variables to the key preassigned parameters. This mapping is sparse and needs only few fine model simulations to be fully established. The algorithm marks an iteration as successful if it results in an improvement of the fine model objective function. It extracts the KPP at each successful iteration and then updates the mapping. The enhanced coarse model (the coarse model with the mapped

KPP) is optimized subject to a trust region size at every iteration. Possible practical stopping criteria are presented. Interfacing with different EM/circuit simulators is also considered.

A comparison between the results obtained by the expanded space mapping algorithm and direct optimization for some examples is presented. The mapping obtained at the final iteration of the algorithm can be utilized in statistical analysis such as yield estimation. We have successfully applied our algorithm to several design problems including microstrip transformer, HTS filter and microstrip bandstop filter with open stubs.

Chapter 6

CONCLUSIONS

This thesis has presented novel approaches to efficient modeling and design of microwave circuits. Reliable and accurate EM simulators (fine models) have been combined with approximate circuit models (coarse models) to facilitate design and modeling of microwave structures. A few fine model simulations are used to create broadband empirical models, enhance the accuracy of available empirical models or design of microwave circuits. Space mapping and its related concepts such as frequency mapping, multiple space mapping and expanded space mapping have been utilized to establish computer-aided modeling and design frameworks for microwave circuits.

A review of some important concepts in circuit design and modeling has been presented in Chapter 2. This includes definition of design responses, design specifications, error functions and objective functions. The space mapping technique (Bandler, Biernacki, Chen, Grobelny and Hemmers 1994) and its variations have been briefly reviewed. Recent developments in space mapping algorithms for modeling and optimization have also been addressed. Dimensional analysis and its application to device modeling have also been presented.

Enhancing available empirical models of microwave devices has been addressed in Chapter 3. The Generalized Space Mapping (GSM) approach is a comprehensive engineering framework for device modeling. The formulation of GSM includes the

original space mapping, frequency mapping and multiple space mapping. Two illustrations are presented: space mapping super model and frequency space mapping super model. Two variations of multiple space mapping (MSM) are also presented: MSM for device responses and MSM for frequency intervals. Algorithms to implement both variations have been also presented. A novel criterion to discriminate between coarse models of the same device is introduced. The GSM concept has been verified on several modeling problems, typically utilizing a few relevant full-wave EM simulations. The examples include a microstrip line, a microstrip right angle bend, a microstrip step junction and a microstrip shaped T-junction, yielding remarkable improvement within regions of interest.

Creating broadband empirical models has been addressed in Chapter 4. A unified computer-aided modeling methodology for developing broadband models of microwave passive components is presented. Full-wave EM simulations, artificial neural networks, multivariable rational functions, dimensional analysis and frequency mapping have been integrated to create broadband empirical models. Two types of models are considered: frequency-independent and frequency-dependent empirical models. Frequency mapping is utilized to develop the frequency-dependent empirical models. Useful properties of frequency mapping have been also exploited in the modeling process. The passivity conditions of the frequency-dependent models as well as transforming them into frequency-independent ones have also been addressed. Dimensional analysis has been utilized to reduce the number of parameters, which the model elements as well as the frequency mapping depend on. Broadband models for a microstrip right angle bend, a microstrip via, a microstrip double-step and a CPW step junction have been created using our approach.

Expanded space mapping is presented in Chapter 5. In the original space mapping, a mapping is established between the optimization variables of the coarse model and those of the fine models. Thus this mapping provides a mathematical link between the same kinds of variables. In the expanded space mapping approach we exploit some selected key preassigned parameters (KPP) in the design process. The coarse model response is very sensitive to the KPP, hence it can be calibrated with the fine model if we allow the KPP to change. The KPP are allowed to change in some components of the coarse model (we call them the "relevant" components). A decomposition technique based on sensitivity analysis to identify the "relevant" components of the coarse model is also presented.

The Expanded Space Mapping Design Framework (ESMDF) algorithm calibrates the coarse model iteratively by extracting the preassigned parameters of the relevant components. It establishes a mapping from some of the optimizable parameters to the preassigned parameters. This mapping is sparse and needs a few fine model simulations to be fully established. Trust region methodology is exploited to optimize the enhanced (calibrated) coarse model. A software implementation and interfacing to commercial EM simulators are also addressed. Several design problems have been solved using our ESMDF algorithm. They include a three-section microstrip transformer, an HTS filter and a bandstop microstrip filter with open stubs. In all these examples we notice that the objective function of the fine model drops dramatically in the first iteration.

The author believes that a number of problems related to the topics in this thesis are worth further research and development

(1) Exploiting the Generalized Space Mapping (GSM) approach (Chapter 3) in yield optimization.

(2) Exploiting key preassigned parameters (Chapter 5) in modeling of microwave circuits. This can be used to calibrate coarse models in regions of interest to match fine models. We expect that very few fine model evaluations would be needed to establish the mapping between the KPP and optimizable parameters. This should have useful application in statistical analyses such as yield estimation and optimization.

(3) Approximating the mapping between the optimizable parameters and the KPP by an artificial neural network. This is expected to enhance coarse models over large regions of interest.

(4) Combining the surrogate model concept with the expanded space mapping to provide a robust optimization algorithm, which can default to direct optimization in the final stages. This is very important when there is no way to achieve a good match between the coarse and fine models (the coarse model is a very poor approximation to the fine model). In this case the algorithm should default to direct optimization.

(5) From a theoretical point of view it is worth investigating optimality conditions for the expanded space mapping formulation.

(6) Applying the expanded space mapping algorithm to waveguide and antenna problems.

(7) A standard framework for interfacing EM simulators to popular programming environments such as C++ or Matlab™ is worth development. This will facilitate communication between different simulators. Matlab has an optimization toolbox, which can be used to design microwave circuits once EM simulators can be driven from inside Matlab. We have developed a driver for Momentum™ (see

Appendix D) but we believe that further developments need to be carried out to provide a standard framework for driving EM/Circuit simulators.

APPENDIX

A PASSIVITY CONDITIONS OF THE FDEMS

The passivity conditions for the FDEM can be proved as follows. The impedance in (4-9a) is written in terms of $s = j\omega$ as

$$Z_L(s) = L\, s \frac{f_1 + s^2 f_2}{f_3 + s^2 f_4} \tag{A-1}$$

By partial fractions we get

$$Z_L(s) = L \frac{f_2}{f_4} \left(1 + \frac{f_1/f_2 - f_3/f_4}{f_3/f_4 + s^2}\right) \tag{A-2}$$

Since the poles of an LC impedance lie on the $j\omega$ axis and have positive residues (Temes and Lapatra 1977), we get the following conditions

$$L \frac{f_2}{f_4} > 0 \tag{A-3}$$

$$f_3/f_4 > 0 \tag{A-4}$$

$$f_1/f_2 - f_3/f_4 > 0 \tag{A-5}$$

The inductance L must be positive, hence, f_1, f_2, f_3, f_4 must have the same sign. If we assume that f_1, f_2, f_3, f_4 are positive, these conditions are equivalent to

$$f_i > 0, i = 1,...,4 \tag{A-6}$$

$$f_1 f_4 - f_2 f_3 > 0 \tag{A-7}$$

Those conditions can be also obtained by applying the same procedure to the impedance in (4-9b).

B APPLYING DIMENSIONAL ANALYSIS TO DETERMINE THE DEPENDENCY OF ω_c ON ω AND THE OTHER PARAMETERS OF THE MICROSTRIP RIGHT ANGLE BEND IN SECTION 4.5.1

We apply dimensional analysis to determine the dependency of the circuit model frequency ω_c (in the microstrip right angle bend example in Section 4.5.1) on the fine model frequency ω and the other parameters. The method of dimensional analysis is based on Buckingham's theorem (Middendorf 1986). This theorem states that "If an equation is dimensionally homogeneous it can be reduced to a relationship among a complete set of dimensionless products of the system variables". The dimensionless products are called Pi (π) terms (Middendorf 1986). In our case we assume that ω_c depends on ω, the device parameters W, H, ε, the free space permittivity ε_0 and the speed of light c (we can replace c with the free space permeability μ_0). A dimensional product π takes the form (see Section 2.3.4)

$$\pi = H^{x_1}\, W^{x_2}\, c^{x_3}\, \varepsilon^{x_4}\, (\varepsilon_0)^{x_5}\, \omega^{x_6}\, (\omega_c)^{x_7} \tag{B-1}$$

where the x's are evaluated by solving the system of homogeneous equations

$$\boldsymbol{C}\ \boldsymbol{x} = \boldsymbol{0} \tag{B-2}$$

The elements of the coefficient matrix $\boldsymbol{C}$ in (B-2) can be obtained directly from TABLE B.1 (Middendorf 1986) where Kg, M, S and A are the units of the SI system. Therefore, $\boldsymbol{C}$ is given by

$$\boldsymbol{C} = \begin{bmatrix} 0 & 0 & 0 & -1 & -1 & 0 & 0 \\ 1 & 1 & 1 & -3 & -3 & 0 & 0 \\ 0 & 0 & -1 & 4 & 4 & -1 & -1 \\ 0 & 0 & 0 & 2 & 2 & 0 & 0 \end{bmatrix} \tag{B-3}$$

TABLE B.1

DETERMINING THE COEFFICIENT MATRIX ***C*** DIRECTLY FROM THE UNITS OF THE DEVICE PARAMETERS

	x_1	x_2	x_3	x_4	X_5	x_6	x_7
	H	W	c	ε	ε_0	ω	ω_c
Kg	0	0	0	−1	−1	0	0
M	1	1	1	−3	−3	0	0
S	0	0	−1	4	4	−1	−1
A	0	0	0	2	2	0	0

The number of independent solutions of (B-2) (the same as the number of independent π-terms) equals the number of elements of ***x*** minus the rank of the matrix ***C***. In our case the number of elements of ***x*** is 7 and the rank of the matrix ***C*** is 3, hence we have 4 independent solutions of (B-2) or 4 π-terms. These independent solutions are given in TABLE B.2. Substituting the value of the x's in (B-1) we get the following π-terms

$$\pi_1 = \omega H / c, \quad \pi_2 = \omega W / c, \quad \pi_3 = \varepsilon / \varepsilon_0 = \varepsilon_r, \quad \pi_4 = \omega_c / \omega \tag{B-4}$$

From π_1 and π_2 we can get $\pi_2' = \pi_2 / \pi_1 = W / H$. Applying Buckingham's theorem (Middendorf 1986) the relation between the independent π-terms can take the form

$$\pi_4 = \varphi(\pi_1, \pi_2', \pi_3) \tag{B-5}$$

Therefore,

$$\omega_c = \omega \ \varphi(W/H, \varepsilon_r, \omega H/c) \tag{B-6}$$

But since ω_c is an odd function of ω (see Section 4.3.1) we get

TABLE B.2

A SOLUTION OF THE SYSTEM OF LINEAR EQUATIONS IN (B-2)

x_1	x_2	x_3	x_4	x_5	x_6	x_7
1	0	−1	0	0	1	0
0	1	−1	0	0	1	0
0	0	0	−1	1	0	0
0	0	0	0	0	−1	1

$$\omega_c = \omega \ f(W/H, \varepsilon_r, (\omega H/c)^2) \tag{B-7}$$

C A ROUGH ESTIMATE OF THE CENTER FREQUENCY AND THE BANDWIDTH OF FILTER TYPE RESPONSES

For filter type responses a rough estimate of the center frequency and bandwidth is as follows. We assume that the response is approximately similar to the pdf curve of a normal distribution. Let the filter response be denoted by $R(\omega)$, where ω is a discrete frequency (assume that we have M frequency points in the frequency range of interest). An approximation to the center frequency μ of the filter response is given by

$$\mu = (\sum_{i=1}^{M} \omega_i \ R(\omega_i)) / \sum_{i=1}^{M} R(\omega_i) \tag{C-1}$$

Similarly, the bandwidth is approximated by

$$\sigma = 2 \ \sqrt{(\sum_{i=1}^{M} \omega_i^2 \ R(\omega_i)) / \sum_{i=1}^{M} R(\omega_i) - \mu^2} \tag{C-2}$$

The response R is taken as $|S_{21}|$ for a bandpass filter and $|S_{11}|$ for a bandstop filter. We have to emphasize that although these approximations are rough they are very useful in extracting the KPP in case of severe misalignment between the coarse and fine model (for example the HTS filter in Section 5.6.2).

D Momentum_Driver

Momentum_Driver is a Windows based program to drive Momentum™ (Momentum 1999) from any programming environment such as C++, Matlab™ (Matlab 1999), Fortran, etc. We have used Momentum_Driver to drive Momentum™ from the SMX-system (Bakr, Bandler, Cheng, Ismail and Rayas-Sánchez 2001) and from our algorithm in Section 5.5.

The operation of the program is illustrated in Fig. D.1. First Matlab (or another Windows based environment) runs the executable file "Momentum_Driver.exe" which opens the input file "Input.dat" (this file is created by Matlab). The input file "Input.dat" contains the necessary information to simulate the microwave structure such as the project name and directory, the design parameters and the frequency bands. Momentum_Driver.exe then runs ADS™ (ADS 1999) and launches Momentum™ with the specified microwave project. Then it creates a structure with the specified parameters. Next it opens the "Simulation" window, fills in frequency bands and launches the simulator. Finally "Momentum_Driver.exe" commands Momentum™ to export the simulated results (S-parameters) to the file "Momentum_Output.dat". Then, it reads this output file and saves its contents in a certain format in the file "Output.dat".

The following command line runs Momentum_Driver

Momentum_Driver [-h] <Input.dat> <Output.dat>

where [-h] is optional and is used for help on how to use Momentum_Driver, "Input.dat" is a text input file containing all the necessary information about the Momentum project and it takes the following format

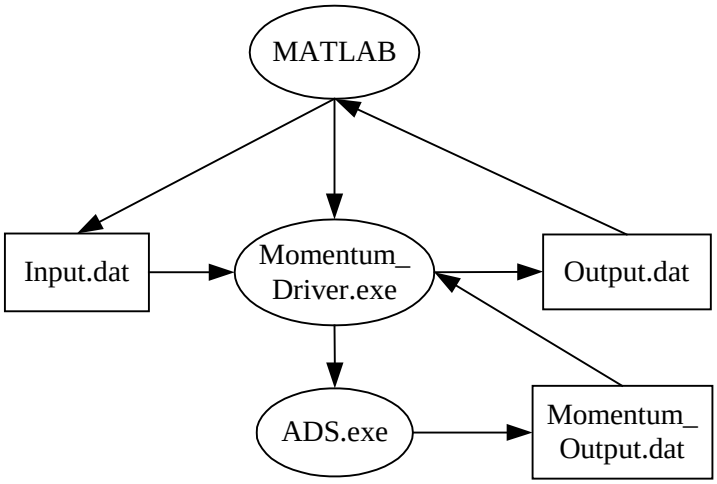

Fig. D.1 Driving Momentum™ from Matlab™.

[Momentum Project Directory]

[Design File Name]

[Number of Parameters] [Number of Points]

[Point Number 1]

[Point Number 2]

⋮

[Point Number n]

[Number of Ports] [Number of Frequency Bands]

[Freq_Start] [Freq_Stop] [Freq_Step]

[Freq_Start] [Freq_Stop] [Freq_Step]

⋮

[Freq_Start] [Freq_Stop] [Freq_Step]

where Freq_Start, Freq_Stop and Freq_Step stand for the lower band edge frequency, the

upper band edge frequency and the incremental frequency step for the band. For example, the input file for the microstrip bandstop filter with open stubs in Section 5.6.4 takes the form

E:\examples\BStopF_mom_prj

BStopF_nom.dsn

5 1

5 10 120 120 120

2 3

5 8 1

9 11 0.25

12 15 1

where the filter is simulated at the point W_1=5 mil, W_2=10 mil, L_0=120 mil, L_1=120 mil and L_2= 120 mil (see Fig. 5.15) over the frequency bands 5 GHz to 8 GHz with a frequency step of 1 GHz, 9 GHz to 11 GHz with a frequency step of 0.25 GHz and 12 GHz to 15 GHz with a frequency step of 1 GHz.

The output file "Output.dat" is generated by Momentum_Driver program and it contains the real and imaginary parts of S-parameters at all points and over all frequency bands. In this file the real and imaginary part of the microwave structure at a single frequency takes the form

$RS_{11}\ IS_{11}\ldots\ RS_{1M}\ IS_{1M}\ RS_{21}\ IS_{21}\ldots RS_{2M}\ IS_{2M}\ RS_{M1}\ IS_{M1}\ldots RS_{MM}\ IS_{MM}$

where RS_{11} and IS_{11} stand for the real and imaginary part of the scattering parameter S_{11} and M is the number of ports. The output file generated by Momentum_Driver corresponding to the microstrip bandstop filter with Open Stubs in Section 5.6.4 is

-0.009119 0.010952 -0.775801 -0.626588 -0.775801 -0.626588 -0.009109 0.010961
0.003383 -0.184941 -0.978425 -0.0177 -0.978425 -0.0177 0.003404 -0.184941
-0.180784 -0.177166 -0.660442 0.694359 -0.660442 0.694359 -0.180754 -0.177198

 0.265666 -0.681888 0.564753 0.264993 0.564753 0.264993 0.265551 -0.681936
-0.832124 -0.520346 0.010263 0.000544 0.010263 0.000544 -0.832166 -0.52028
-0.915579 -0.354741 0.002534 0.015021 0.002534 0.015021 -0.915606 -0.354671
-0.963203 -0.189628 0.003808 0.017706 0.003808 0.017706 -0.963218 -0.189554
-0.980776 -0.023784 0.006914 0.012963 0.006914 0.012963 -0.980778 -0.023707
-0.969209 0.144564 0.008633 0.005253 0.008633 0.005253 -0.969197 0.144644
-0.925085 0.317589 0.009219 1.9e-005 0.009219 1.9e-005 -0.925056 0.317673
-0.838206 0.498008 0.015747 0.005309 0.015747 0.005309 -0.838154 0.498094
-0.68088   0.68758   0.052362 0.029807 0.052362 0.029807 -0.680792 0.687665
-0.367492 0.857775 0.201777 0.054805 0.201777 0.054805 -0.367341 0.857836
-0.258549 0.366671 -0.699751 -0.511677 -0.699751 -0.511677 -0.258594 0.366637
 0.077751 0.177318 -0.889097 0.35538 -0.889097 0.35538   0.07773   0.177327
-0.092225 -0.050086 -0.390055 0.88509 -0.390055 0.88509 -0.092236 -0.050063
-0.243701 0.034075 0.17604   0.920942 0.17604   0.920942 -0.243697 0.034103

BIBLIOGRAPHY

ADS™ (1999), Agilent Technologies, 1400 Fountaingrove Parkway, Santa Rosa, CA 95403-1799.

N. Alexandrov, J.E. Dennis, Jr., R.M. Lewis and V. Torczon (1998), "A trust region framework for managing the use of approximation models in optimization," *Structural Optimization*, vol. 15, pp. 16-23.

M.H. Bakr, J.W. Bandler, R.M. Biernacki, S.H. Chen and K. Madsen (1998), "A trust region aggressive space mapping algorithm for EM optimization," *IEEE Trans. Microwave Theory Tech.*, vol. 46, pp. 2412-2425.

M.H. Bakr, J.W. Bandler, Q.S. Cheng, M.A. Ismail and J.E. Rayas-Sánchez (2001), "SMX—a novel object-oriented optimization system," *IEEE MTT-S Int. Microwave Symp. Dig*. (Phoenix, AZ), pp. 2083-2086.

M.H. Bakr, J.W. Bandler and N. Georgieva (1999), "Modeling of microwave circuits exploiting space derivative mapping," *IEEE MTT-S Int. Microwave Symp. Dig*. (Anaheim, CA), pp. 715-718.

M.H. Bakr, J.W. Bandler, N. Georgieva and K. Madsen (1999), "A hybrid aggressive space mapping algorithm for EM optimization," *IEEE Trans. Microwave Theory Tech.*, vol. 47, pp. 2440-2449.

M.H. Bakr, J.W. Bandler, M.A. Ismail, J.E. Rayas-Sánchez and Q.J. Zhang (2000), "Neural space-mapping optimization for EM-based design," *IEEE Trans. Microwave Theory Tech*., vol. 48, pp. 2307-2315.

M.H. Bakr, J.W. Bandler, K. Madsen, J.E. Rayas-Sánchez and J. Søndergaard (2000), "Space-mapping optimization of microwave circuits exploiting surrogate models," *IEEE Trans. Microwave Theory Tech*., vol. 48, pp. 2297-2306.

M.H. Bakr, J.W. Bandler, K. Madsen and J. Søndergaard (2000), "Review of the space mapping approach to engineering optimization and modeling," *Optimization and Engineering*, vol. 1, pp. 241-276.

J.W. Bandler (1969), "Optimization methods for computer-aided design," *IEEE Trans. Microwave Theory Tech.*, vol. MTT-17, pp. 533-552.

J.W. Bandler, M.H. Bakr, N. Georgieva, M.A. Ismail and D.G. Swanson, Jr. (1999), "Recent results in electromagnetic optimization of microwave components including microstrip T-junctions," *Applied Computational Electromagnetics Society Conf.* (Monterey, CA), pp. 326-333.

J.W. Bandler, R.M. Biernacki and S.H. Chen (1996), "Parameterization of arbitrary geometrical structures for automated electromagnetic optimization," *IEEE MTT-S Int. Microwave Symp. Dig.* (San Francisco, CA), pp. 1059-1062.

J.W. Bandler, R.M. Biernacki and S.H. Chen (1999), "Parameterization of arbitrary geometrical structures for automated electromagnetic optimization," *Int. J. RF and Microwave CAE*, vol. 9, pp. 73-85.

J.W. Bandler, R.M. Biernacki, S.H. Chen, W.J. Getsinger, P.A. Grobelny, C. Moskowitz and S.H. Talisa (1995), "Electromagnetic design of high-temperature superconducting microwave filters," *Int. J. RF and Microwave CAE*, vol. 5, pp. 331-343.

J.W. Bandler, R.M. Biernacki, S.H. Chen, P.A. Grobelny and R.H. Hemmers (1994), "Space mapping technique for electromagnetic optimization," *IEEE Trans. Microwave Theory Tech.,* vol. 42, pp. 2536-2544.

J.W. Bandler, R.M. Biernacki, S.H. Chen, P.A. Grobelny and S. Ye (1993), "Yield-driven electromagnetic optimization via multilevel multidimensional models," *IEEE Trans. Microwave Theory Tech.,* vol. 41, pp. 2269-2278.

J.W. Bandler, R.M. Biernacki, S.H. Chen, R.H. Hemmers and K. Madsen (1995), "Electromagnetic optimization exploiting aggressive space mapping," *IEEE Trans. Microwave Theory Tech.*, vol. 43, pp. 2874-2882.

J.W. Bandler, R.M. Biernacki, S.H. Chen, L.W. Hendrick and D. Omeragić (1997), "Electromagnetic optimization of 3-D structures," *IEEE Trans. Microwave Theory Tech.*, vol. 45, pp. 770-779.

J.W. Bandler, R.M. Biernacki, S.H. Chen and D. Omeragić (1997), "Space mapping optimization of waveguide filters using finite element and model-matching electromagnetic simulators," *IEEE MTT-S Int. Microwave Symp. Dig*. (Denver, CO), pp. 635-638.

J.W. Bandler, R.M. Biernacki, S.H. Chen and D. Omeragić (1999), "Space mapping optimization of waveguide filters using finite element and mode-matching electromagnetic simulators," *Int. J. RF and Microwave CAE*, vol. 9, pp. 54-70.

J.W. Bandler, R.M. Biernacki, S.H. Chen, D.G. Swanson, Jr. and S. Ye (1994), "Microstrip filter design using direct EM field simulation," *IEEE Trans. Microwave Theory Tech.*, vol. 42, pp. 1353-1359.

J.W. Bandler, R.M. Biernacki, S.H. Chen and Q.H. Wang (1998), "Multiple space mapping EM optimization of signal integrity in high-speed digital circuits," *Proc. 5th Int. Workshop on Integrated Nonlinear Microwave and Millimeterwave Circuits* (Duisburg, Germany), pp. 138-140.

J.W. Bandler and C. Charalambous (1972), "Practical least *p*th optimization of networks," *IEEE Trans. Microwave Theory Tech.*, vol. 34, pp. 834-840.

J.W. Bandler and S.H. Chen (1988), "Circuit optimization: the state of the art," *IEEE Trans. Microwave Theory Tech.*, vol. 36, pp. 424-443.

J.W. Bandler, S.H. Chen, R.M. Biernacki, L. Gao, K. Madsen and H. Yu (1993a), "Robustizing circuit optimization using Huber functions," *IEEE MTT-S Int. Microwave Symp. Dig*. (Atlanta, GA), pp. 1009-1012.

J.W. Bandler, S.H. Chen, R.M. Biernacki, L. Gao, K. Madsen and H. Yu (1993b), "Huber optimization of circuits: a robust approach," *IEEE Trans. Microwave Theory Tech.*, vol. 41, pp. 2279-2287.

J.W. Bandler, S.H. Chen and S. Daijavad (1986), "Microwave device modeling using efficient l_1 optimization: a novel approach," *IEEE Trans. Microwave Theory Tech.*, vol. 34, pp. 1282-1293.

J.W. Bandler, N. Georgieva, M.A. Ismail, J.E. Rayas-Sánchez and Q.J. Zhang (1999), "A generalized space mapping tableau approach to device modeling," 29*th European Microwave Conf.* (Munich, Germany), pp. 231-234.

J.W. Bandler, N. Georgieva, M.A. Ismail, J.E. Rayas-Sánchez and Q.J. Zhang (2001), "A generalized space mapping tableau approach to device modeling," *IEEE Trans. Microwave Theory Tech.*, vol. 49, pp. 67-79.

J.W. Bandler, M.A. Ismail and J.E. Rayas-Sánchez (2000), "Broadband physics-based modeling of microwave passive devices through frequency mapping," *IEEE MTT-S Int. Microwave Symp. Dig.* (Boston, MA), pp. 969-972.

J.W. Bandler, M.A. Ismail and J.E. Rayas-Sánchez (2001a), "Broadband physics-based modeling of microwave passive devices through frequency mapping," *Int. J. RF and Microwave CAE*, vol. 11, pp. 156-170.

J.W. Bandler, M.A. Ismail and J.E. Rayas-Sánchez (2001b), "Expanded space mapping design framework exploiting preassigned parameters," *IEEE MTT-S Int. Microwave Symp. Dig.* (Phoenix, AZ), pp. 1151-1154.

J.W. Bandler, M.A. Ismail and J.E. Rayas-Sánchez (2001c), "Expanded space mapping EM based design framework exploiting preassigned parameters," *IEEE Trans. Microwave Theory Tech.*, submitted.

J.W. Bandler, M.A. Ismail, J.E. Rayas-Sánchez and Q.J. Zhang (1999), "Neuromodeling of microwave circuits exploiting space mapping technology," *IEEE Trans. Microwave Theory Tech.*, vol. 47, pp. 2417-2427.

J.W. Bandler, M.A. Ismail, J.E. Rayas-Sánchez and Q.J. Zhang (2001), "Neural inverse space mapping EM-optimization," *IEEE MTT-S Int. Microwave Symp. Dig.* (Phoenix, AZ), pp. 1007-1010.

J.W. Bandler, W. Kellermann and K. Madsen (1985), "A superlinearly convergent minimax algorithm for microwave circuit design," *IEEE Trans. Microwave Theory Tech.*, vol. 33, pp. 1519-1530.

J.W. Bandler and M.R.M. Rizk (1979), "Optimization of electrical circuits," *Math. Program. Study*, vol. 11, pp. 1-64.

J.W. Bandler and A.E. Salama (1985), "Fault diagnosis of analog circuits," *Proc. IEEE*, vol. 73, pp. 1279-1325.

J.W. Bandler and Q.J. Zhang (1987), "An automatic decomposition approach to optimization of large microwave systems," *IEEE Trans. Microwave Theory Tech.*, vol. 35, pp. 1231-1239.

R.M. Biernacki, J.W. Bandler, J. Song and Q.J. Zhang (1989), "Efficient quadratic approximation for statistical design," *IEEE Trans. Circuits Syst.*, vol. 36, pp. 1449-1454.

C.G. Broyden (1965), "A class of methods for solving nonlinear simultaneous equations," *Math. Comp.*, vol. 19, pp. 577-593.

P. Burrascano, M. Dionigi, C. Fancelli and M. Mongiardo (1998), "A neural network model for CAD and optimization of microwave filters," *IEEE MTT-S Int. Microwave Symp. Dig.* (Baltimore, MD), pp. 13-16.

C. Charalambous (1973), *Nonlinear Least pth Approximation and Nonlinear Programming with Applications in the Design of Networks and Systems*. Ph.D. Thesis, Department of Electrical and Computer Engineering, McMaster University, Hamilton, Ontario, Canada.

S. Chen (1987), *A Unified, Integrated Approach to Generalized ℓ_p Circuit Optimization*. Ph.D. Thesis, Department of Electrical and Computer Engineering, McMaster University, Hamilton, Ontario, Canada.

R. Collin (1966), *Foundations for Microwave Engineering*. New York: McGraw-Hill, Inc.

T. Dhaene, J. Ureel, N. Faché and D. De Zutter (1995) "Adaptive frequency sampling algorithm for fast and accurate S-parameters modeling of general planar structures," *IEEE MTT-S Int. Microwave Symp. Dig*. (Orlando, FL), pp. 1427-1430.

A. Dounavis, E. Gad, R. Achar and M.S. Nakhla (2000), "Passive model reduction of multiport distributed interconnects," *IEEE Trans. Microwave Theory Tech.*, vol. 48, pp. 2325-2334.

M. Dydyk (1977), "Master the T-junction and sharpen your MIC designs," *Microwaves*, pp. 184-186.

em™ Version 4.0b (1997), Sonnet Software, Inc., 1020 Seventh North Street, Suite 210, Liverpool, NY 13088.

Empipe™ Version 4.0 (1997), formerly Optimization Systems Associates Inc., P.O. Box 8083, Dundas, Ontario, Canada L9H 5E7, now Agilent Technologies, 1400 Fountaingrove, Parkway, Santa Rosa, CA 95403-1799.

Empipe3D™ Version 4.0 (1997), formerly Optimization Systems Associates Inc., P.O. Box 8083, Dundas, ON, Canada, L9H 5E7, 1997, Chapter 5, now Agilent Technologies, 1400 Fountaingrove Parkway, Santa Rosa, CA 95403-1799.

P.A. Grobelny (1995), *Integrated Numerical Modeling Techniques for Nominal and Statistical Circuit Design*. Ph.D. Thesis, Department of Electrical and Computer Engineering, McMaster University, Hamilton, Ontario, Canada.

K.C. Gupta, R. Garg and I.J. Bahl (1979), *Microstrip Lines and Slotlines*. Dedham, MA: Artech House.

R.F. Harrington (1967), "Matrix methods for field problems," *Proc. IEEE*, vol. 55, pp. 136-149.

Agilent HFSS™ Version 5.5 (1999), Agilent Technologies, 1400 Fountaingrove Parkway, Santa Rosa, CA 95403-1799.

Ansoft HFSS™, Ansoft Corporation, Four Station Square, Suite 660, Pittsburgh, PA 15219, USA.

W.J.R. Hoefer (1992), "Time domain electromagnetic simulation for microwave CAD applications," *IEEE Trans. Microwave Theory Tech*., vol. 40, pp. 1517-1527.

P. Huber (1981), *Robust Statistics*. New York: Wiley.

N. Jain and P. Onno (1997), "Methods of using commercial electromagnetic simulators for microwave and millimeter-wave circuit design and optimization," *IEEE Trans. Microwave Theory Tech*., vol. 45, pp. 724-746.

M. Kirschning, R. Jansen and N. Koster (1983), "Measurement and computer-aided modeling of microstrip discontinuities by an improved resonator method," *IEEE MTT-S Int. Microwave Symp. Dig*. (Boston, MA), pp. 495-497.

H. Leung and S. Haykin (1993), "Rational function neural network," *Neural Computation*, vol. 5, pp. 928-938.

Matlab™ Version 5.3 (1999), The MathWorks, Inc., 3 Apple Hill Drive, Natick, MA 01760-2098.

W.H. Middendorf (1986), *Design of Devices and Systems*. New York: Marcel Dekker, Inc., Chapter 7.

Momentum™ Version 3.5 (1999), Agilent Technologies, 1400 Fountaingrove Parkway, Santa Rosa, CA 95403-1799.

D.C. Montgomery (1991), *Design and Analysis of Experiments*. New York: Wiley.

OSA90/hope™ Version 4.0 (1997), formerly Optimization Systems Associates Inc., P.O. Box 8083, Dundas, Ontario, Canada L9H 5E7, now Agilent Technologies, 1400 Fountaingrove, Parkway, Santa Rosa, CA 95403-1799.

A.M. Pavio (1999), "The electromagnetic optimization of microwave circuits using companion models," *Proc. Workshop on Novel Methodologies for Device Modeling and Circuit CAD*, *IEEE MTT-S Int. Microwave Symp*. (Anaheim, CA).

S.F. Peik, R.R. Mansour and Y.L. Chow (1998), "Multidimensional Cauchy method and adaptive sampling for an accurate microwave circuit modeling," *IEEE Trans. Microwave Theory Tech.*, vol. 46, pp. 2364-2371.

D.M. Pozar (1990), *Microwave Engineering*. New York: Addison-Wesley.

J.C. Rautio and R.F. Harrington (1987a), "An efficient electromagnetic analysis of arbitrary microstrip circuits," *IEEE MTT-S Int. Microwave Symp. Dig*. (Las Vegas, NV), pp. 295-298.

J.C. Rautio and R.F. Harrington (1987b), "An electromagnetic time-harmonic analysis of shielded microstrip circuits," *IEEE Trans. Microwave Theory Tech.*, vol. 35, pp. 726-730.

M.R.M. Rizk (1979), *Advances in Simulation and Optimization of Electrical Networks*. Ph.D. Thesis, Department of Electrical and Computer Engineering, McMaster University, Hamilton, Ontario, Canada.

J. Søndergaard (1999), *Non-linear Optimization Using Space Mapping*. Masters Thesis, Department of Mathematical Modeling (IMM), Technical Uinversity of Denmark (DTU), Lyngby, Denmark.

D.G. Swanson, Jr. (1992), "Grounding microstrip lines with via holes," *IEEE Trans. Microwave Theory Tech.*, vol. 40, pp. 1719-1721.

D.G. Swanson, Jr. (1995), "Optimizing a microstrip bandpass filter using electromagnetics," *Int. J. Microwave and Millimeter-wave CAE*, vol. 5, pp. 344-351.

D.G. Swanson, Jr. (1998), "EM field simulators made practical," Field-Solver Course, M/A-COM Division of AMP, Lowell, MA.

G.C. Temes and D.A. Calahan (1967), "Computer-aided network optimization the state-of-the-art," *Proc. IEEE*, vol. 55, pp. 1832-1863.

G.C. Temes and J.W. Lapatra (1977), *Introduction to Circuit Synthesis and Design*. New York: McGraw-Hill, Inc.

F. Wang and Q.J. Zhang (1997), "Knowledge-based neural models for microwave design," *IEEE Trans. Microwave Theory Tech.*, vol. 45, pp. 2333-2343.

P. Watson and K.C. Gupta (1996), "EM-ANN models for microstrip vias and interconnects in multilayer circuits," *IEEE Trans. Microwave Theory Tech.*, vol. 44, pp. 2495-2503.

P. Watson and K.C. Gupta (1997), "Design and optimization of CPW circuits using EM-ANN models for microstrip CPW components," *IEEE Trans. Microwave Theory Tech.*, vol. 45, pp. 2515-2523.

P. Watson, M.Y. Mah and L.L. Liou (1999), "Input variable space reduction using dimensional analysis for artificial neural network modeling," *IEEE MTT-S Int. Microwave Symp. Dig*. (Anaheim, CA), pp. 269-272.

S. Ye and R.R. Mansour (1997), "An innovative CAD technique for microstrip filter design," *IEEE Trans. Microwave Theory Tech*., vol. 45, pp. 780-786.

A.H. Zaabab, Q.J. Zhang and M.S. Nakhla (1994), "Analysis and optimization of microwave circuits & devices using neural network models," *IEEE MTT-S Int. Microwave Symp. Dig*. (San Diego, CA), pp. 393-396.

A.H. Zaabab, Q.J. Zhang and M.S. Nakhla (1995), "A neural network modeling approach to circuit optimization and statistical design," *IEEE Trans. Microwave Theory Tech.*, vol. 43, pp. 1349-1358.

AUTHOR INDEX

J

K

L

M

N

O

Z

SUBJECT INDEX

D

E

F

G

H

I

K

L

M

T

W

Y